Magnetic Resonance Spectroscopy at ultra-high field in humans

Vincent Oltman Boer

ISBN: 978-90-393-5706-4
Lay-out and cover: Simon Boer, GBver Design
Printed by: Ipskamp Drukkers, Enschede, The Netherlands
The publication of this thesis was financially supported by Philips Medical Solutions.

Magnetic Resonance Spectroscopy at ultra-high field in humans

Magnetische Resonantie Spectroscopie op ultrahoogveld in de mens

(met een samenvatting in het Nederlands)

Proefschrift

ter verkrijging van de graad van doctor aan de Universiteit Utrecht
op gezag van de rector magnificus, prof.dr. G.J. van der Zwaan,
ingevolge het besluit van het college voor promoties in het openbaar te verdedigen op
donderdag 12 januari 2012 des ochtends te 10.30 uur

door

Vincent Oltman Boer

geboren op *22 augustus 1984* te *Nieuwegein*

Promotor: Prof. dr. P.R. Luijten

Co-promotor: Dr. D.W.J. Klomp

Voor mijn ouders en grootouders

Content

Chapter 1

Introduction

1.1 Introduction

MR spectroscopy (MRS) is a technique to non-invasively measure the concentration of biochemical molecules in the human body. It obviates the need for tissue excisions or biopsies and provides direct tissue biomarkers, rather than indirect parameters derived from blood, plasma or urine samples. MRS is a unique tool to study the *in vivo* metabolism.

The local biochemistry in the human body can give important information in the (early) diagnosis, staging or treatment monitoring of disease and hence MR spectroscopy has attracted a large interest over the last decades. However, since the concentration of the metabolites in the human body is relatively low, the signal-to-noise (SNR) ratio is often the limiting factor in MRS measurements and only a selective number of metabolites are under physiological conditions concentrated enough (millimolar range) to result in a MR detectable signal. Other imaging techniques, such as Positron Emission Tomography (PET) can resolve metabolites in the picomolar range. However, these techniques need radioactive exogenous tracers, whereas MR spectroscopy makes use of the signal of endogenous metabolites without the use of ionizing radiation.

With the recent development of ultra-high field magnets, the intrinsic SNR is increased, improving the reliability and reproducibility of the MR spectroscopy measurements. These stronger magnetic fields allow for a leap forward in higher spectral and spatial resolutions in MR spectroscopy of the human body.

At ultra-high field, the localization accuracy, and spectral quality over the different regions in the body is severely compromised due to low transmit radio frequency fields (B_1) in the human body and increased inhomogeneity in the radio frequency field and the static magnetic field (B_0). Although the increased SNR allows relatively low concentrated metabolites to be detected at increased spatial resolutions, a stronger suppression of the overlapping background signals is required. This is however complicated by the inhomogeneity in both B_0 and B_1 fields. In this thesis, several methods are described for counteracting these spatial and temporal instabilities at ultra-high field, allowing for the robust and sensitive acquisition of metabolic information in the human body.

1.2 Outline of this thesis

Chapter 1 will continue with a short overview of the basis of *in vivo* MR spectroscopy and the typical opportunities and challenges that ultra-high field brings us for MR spectroscopy.

At ultra-high field, accurate localization of the MR signal in the human body is one of the major challenges. Therefore a newly developed single-voxel sequence with high localization accuracy is described in **Chapter 2**, with which the signal of several metabolites can be robustly and accurately detected in the human brain.

An alternative localization technique is described in **Chapter 3**, where a novel B_0 field inhomogeneity correction strategy is combined with frequency selective suppression to remove overlapping background signals from water and lipids. To this end, slice selection with phase encoding can be used to spatially resolve the signal in a two-dimensional (2D) matrix with a very short echo time and high temporal efficiency.

In **Chapter 4**, this technique is extended to a multi-slice acquisition, where dynamic B_0 and B_1 field optimization was incorporated to correct field inhomogeneity and ensure high quality MR spectroscopy data throughout the human brain.

At ultra-high field, not only the spatially varying B_0 fields have to be compensated. Also the temporal B_0 field fluctuations, as for example caused by breathing, have to be considered. **Chapter 5** discusses the stability problems associated with a dynamically changing B_0 field, and how these can be monitored and compensated for in real-time.

With the overall high SNR and the spatial and temporal stability that was demonstrated at 7T, the detection of metabolites with very low concentrations becomes possible. This is demonstrated in **Chapter 6**, where the signal from γ-Aminobutyric acid (GABA) (with a concentration of ± 1 mM) is robustly measured in the human brain. This is challenging due to the overlap with signals of macromolecules and a more than 10 times higher creatine signal.

This concept is further developed in **Chapter 7**, where a novel refocused double quantum filter was employed to detect the lactate resonance, which was overlapped by a more than 1000 fold higher lipid signal.

Finally, in **Chapter 8**, after summarizing the main conclusions obtained from the results in this thesis we can conclude that after applying the recently developed methodology, ultra-high field brings MR spectroscopy to a higher level in clinical research in humans.

1.3 MR spectroscopy at ultra high field

1.3.1 Level splitting; the Zeeman effect

When atoms, the building blocks of all matter around us, are placed into a strong magnetic field (B_0), an interesting phenomenon occurs. The nucleus of the atoms, consistent of protons (and neutrons), has a fundamental quantum mechanical property known as spin. For example, if we look at the nucleus of the simplest atom, the hydrogen atom (^{1}H), it has spin ½, and can be in either of two states. It can either have an up (+½) or a down (-½) spin. Due to the Zeeman effect, the energy level of the up state in a strong magnetic field is slightly lower than the energy level of the down state (Figure 1).

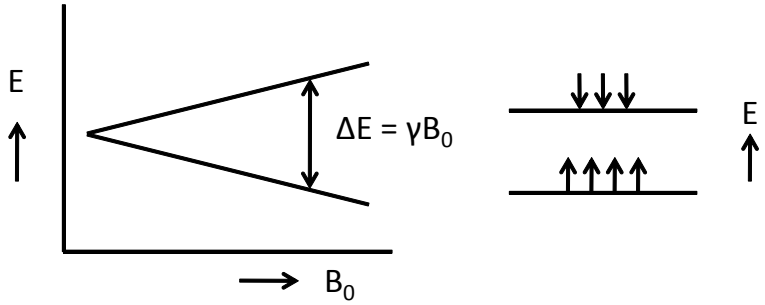

Figure 1. The Zeeman effect. The energy levels of the ^{1}H nucleus show a field strength dependent splitting, which can be probed with RF energy. The higher the static magnetic field, the larger the energy associated with RF absorption and transmission. Also the amount of spin nuclei with a preference for the low energy state increases with B_0 field, leading to a higher polarization at higher static magnetic field.

The difference in energy between the levels corresponds to the energy in the radio frequency (RF) band of the electromagnetic spectrum. Therefore, if a ^{1}H nucleus encounters a radiofrequency wave (B_1 field) with the correct energy, it can interact with the radio wave and flip its state, from up to down, or from down to up. If the radio waves are turned off, the ensemble of nuclei will have absorbed a certain amount of energy and will slowly return to thermal equilibrium. As the nuclei relax back to the original state, they will emit radio waves of similar energy. This process of absorption and radiation of radio waves is the basis of MRI. When first discovered in 1946 (1-2), relatively simple one-pulse experiments were performed, but it has since then evolved to one of the pillars of worldwide diagnostic healthcare and is used in fundamental as well as clinical research.

Sophisticated hardware is required to allow for this absorption and subsequent emission of radio frequency waves in the human body, while in a strong magnetic field. Especially so, since the difference in power between the transmission RF field and the received echo can be as large as 20 orders of magnitude.

The energy difference between these two levels, and therefore the strength of the echo that can be detected, depends on the magnetic field in which the substance is placed. The higher the magnetic field, the larger the energy difference between the states;

$$\omega = \gamma B_0, \tag{1}$$

where ω is the frequency of the RF waves, γ is the gyromagnetic ratio, which is dependent on the nucleus, and B_0 is the strength of the local magnetic field. For 1.5 tesla results in a frequency of 64 MHz, where at 7T the frequency of the RF field is 298 MHz.

1.3.2 Boltzmann equation

In typical MR experiments, a sample of many atoms is studied. Therefore instead of looking at a single nucleus, a large collection (ensemble) of spins must be considered. Therefore, since the chance of a nucleus for being in a spin up or down state is almost equal, the total net magnetization of a sample at room temperature will be low. Only in a very strong magnetic field there is a detectable but small preference for spins to be in the low energy level. Typically in a clinical used MRI scanner of 1.5 tesla and at room temperature, only a surplus of 0.0005% of the ^1H nuclei are in an up state rather than in a down state. The higher the magnetic field, the larger the preference for the low energy state, as is described by the Boltzmann equation,

$$\frac{Na}{Nb} = e^{\frac{dE}{kT}}, \tag{2}$$

where Na/Nb is the ratio between the populations of the energy levels, dE is the energy difference between the up and down state, k is the Boltzmann constant, and T is the temperature of the sample.

Despite the very low number of nuclei that actually contribute to the detected signal, the sensitivity of the measurements is in practice high enough to detect the weak MR signals from inside the human body. As seen from equation 2, if the difference in energy level increases, also the preference for the low energy state will become higher. So at higher magnetic fields, there will be a larger population of spins that contribute to the net magnetization of the sample (M_0); leading to a higher detectable signal.

1.3.3 Spin perturbation

To be able to detect an MR signal, the nuclei will first have to absorb a certain amount of energy from a radiofrequency source. In thermal equilibrium, the net magnetization of a sample will point along the z-axis (Mz), and will not result in any observable signal. If the system is disturbed (excited) and the magnetization is rotated away from the z-axis to the x- or y-axis by an RF pulse, the ensemble of nuclei will relax back to the thermal equilibrium Mz through spin lattice interactions, a process known as T_1 relaxation, which

is in the order of seconds. The observable signal (the free induction decay or FID) decays much faster, since the net magnetization is only observable if all spins show precession with a similar phase (e.g. phase coherence). However, the spins interact due to coupling between the spins through space (dipolar coupling), through chemical bonds (scalar coupling), or chemical exchange. Due these interactions, but also due to tissue inhomogeneity, diffusion etc, the spins in the sample will start to lose their phase coherence after excitation within several milliseconds. This is generally described by an exponential signal decay; T2* relaxation. Some of these sources of signal dephasing can be made undone, for example the local inhomogeneity in magnetic field will cause some spins in the sample to dephase faster than others. By flipping the spins with an RF refocusing pulse, the phase of the spins is inverted, and a spin echo signal is generated after a short delay time (Figure 2). Some of the other sources of signal loss however, cannot be reversed; therefore the intensity of the spin echo decays (T2 decay) with increasing echo time.

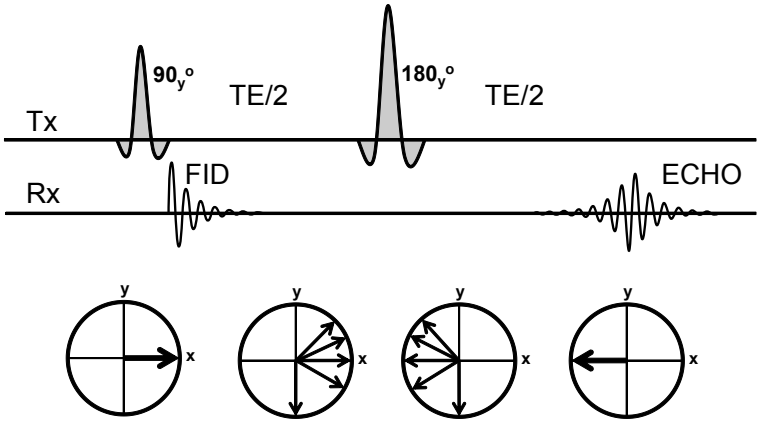

Figure 2. Spin echo generation. After excitation the FID signal decays due to T2 dephasing. After a delay time (TE/2) and a 180 refocusing pulse, the phase of the spins is inverted, leading to a spin echo signal after twice this delay time (TE). The recovered signal has a lower intensity due to irreversible T2 relaxation.*

1.3.4 Chemical shift

Since the energy levels of the nucleus depend on the local magnetic field (equation 1), the relative frequency of the observed signal depends on the local magnetic field at the nucleus, and is generally expressed in parts per million (ppm). This local magnetic field depends on the externally applied magnetic field of the MR scanner, the electron cloud surrounding the nucleus and the chemical bonds of the atom with other atoms. Therefore the energy levels in the nucleus of a ^{1}H-atom in for example an oxygen (OH) bond are slightly different from those in a carbon (CH) bond. Thus, a molecule with a several different chemical bonds will generate a signal at several different frequencies (chemical shifts). And as such,

every molecule has its own fingerprint in the chemical shift spectrum. For example, the CH3 resonance of N-acetyl aspartate resonates at 2.0 ppm, whereas the CH3 resonance of creatine resonates at 3.0 ppm (Figure 3).

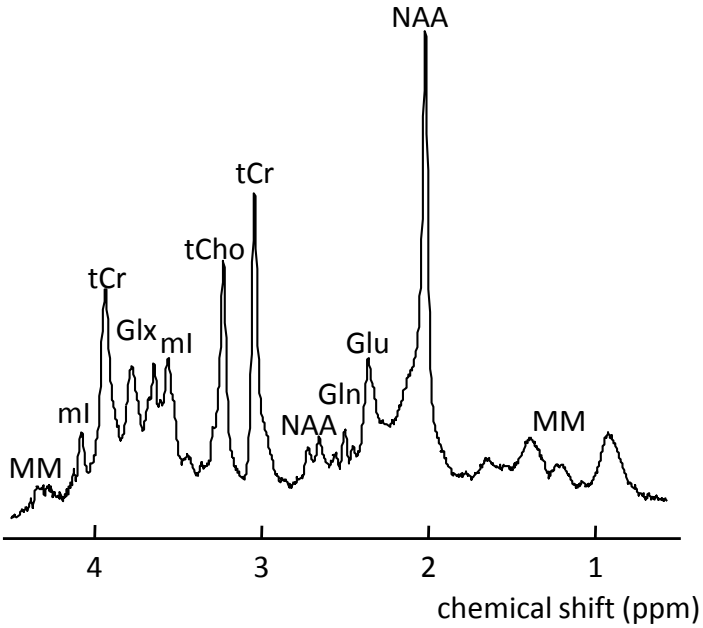

Figure 3. MR spectrum from the human brain at 7T, where several metabolites can be distinguished at high SNR; glutamate (Glu), glutamine (Gln), glutamate+glutamine (Glx) N-acetyl aspartate (NAA), total choline (tCho), total creatine (tCr), myo-inositol (mI) and several macromolecular resonances (MM).

By analyzing the frequency spectrum of the MR signal generated in in tissue, the chemical composition can be deducted, allowing for the study of chemical compounds (e.g. metabolites) in the human body. *In vivo* MR spectroscopy encompasses the study of metabolites by manipulating and studying frequency profiles, mainly of the ^{1}H nuclei but also of any other nucleus that possesses a spin (e.g. ^{31}P, ^{19}F, ^{13}C, ^{16}O etc). At higher static magnetic field, the difference in resonance frequency between individual resonances becomes bigger (equation 1) making it easier to separate resonances which appear close together in the spectrum. For example, the resonances of glutamate and glutamine show significant overlap at 1.5T, where at 7T both molecules can be separately observed.

1.3.5 Localization

Several methods can be applied for obtaining the MR spectrum from a specific region of interest in the human body. The two methods that have been applied in this work are (1) single voxel localization, where three perpendicular slices are used to generate signal from only the overlapping cube and (2) slice selection with chemical shift imaging (CSI), for acquisition of a (multi-slice) 2D dataset consisting of several voxels. By slice selection, only signal from a single slice in space is excited by turning on a magnetic field gradient in combination with an RF frequency pulse with a certain frequency and bandwidth. By changing the carrier frequency, the RF pulse bandwidth or the gradient strength, the slice position and thickness can be varied. However, since different resonances in the MR spectrum have a different frequency, the slice selection is shifted between the metabolites. A severe case is shown in Figure 4 where the slice selected for water and NAA do not show any overlap any more. The NAA signal in a spectrum might be originating from the brain, where the water signal would be generated in a location outside of the head. This will result in the peculiar situation that all resonances in a spectrum can be generated at a different location in the human body.

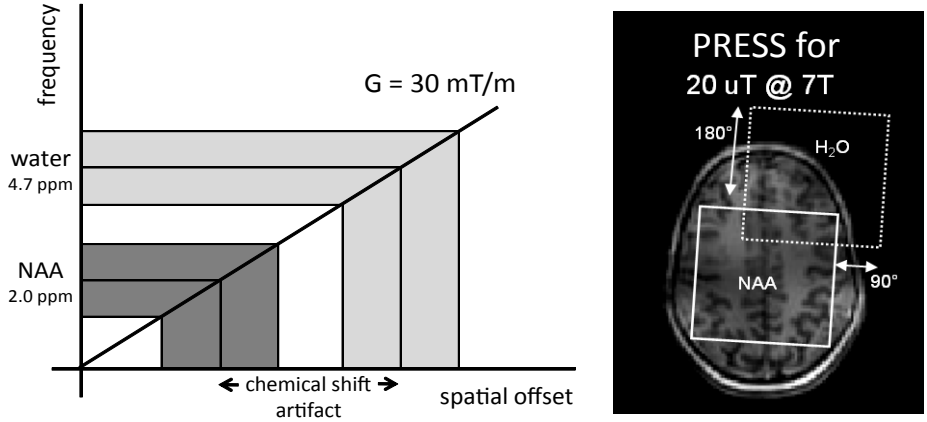

Figure 4. MR slice selection. When a linear gradient is applied in the magnetic field, together with a RF pulse with a specified offset frequency and bandwidth, a slice in space can be excited. However, since different resonances have a different frequency, here depicted with water (4.7 ppm) and NAA (2.0 ppm), the slice for NAA will be excited at a different spatial location than the slice for water. In some cases the NAA signal in a spectrum might be originating from the brain, where the water selection is acquired from a location outside of the head. Especially at high field this effect increases due to the increase in chemical shift dispersion.

To minimize this effect, it is import to maximize the bandwidth of the RF pulses in order to keep the ratio between the chemical shift of the different resonances, and the bandwidth of the pulse as small as possible. Especially for traditional refocusing pulses it is difficult to generate a sufficiently high bandwidth at 7T, since the B_1 fields of a volume coil are not particularly high, while the chemical shift differences between the resonances are enlarged at ultra-high field. In literature, three 90 degree slice selective RF pulses are used to generate a localized stimulated echo (STEAM), which can be employed at ultra-high field, since the bandwidth requirement of these RF pulses is not as demanding as a refocusing pulse. A stimulated echo acquisition comes however at an SNR penalty of 50% compared to obtaining a full echo. High bandwidth refocusing pulses can however be obtained with frequency swept (adiabatic) RF pulses. Particularly when applying RF focusing with a dual-channel transmit setup such a semi Localization with Adiabatic SElective Refocusing sequence (sLASER) can ensure full signal acquisition with a low chemical shift displacement artifact at ultra-high field (Chapter 2).

Alternatively, 2D phase encoding can be used to localize the signal, so that no slice selective refocusing pulses are required. This is explored at high spatial resolution at 7T for single slices in the human brain in Chapter 3 and even in the entire brain using multi-slice techniques in Chapter 4.

1.3.6 Spectral editing; J-coupling

Apart from relaxation, the interaction between spins also causes other phenomena. One particular effect, which is caused by interaction between nuclear spins through chemical bonds, is J-coupling. The magnetic field experienced by a nucleus depends on the state of the nuclear spin of the surrounding atoms. For example, the energy levels of the three (identical) ^{1}H nuclei in the methyl (CH_3) group in the lactate molecule (CH_3-CHOH-COOH) are influenced by the state of the ^{1}H nucleus in the methine (CH) bond. Dependent on whether the methine ^{1}H nucleus is in an up or down state, the methyl ^{1}H nuclei experience a different local magnetic field. Therefore, instead of only an up or down state, there are now more energy levels as both the methine ^{1}H nucleus and the methyl ^{1}H nuclei can each be either up or down, leading to four energy levels and multiple possible transitions between the levels.

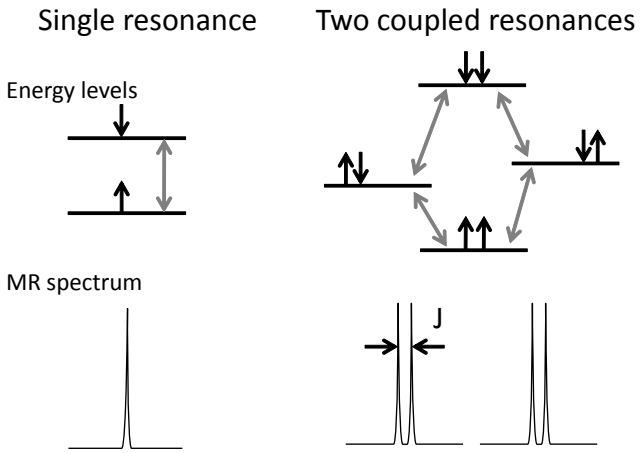

Figure 5. Scalar coupling. On the left the situation for a single resonance is depicted, where only a single transition is possible between the up and down state. On the right, where two spins are present which influence each other, the energy levels in one nucleus become dependent on the state of the other nucleus. Therefore, where one would expect only two resonances from the two nuclei, the J-coupling causes the resonances of both nuclei to split up into four energy levels, where the splitting is dependent on the strength of the interaction (J).

The state of the spins in one group can now be influenced by selectively manipulating the coupling partner. For example, due to the J-coupling, the lactate methyl resonance at 1.3 ppm will show as an inverted doublet at an echo time of 144 ms. Two different experiments can be performed, where in one the J-coupling is allowed to evolve, and in the other experiment the effects of the J-coupling are reverted by an additional selective refocusing pulse on the coupling partner (the methine group). The lactate signal now shows as a negative peak in one experiment, and as a positive peak in the second. By overlapping or subtracting the two spectra, the lactate peak can be distinguished from overlapping signals of other compounds.

A similar approach can be used for the detection of signals from low concentrated molecules that are overlapped by other signals, for instance in the detection of GABA (Chapter 6). As such an approach requires a subtraction technique, the method remains sensitive to instabilities during data acquisition. Therefore, more advanced editing techniques are required when overlapping signals are many orders of magnitude higher, or when severe instability is expected. For instance the detection of lactate in lipid rich environments requires single shot editing techniques.

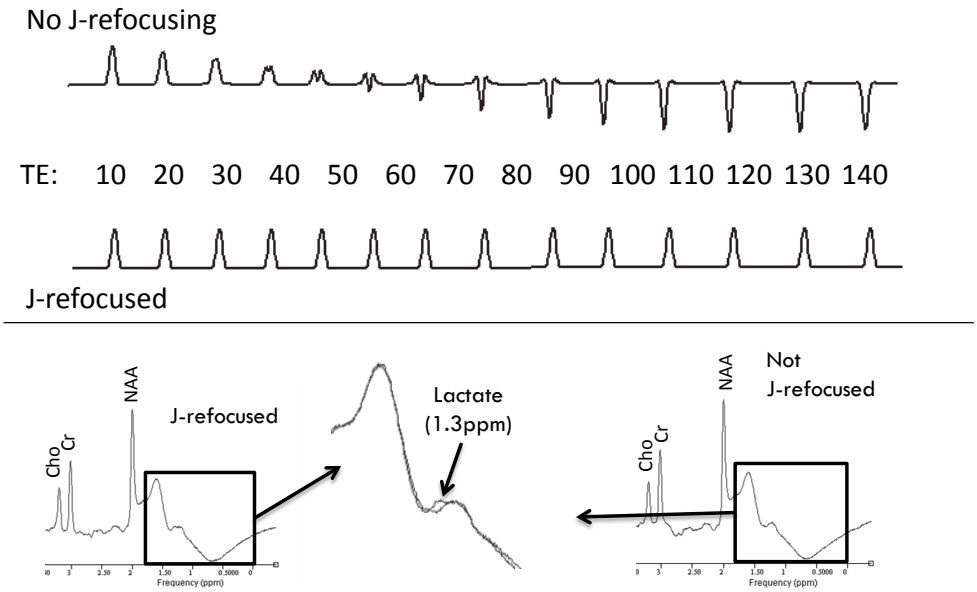

Figure 6. J-difference lactate editing. With longer echo times, the J-evolution causes the doublet lactate signal at 1.3 ppm to dephase (1st row). At an echo time of 144 ms, the signal is fully inverted. When an additional refocusing pulse is used to cancel the J-coupling effects (2nd row) the lactate signal remains upright. By overlapping an in vivo acquisition with and without J-refocusing (bottom) the small lactate signal can be detected despite the relatively large overlapping signals of other molecules.

1.3.7 Multiple quantum filtering

The detection of lactate is clinically relevant, since it is a marker for anaerobic glucose metabolism. This is however complicated due to the relatively low concentration *in vivo*, but also by the overlap of lipid resonances, which might even originate from the same location, as is the case with muscle tissue (3) or in a tumors (4). Therefore frequency selective (Chapter 3), or spatially selective (Chapter 4) lipid suppression is not an option in these cases, where the lipid resonance can be more than 1000× fold higher than the lactate peak. Also subtraction based J-difference editing techniques should not be applied in these cases, as the stability of the measurements *in vivo* are insufficient to overcome the artifacts arising from the 3 orders of magnitude stronger lipid signals. Therefore a different type of J-editing can be performed, the so-called multiple quantum filtering. This is based on the principle that coupled spin systems, such as lactate, can be brought into a double quantum state, where it is twice as sensitive to dephasing gradients, and therefore dephase with twice the gradient area (-2). All overlapping metabolites which do not exhibit J-coupling (e.g. lipids at 1.3 ppm), cannot be converted to double quantum states, and therefore experience only a single dephasing (-1). Afterwards, the lactate is brought back to a single quantum

state, where it is rephased (0) with a double gradient (+2). Therefore, the lactate signal is rephased, where the overlapping signals have experienced (+1) gradient dephasing, and therefore show a large signal reduction. When applied with additional refocusing pulses, up to several thousand fold reduction in overlapping lipids can be reached in this way (Chapter 7).

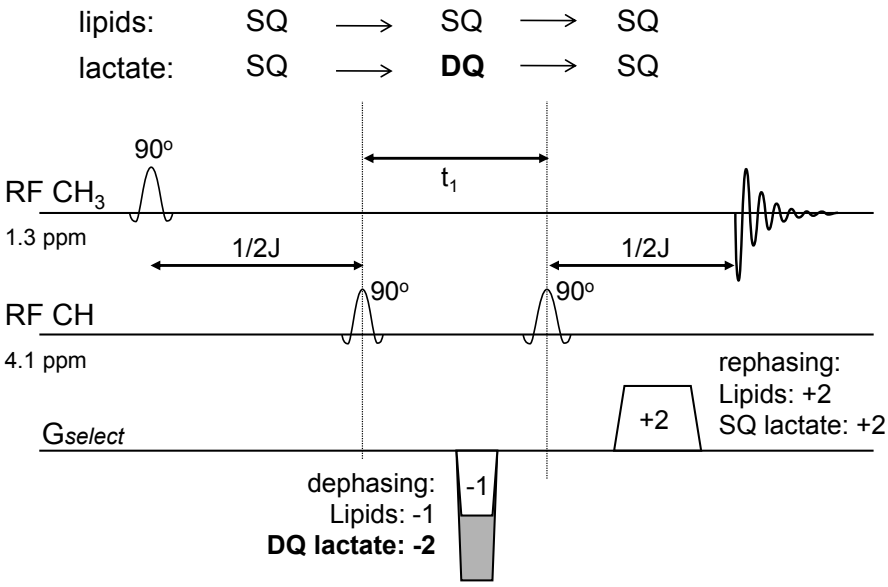

Figure 7. Double quantum filter technique. The J-coupled lactate signal is brought into a double quantum state where it is twice as sensitive to the dephasing gradients. The overlapping lipid signal remains in a single quantum state, and experiences only single dephasing. The lactate is converted back to a single quantum state where it has to be rephased with a double gradient. The lipid signal experiences a spin echo with asymmetric gradients, and is therefore effectively suppressed.

1.3.8 Sensitivity

The sensitivity of MR spectroscopy measurements puts a lower limit on the concentration of the metabolites that can be measured in the human body. Up to 30 metabolites have been detected in the human brain (5), such as choline compounds that are studied in cancer staging and treatment monitoring, or neurotransmitters such as glutamate or GABA that are of interest in studying brain disorders, or lactate or inorganic phosphate in skeletal muscle disorders. However, for MR spectroscopic measurement, the SNR is typically low, since the concentration of these metabolites is several orders of magnitude lower than the water concentration (1-10 mM vs 50 M). Voxel sizes for MR spectroscopy are therefore larger than those often used for MR imaging, where the bulk water is spatially resolved. To compare, current state of the art MRI of the human brain allows voxel volumes of smaller

than 0.1 μL (6), while voxel sizes regarded very small for MR spectroscopy are currently 250 μL (Chapter 3). Ultra-high field MR can provide a novel opportunity to maximize the sensitivity of the MR spectroscopy measurements, since the intrinsic SNR goes up with static magnetic field strength (7-8). MR spectroscopy (9-10), but also gradient echo imaging (11), MR angiography sequences (12-13), and diffusion imaging (14) benefits from the increased signal-to-noise at 7T. Neglecting the relaxation effects, the increase in SNR is approximately linear. The frequency, and therefore induced current in the receiver coil, increases with B_0, and the net magnetization also increases with B_0. If only these two effects were present, this would lead to a quadratic increase in SNR, however, the coil loading and tissue losses also increase with field strength, resulting in an approximately linear dependence of the SNR on field strength.

1.3.9 B_0 inhomogeneity – B_0 shimming

Although the increase in SNR with the static magnetic field strength is beneficial for MR spectroscopy, not everything improves for MR spectroscopy of the human at higher static field. Several technical challenges complicate the use of MR spectroscopy techniques at ultra-high field and, if not accounted for, can lead to severely reduced data quality.

A major challenge at ultra-high field is the disturbance of the homogeneity of the magnetic field. The difference in resonance frequencies between different chemical compounds is typically 6 orders of magnitude lower than the value of the static magnetic field. Therefore the magnetic field inside the MR scanner must be made as homogeneous as possible to be able to discriminate between different metabolites. However, different tissue types have a different magnetic susceptibility, leading to a varying static magnetic field throughout the body. Especially on interfaces of tissue and air, bone or lipids, large jumps in the static magnetic field can occur. Furthermore, these induced inhomogeneities in the magnetic field increase with static magnetic field strength. Therefore at ultra-high field, more effort has to be put on homogenizing the magnetic field, a process known as shimming. Traditionally, several external electromagnetic coils are installed in the magnet bore to generate spatially varying magnetic fields. When the subject is placed into the scanner and the location of interest is determined, the magnetic field homogeneity in this area is measured, and the external magnetic field coils (shim coils) appropriately steered to compensate the local field inhomogeneity. In the 7 tesla systems used in this research, up to third order spherical harmonic shim coils were available; meaning that up to cubic spatial terms can be compensated for. Although shimming is sometimes still considered a 'dark art', recent developments in automated and image based shimming routines allow for reproducible and fast magnetic field optimization. In general for MR spectroscopy, it is a good approach to take the shimming volume only slightly bigger than the region of interest, so that the magnetic field inhomogeneity inside the region of interest can be corrected for as good as possible, as used in Chapter 2. However, if steep second or third order shims are employed on a small region, this will lead to high field offsets

outside this region, complicating the use of frequency selective suppression pulses. As an alternative, a cost function based shimming approach can be applied, where both the homogeneity inside as well as outside the region of interest is taken into account (Chapter 3). The shimming quality can even be taken one step further by optimizing the B_0 magnetic field for several different regions within one scanning sequence, by employing dynamic shimming (Chapter 4).

The B_0 magnetic field also fluctuates over time, causing a variety of artifacts in the experimental data. The major source of temporal B_0 field variation is subject motion as for example caused by breathing and heartbeat. These temporal instabilities can be monitored during a measurement, and can be corrected for in real-time (Chapter 5).

1.3.10 B_1 inhomogeneity – B_1 shimming

Another challenge at ultra-high field is caused by the increased RF frequency, which leads to specific high field problems, due to the fact that the decreased wavelength of the electromagnetic fields for ^{1}H MR at a field strength of 7 tesla is typically smaller than the human body. The higher frequency of the RF leads to severe absorption and wave interference effects in the RF field, resulting in problems with B_1 penetration into the body, and inhomogeneous excitation and reception fields (15). A solution to compensate for the disturbed B_1 fields at ultra-high field can be found in the use of multiple RF coils, where the phase and amplitude of the different elements can be adapted, in order to generate a more homogeneous transmit field in the body (16). This can be applied dynamically, through a slice-by-slice optimization of the B_1 field, which significantly improves the B_1 homogeneity (Chapter 4). Alternatively, the RF energy of several RF transmitters can be applied to a specific area, such as the skull for lipid suppression (Chapter 4) or focused in a single location to boost the local RF field to enable the use of high-bandwidth RF pulses (Chapters 2 and 6).

References

1. Purcell EM, Torrey HC, Pound RV. Resonance Absorption by Nuclear Magnetic Moments in a Solid. Phys Rev 1946;69:37-38.
2. Bloch F, Hansen WW, Packard M. Nuclear Induction. Phys Rev 1946;69:127-127.
3. Torriani M, Townsend E, Thomas BJ, Bredella MA, Ghomi RH, Tseng BS. Lower leg muscle involvement in Duchenne muscular dystrophy: an MR imaging and spectroscopy study. Skeletal Radiol 2011.
4. Delikatny EJ, Chawla S, Leung DJ, Poptani H. MR-visible lipids and the tumor microenvironment. NMR Biomed 2011;24:592-611.
5. de Graaf RA. in Vivo NMR Spectroscopy: Principles and Techniques: John Wiley & Sons Ltd; 2007.
6. Conijn MMA, Geerlings MI, Luijten PR, Zwanenburg JJM, Visser F, Biessels GJ, Hendrikse J. Visualization of cerebral microbleeds with dual-echo T2*-weighted magnetic resonance imaging at 7.0 T. JMRI 2010;32:52-59.
7. Hoult D. The sensitivity of the zeugmatographic experiment involving human samples. Journal of Magnetic Resonance (1969) 1979;34:425-433.
8. Edelstein WA, Glover GH, Hardy CJ, Redington RW. The intrinsic signal-to-noise ratio in NMR imaging. MRM 1986;3:604-618.
9. Tkáć I, Gruetter R. Methodology of ^{1}H NMR spectroscopy of the human brain at very high magnetic fields. Applied Magnetic Resonance 2005;29:139-157.
10. Otazo R, Mueller B, Ugurbil K, Wald L, Posse S. Signal-to-noise ratio and spectral linewidth improvements between 1.5 and 7 Tesla in proton echo-planar spectroscopic imaging. MRM 2006;56:1200-1210.
11. Duyn JH, van Gelderen P, Li T-Q, de Zwart JA, Koretsky AP, Fukunaga M. High-field MRI of brain cortical substructure based on signal phase. PNAS 2007;104:11796-11801.
12. Cho Z-H, Kang C-K, Han J-Y, Kim S-H, Kim K-N, Hong S-M, Park C-W, Kim Y-B. Observation of the Lenticulostriate Arteries in the Human Brain In Vivo Using 7.0T MR Angiography. Stroke 2008;39:1604-1606.
13. Hendrikse J, Zwanenburg JJ, Visser F, Takahara T, Luijten P. Noninvasive Depiction of the Lenticulostriate Arteries with Time-of-Flight MR Angiography at 7.0 T. Cerebrovascular Diseases 2008;26:624-629.
14. Polders DL, Leemans A, Hendrikse J, Donahue MJ, Luijten PR, Hoogduin JM. Signal to noise ratio and uncertainty in diffusion tensor imaging at 1.5, 3.0, and 7.0 Tesla. JMRI 2011;33:1456-1463.
15. Vaughan JT, Garwood M, Collins CM, Liu W, DelaBarre L, Adriany G, Andersen P, Merkle H, Goebel R, Smith MB, Ugurbil K. 7T vs. 4T: RF power, homogeneity, and signal-to-noise comparison in head images. MRM 2001;46:24-30.
16. Van de Moortele P-F, Akgun C, Adriany G, Moeller S, Ritter J, Collins CM, Smith MB, Vaughan JT, Uğurbil K. B1 destructive interferences and spatial phase patterns at 7 T with a head transceiver array coil. MRM 2005;54:1503-1518.

Chapter 2

7T ^{1}H-MRS with adiabatic refocusing at short TE using RF focusing with a dual-channel volume transmit coil

NMR in Biomedicine 2011; 24(9):1038-46

V.O.Boer[1]; A.L.H.M.W. van Lier[2]; J.M. Hoogduin[1]; J.P.Wijnen[1]; P.R.Luijten[1], D.W.J.Klomp[1]

[1]Department of Radiology, UMC Utrecht, the Netherlands
[2]Department of Radiotherapy, UMC Utrecht, the Netherlands

Abstract

In vivo MRS of the human brain at ultra-high field allows for the identification of a large number of metabolites at higher spatial resolutions than currently possible in clinical practice. However, *in vivo* localization of single-voxel spectroscopy has shown to be challenging at ultra-high field due to the low bandwidth of refocusing RF pulses. Thus far, the proposed methods for localized MRS at 7 tesla suffer from long TE, inherent signal loss and/or a large chemical shift displacement artifact that causes a special displacement between resonances, and results in a decreased efficiency in editing sequences. In this work we show that by driving a standard volume coil with two RF amplifiers, focusing the B_1^+ field in a certain location, and using high bandwidth adiabatic refocusing pulses, a semi-LASER localization is feasible at short echo time in the human brain with full signal acquisition and a low chemical shift displacement artifact at 7 tesla.

2.1 Introduction

^{1}H MR spectroscopy (MRS) is a valuable technique to monitor metabolite levels *in vivo*. As the concentrations of the detected metabolites are low, in practice MRS is limited to large detection volumes and long scan times. Using a higher B_0 field strength for human MRI and MRS increases the signal-to-noise ratio, which allows for a shorter acquisition time or a smaller detection volume. Furthermore, the chemical shift dispersion is increased at a higher B_0 field strength, leading to better resolved metabolic information. However, the increased chemical shift dispersion sets a higher demand on the bandwidth of RF pulses that are used in localization schemes for human MRS at ultra-high field. In addition, the available RF power is limited. Using the maximum available RF peak power with a dedicated head coil, still leads to a relatively low B_1^+ field, resulting in long RF pulses with low bandwidth, particularly for refocusing pulses. The consequences are severe spatial misalignment of the metabolic components in the spectrum (1) and decreased efficiency in editing sequences known as the four compartment effect (2,3). Furthermore the long RF pulses lead to long echo times which cause a loss of potentially valuable metabolic information from coupled spin systems and metabolites with a short T2 relaxation time. Several publications have shown how MRS at 7 tesla can be performed at short echo times, mostly with the use of surface coils. These coils allow an increase of the B_1^+ field and thus the RF bandwidth at the cost of a small field of view. For whole brain applications the use of a stimulated echo acquisition mode (STEAM) was promoted (4). The STEAM sequence does not require refocusing pulses, and can therefore be used at short echo time with a limited chemical shift displacement artifact. However, the STEAM sequence comes at a severe penalty on the signal-to-noise ratio (SNR) since only half of the available signal is acquired. To acquire the full signal intensity the spin-echo full-intensity acquired localized (SPECIAL) sequence (5) was proposed, a hybrid sequence that combines a one-dimensional preselection (6) in one direction with a slice selective excitation and refocusing in the other two directions. This allows for full signal acquisition at short echo time, however the necessary subtraction scheme for the preselection is prone to motion artifacts and magnetization transfer effects. With the SPECIAL sequence the chemical shift displacement artifact can be minimized in one direction by using a high bandwidth (BW) adiabatic inversion pulse for the preselection, however a large chemical shift displacement artifact remains present in the direction of the refocusing pulse. To overcome the problems regarding limited refocusing bandwidth, and still acquire the full signal intensity it was proposed to use adiabatic refocusing pulses in a spatially selective adiabatic refocusing (semi-LASER) sequence (7,8). The adiabatic refocusing pulses provide a high bandwidth, but since four refocusing pulses have to be used, this sequence has so far only been applied to the human brain at echo times of 50 ms or more at 7T. (9)

At 7 tesla, the B_1^+ field in the brain as generated by a birdcage volume coil shows significant spatial variation. With a default 90 degree phase difference between the two

feeding points of a birdcage coil, a central brightening is typically seen (10). In single-voxel spectroscopy only a small region of the brain is measured. Therefore the maximum in the B_1^+ field can be steered to this location by driving the two input channels of the volume coil with an appropriate phase. In this work it is shown how, with a standard volume coil for the human brain, the B_1^+ can be focused in a region of interest in the brain, thereby maximizing the transmit efficiency. With the increased B_1^+ it becomes possible to use short adiabatic refocusing pulses. We present a method for a semi-LASER localization with short echo time (TE = 25 ms) and compare the spectral quality with two methods for localization of single-voxel MRS with even shorter echo time: the STEAM (TE = 6 ms) and the SPECIAL (TE = 11 ms) sequence. In the comparison, the bandwidth of all RF pulses was maximized for the available B_1^+ and the shortest possible echo time was used for each sequence. Our results demonstrate that the semi-LASER sequence provides twice the SNR as compared to the STEAM sequence, and similar SNR as compared to the SPECIAL sequence. Moreover, in both comparisons, the semi-LASER localization has a greatly reduced chemical shift displacement artifact.

2.2 Methods

Electromagnetic field simulations were performed to assess the maximal achievable B_1^+ in the human brain and the corresponding 1 gram averaged specific absorption rate (SAR) when the transmit phase of the two channels is optimized for a specific location. The simulations were performed using an in-house implementation of the FDTD (finite-difference time-domain) algorithm (11). The coil was modeled as a birdcage transmit head coil, with properties similar as used for the MR measurements. A dielectric model of the human head (12) was used. The simulations were performed using isotropic voxels with a size of 2.5×2.5×2.5 mm^3, and after 20000 time steps the simulations were terminated and the stability of the simulations checked. The electric (E) and magnetic fields (B) of the two transmit channels were processed by calculating the optimal transmit phase difference between the channels for every voxel in the brain. After this the B_1^+ and the E field of the two channels were combined using this phase difference to find the optimal B_1^+ per location and its corresponding 1 gram averaged SAR.

MR experiments were performed on a 7 tesla whole body MR scanner (Philips, Cleveland, USA). A birdcage transmit head coil (Nova Medical, Inc, Burlington, MA, USA) with two input channels was used in combination with a 16-channel receive coil (Nova Medical, Inc, Burlington, MA, USA). Written informed consent was given by all volunteers prior to the exam, and the study was approved by the local ethical committee.

After selecting the volume of interest, the transmit phase of both channels was optimized to minimize local destructive interferences between the two channels, generating the highest possible B_1^+ field with the available power. The phase between the two transmit channels

was varied while performing a series of single shot, localized B_1^+ measurements (13) on the volume of interest to find the phase setting with optimal constructive interference. The two transmit channels of the volume coil were both driven with a 4 kW RF amplifier. Approximately half of the power was dissipated in the radio frequency (RF) chain, mainly due to cable losses.

The finite bandwidth of RF pulses typically leads to a chemical shift displacement artifact, resulting in a varying spatial origin of the signal, dependent on the resonance frequency of the spins. Bloch simulations to assess the bandwidth (BW) performance were performed using the Matpulse software package (14) in Matlab (The Mathworks Inc., Natick, MA). The chemical shift displacement artifact is reported here as a the percentage of voxel overlap between two resonances with a 1 ppm frequency shift at 7 T,

$$\text{voxel overlap for 1ppm} = \left(1-\frac{298}{BW_{RFx}}\right)\left(1-\frac{298}{BW_{RFy}}\right)\left(1-\frac{298}{BW_{RFz}}\right)\times 100\%,$$

where $BW_{RFx,y,z}$ denotes the bandwidth in Hz of the RF pulse in the x,y,z direction. For example, using a traditional point-resolved spectroscopy (PRESS) sequence with a high BW excitation pulse (4.4 kHz) and two sinc shaped refocusing pulses (BW of 1.2 kHz) gives a 52% voxel overlap for two resonances with 1 ppm frequency difference at 7 T.

The three single-voxel measurements were performed on a volume of 2×2×2 cm^3, and were planned to contain mostly grey matter in the occipital lobe. B_0 field homogenization was performed with an image based shimming algorithm (15) where a measured B_0 field map was used to calculate a 2nd order shim setting on a 2.5×2.5×2.5 cm^3 volume covering the spectroscopy voxel.

To allow for absolute quantification without the need for T_1 corrections (16) a repetition time (TR) of 8 seconds was used, which is approximately 5 times the T_1 value of the singlet of N-acetylaspartate (NAA) at 2.01 ppm at 7 tesla (17). Water suppression was performed using variable-pulse power and optimized relaxation delays (VAPOR) (18). The readout time was 512 ms at a 4 kHz bandwidth. 16 averages were taken, leading to an acquisition time of 128 seconds per spectrum. An acquisition without water suppression (two averages) was performed to estimate the phase and amplitude of the MR signal for a coil sensitivity weighted reconstruction of the data from the 16 receive channels (19) and to apply an eddy current correction.

A semi-LASER sequence (Figure 1a) was implemented with an asymmetric sinc excitation pulse (3.2 ms, BW=4.4 kHz, Figure 2a) and four adiabatic refocusing pulses. The adiabatic refocusing pulses (Figure 2c) consisted of a trapezoid amplitude envelope, with a linear frequency modulation under the constant amplitude part and a quadratic frequency modulation under both ramps, resulting in a smooth frequency sweep from –BW/2 to BW/2. This adiabatic refocusing pulse provides a high bandwidth for a relatively short RF pulse duration. A pulse duration of 3.7 ms was used, providing an 8.2 kHz BW assuming an adiabatic threshold of 24 μT (figure 2).

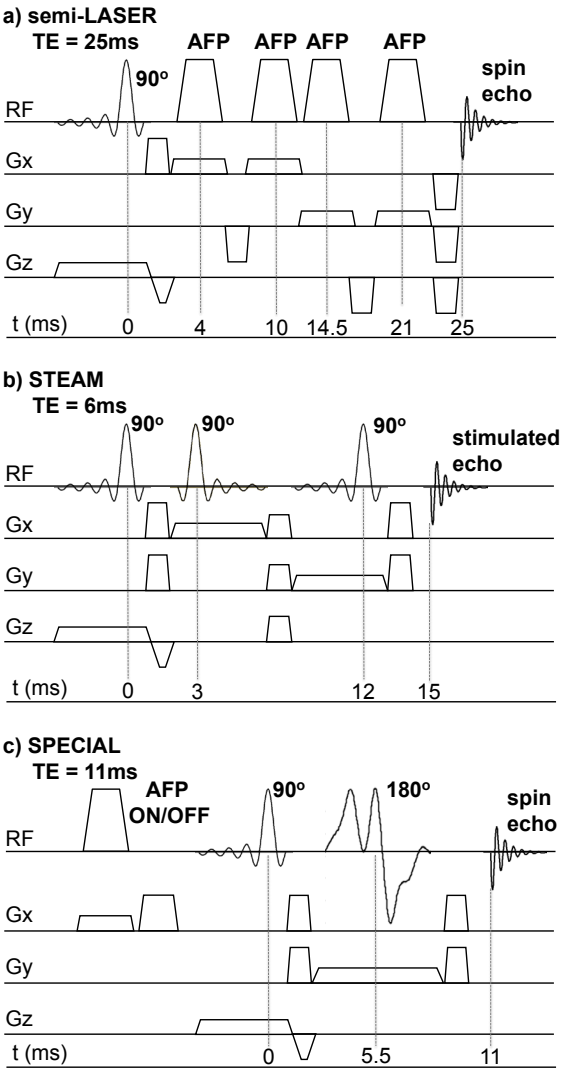

Figure 1. Semi-LASER (a), STEAM (b) and SPECIAL (c) localization sequences that were used in the single-voxel MRS experiments. For the semi-LASER localization the echo time was minimized by using optimized crusher gradients in combination with four short adiabatic refocusing pulses to generate a spin echo at 25 ms echo time. The STEAM sequence consists of three 90° pulses that generate a stimulated echo at 6 ms echo time. The SPECIAL sequence consists of a bar-like volume selection using a slice selective excitation and refocusing pulse. This spin echo is preceded by a slice selective (adiabatic) inversion pulse which is turned on and off in consecutive experiments. Combining the signal of the odd and even results in a volume selection.

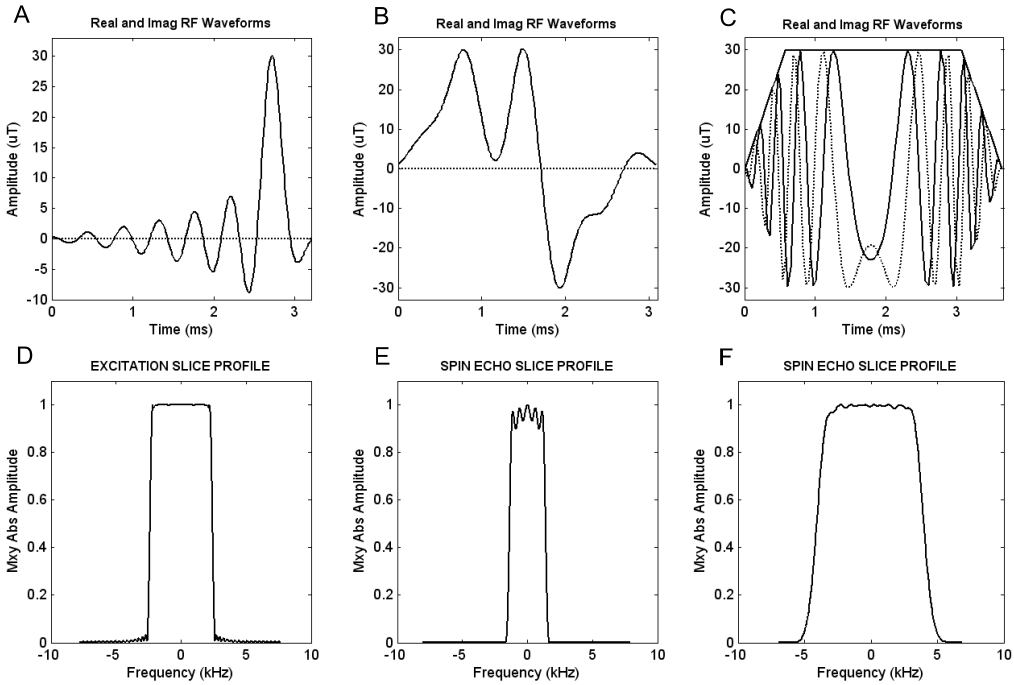

Figure 2. Simulated RF pulse profiles for the three RF pulses that were used in the STEAM, SPECIAL and semi-LASER sequences, simulated for a peak B_1^+ of 30 μT. An asymmetric sinc shaped pulse (A,D) was used for excitation in all sequences. It was also used for refocusing in the STEAM measurement. A numerically optimized, amplitude modulated refocusing pulse (B,E) was used for refocusing in the SPECIAL sequence and a high bandwidth adiabatic refocusing pulse (C,F) was used in the semi-LASER sequence. The adiabatic refocusing pulse clearly provides the highest bandwidth performance with the available B_1^+ and still has a relatively short pulse duration.

The use of high bandwidth adiabatic refocusing pulses in the semi-LASER sequence improves the spatial localization quality, however it also increases the chance of spurious signal generated by the four refocusing pulses. To minimize artifacts from unwanted excitations and spurious echoes generated by the refocusing pulses, care was taken to design gradient spoilers surrounding the refocusing pulses. A combination of minimized crusher gradients and phase cycling (20) was used. The maximum crusher gradient strength of 33 mT/m was used with a duration of 1.6 ms each. To further increase the suppression efficiency while using the shortest possible dephasing gradients, a 16-step phase cycling scheme was implemented, consisting of a 2-step cycle of the excitation pulse (0-180 degrees), a two-step phase cycle of the third refocusing pulse (0-180 degrees) and a four-step phase cycle of the last refocusing pulse (0-90-180-270 degrees).

The duration of the crusher gradients and the four RF pulses led to a minimum echo

time of 25 ms for the semi-LASER sequence. With a single spin echo sequence an echo time of 25 ms would lead to severe signal loss in coupled spin systems (Glutamate (Glu), Glutamine (Gln), myo-Inositol (myo-Ins) etc.) due to the J-coupling evolution. However with a semi-LASER localization part of the J-coupling is refocused for strongly coupled spin systems (21), which results in reduced signal loss at longer echo times. An example is shown in Figure 3, where a simulation of the spectrum of Glutamate is shown for the semi-LASER localization at 25 ms, a spin echo at 25 ms and a spin echo at 11 ms (the shortest echo time for the SPECIAL localization). The signal loss due to J-coupling for the semi-LASER localization at 25 ms is similar to a spin echo at 11 ms. To minimize the signal loss due to J-coupling and T_2 in the experimental comparison between the semi-LASER, the STEAM and the SPECIAL, the shortest possible echo time was used with all sequences and therefore the bandwidth of all RF pulses was maximized.

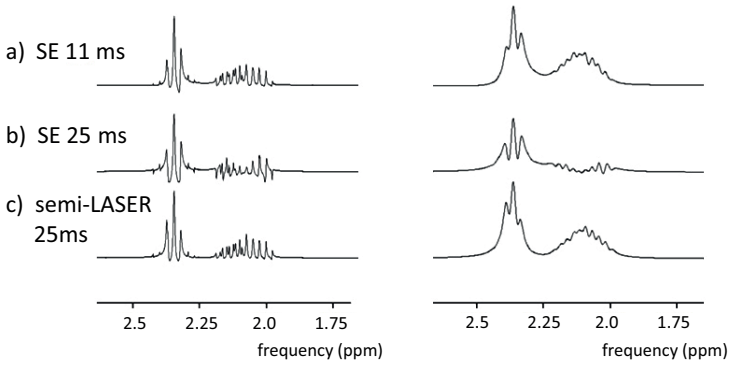

Figure 3: Simulations of the spectral profile of the coupled spin system of Glutamate on the left, line-broadened with 14 Hz to the in vivo situation at the right. A spin echo (SE) at 25 ms echo time with a single refocusing pulse time leads to severe signal loss due to the J-coupling evolution (b), however with the semi-LASER sequence the signal remain in phase(c), and is comparable to the spin echo signal at the shortest echo time of the SPECIAL sequence (a). Note that T2 relaxation has not been considered in these simulations.

A STEAM sequence was used (Figure 1b), consisting of three slice selective asymmetric 90° sinc pulses (3.2 ms, BW=4.4 kHz, B_1^+=30 μT, Figure 2a) resulting in a short echo time of 6 ms.

A SPECIAL localization sequence (Figure 1c) was adapted from Merkle et al. (5). A bar-like excitation was performed by an asymmetric slice selective excitation pulse and a perpendicular slice selective refocusing pulse. For the refocusing a numerically optimized, amplitude modulated pulse was used (3.1 ms, BW = 2.8 kHz, B_1^+=30 μT, Figure 2b) which provided a significantly higher bandwidth compared to a sinc shaped refocusing pulse (1.2 kHz for the same B_1^+ of 30 μT). This bar like volume selection was combined with a perpendicular high bandwidth adiabatic inversion pulse to localize a voxel by adding the signal of experiments with the inversion pulse turned on and off. The inversion pulse was placed in front of the excitation pulse, between the last two water suppression pulses. The

additional inversion pulse was switched on and off in successive measurements to minimize the chance of motion artifacts. An echo time of 11 ms was used with this sequence.

Metabolite quantification for the semi-LASER spectra was performed by calculating the best fit to the spectrum with 16 metabolite model spectra for aspartate (Asp), γ-aminobutyric acid (GABA), Glu, Gln, glutathione (GSH), lactate (Lac), myo-Ins, phosphorylethanolamine (PE), taurine (Tau), Scyllo-Inositol (scyllo-Ins), NAA, N-acetylaspartylglutamate (NAAG), phosphocreatine (PCr), creatine (Cr), phosphocholine (PC) and glycerophosphocholine (GPC) which were generated using NMRSim (v5.2b Bruker Biospin, Billerica, MA) with chemical shifts and coupling constants taken from literature (22). Measurements of the macromolecular (MM) baseline were performed with the semi-LASER sequence, also in the occipital grey matter. The MM signal in the grey matter was measured by nulling of the metabolites with an additional inversion pulse (23) at an inversion time of 1040 ms, where 64 averages were obtained to reduce the noise contribution. This MM spectrum was included as an additional model spectrum for the fitting procedure. Average and standard deviation of the concentration for measurements over five volunteers is reported. Normalization was performed by scaling the tCr concentration to a reference value of 8 mM (5).

2.3 Results

The maximum available B_1^+ field for the available input power after RF phase optimization on a pixel by pixel basis is shown in Figure 4, as well as the optimal phase difference between the two channels and the maximum local 1 gram averaged SAR in the brain for that phase setting for the semi-LASER sequence. The generated B_1^+ field ranges from a low 10 μT in the temporal lobes and the cerebellum to a maximum of 40 μT in the center of the brain. Maximum local SAR values vary from 4 to 6 W/kg for the fixed input power of 2×2 kW (including cable losses) and taking the duty cycle of the semi-LASER sequence into account. The normalized SAR/(B_1^+)2 map (Figure 4e) shows that there is a severe SAR penalty for generating a high B_1^+ field in lower parts of the brain with the current setup. All single-voxel spectroscopy measurements were performed in the occipital grey matter where a measured B_1^+ value of 30 μT (range 28 μT -32 μT over the five volunteers) was reached.

The chemical shift displacement artifact of a traditional PRESS sequence, using sinc shaped RF pulses with a BW of 1.2 kHz, would give a 52% voxel overlap for two resonances with 1 ppm frequency difference at 7 T. Using amplitude modulated pulses, as shown in Figure 2b, improves the bandwidth, and would lead to a voxel overlap of 75% for a 1 ppm frequency difference. The STEAM and the SPECIAL sequences perform better with respectively 81% and 80% voxel overlap where the artifact for the STEAM sequence is uniform in all three directions, but for the SPECIAL is mainly generated by the low BW of the refocusing pulse. The semi-LASER sequence with high bandwidth adiabatic refocusing

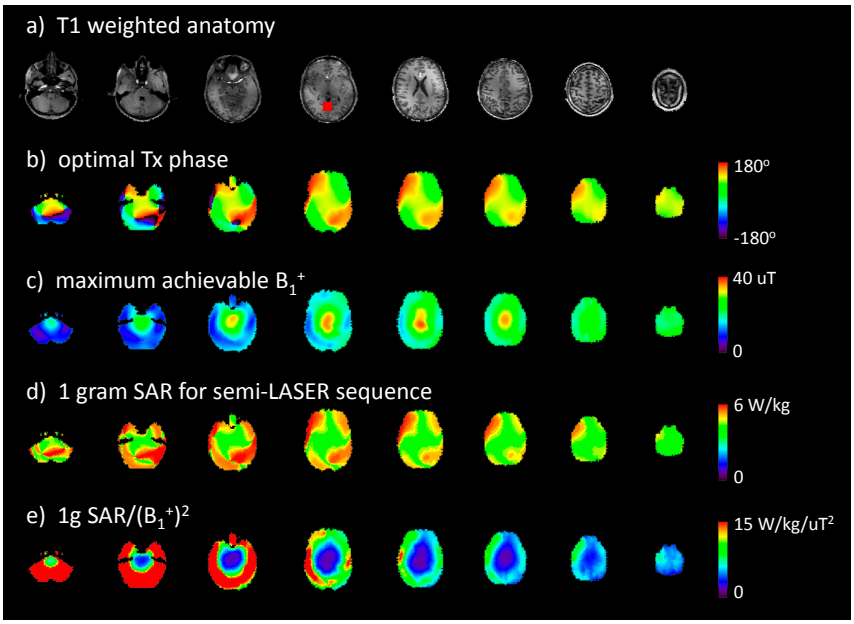

Figure 4. B_1^+ and SAR values as determined by FDTD simulations, an anatomical T_1 scan from a healthy volunteer is shown as a reference, with the location which was used for the MRS indicated in red (a). The optimal pixel by pixel transmit phase setting (b) was determined by calculating the phase difference between the B_1^+ fields of the two channels of the birdcage coil. For a fixed coil input power (2×2 kW) the maximum achievable B_1^+ per voxel was calculated (c) as well as the corresponding maximum local 1 gram averaged SAR value in the brain (d) for the phase optimization for that voxel. Maximum local SAR per unit of $(B_1^+)^2$ (e) shows that regions in the temporal lobes and cerebellum have a high SAR penalty. For these regions stronger RF amplifiers or a more efficient coil setup is desired. All single-voxel MRS measurements were performed in the occipital cortex, corresponding to a B_1^+ of 30 μT and 4.6 W/kg local 1 gram SAR.

in two directions results in the lowest chemical shift displacement artifact and has 87% voxel overlap for resonances with a frequency difference of 1 ppm. Here, the chemical shift displacement artifact is now limited by the bandwidth of the excitation pulse. Figure 5 shows single-voxel measurements in the occipital lobe of a healthy volunteer. The acquisition of the semi-LASER, the STEAM and the SPECIAL sequences were reconstructed in a similar way so that the noise level is equal and peak heights can directly be compared between sequences. The semi-LASER localization results in twice the SNR of the STEAM localization and in similar SNR as the SPECIAL localization. Furthermore the semi-LASER has a higher localization accuracy. Note that despite of the longer echo time of the semi-LASER sequence, the signal level of coupled spin systems like Glu is comparable to that of the shorter echo time measurements. Metabolite fitting results of one semi-

LASER localized spectrum in the occipital grey matter is shown in Figure 6. Metabolite concentrations (averages and standard deviation over five volunteers) are shown in Table 1.

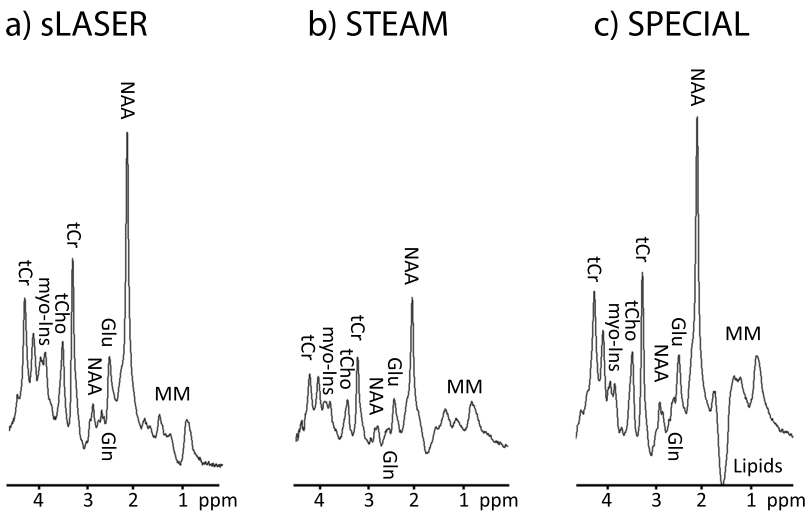

Figure 5. Single-voxel localized spectra (2×2×2 cm³, TE=25 ms, 16 averages) from the occipital lobe in one volunteer. Reconstruction parameters for the three sequences were identical, leading to an equal noise level, so that signal levels can directly be compared. Semi-LASER localization (a) results in twice the SNR of the STEAM localization (b) and in similar SNR as the SPECIAL localization for most metabolites, and a lower baseline due to higher signal loss on the MM. Note that despite of the longer echo time of the semi-LASER sequence, the signal level of coupled spin systems like Glu is comparable due to the inherent J-refocusing of the semi-LASER. Because no additional outer volume suppression was used, lipid artifacts are still visible in the STEAM and SPECIAL sequences. The semi-LASER sequence shows to be less sensitive to signal generated outside of the VOI due to the double refocusing pulses.

2.4 Discussion

The semi-LASER sequence using adiabatic refocusing pulses has shown to be a reliable measurement for single-voxel MR spectroscopy at 7 T. Although traditionally long RF pulses and long crusher gradients had prevented the use of a semi-LASER at short echo time, we have shown in this study that a short echo time of 25 ms can be realized in the human head even when using a conventional volume head coil. As such, MRS with full signal acquisition can be obtained with a small chemical shift displacement artifact at 7T.

A maximized B_1^+ field was generated by independently steering the two transmit channels in a standard volume head coil with two input channels. When B_1^+ homogeneity over larger regions is of importance for MRI or MRSI, more than two transmit elements

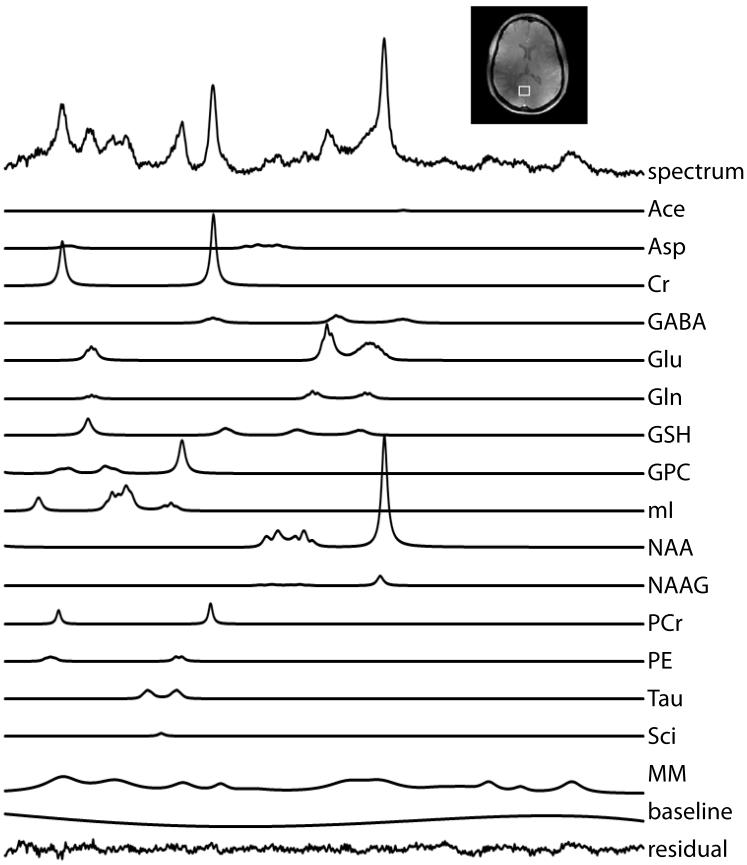

Figure 6. Result of the metabolite fitting for the short echo time semi-LASER sequence (2×2×2 cm^3, TE=25, 16 averages) in the occipital grey matter in a healthy volunteer. The inset shows how the MRS volume was planned in the occipital grey matter.

are necessary at ultra-high field (24,25). However, as single-voxel MRS only focuses on a relatively small ROI, a relatively simple two channel system can be used. With the standard volume coil driven by two 4 kW RF amplifiers, most of the human brain is available for single-voxel MRS examination at B_1^+ levels above 24 μT, including most of the cerebrum and the brain stem, enabling the use of short adiabatic refocusing pulses. For regions in the temporal lobes and the cerebellum however, a very low B_1^+ transmit efficiency is observed (Figure 4c), indicating that either stronger RF amplifiers or a more efficient RF coil is required to obtain similar measurements in these regions.

The SAR was analyzed by calculating the optimal transmit phase for maximum B_1^+ in all voxels of the brain model. Sequentially the maximum local 1 gram averaged SAR in the whole brain was calculated, for the optimal phase setting per pixel, resulting in a 4 to 6 W/kg power deposition for the semi-LASER sequence when using the maximum available RF

Metabolite	Average concentration (mM)	Standard deviation (mM)
Asp	3.5	1.2
GABA	1.4	0.8
Glu	9.2	1.2
Gln	2.0	0.4
GSH	1.3	0.4
Lac	0.3	0.4
myo-Ins	4.8	1.7
PE	1.3	0.6
Tau	2.6	0.4
scyllo-Ins	0.4	0.2
NAA+NAAG	11.8	1.6
Cr+PCr	8.0	-
PC+GPC	1.2	0.4

Table 1: Metabolite concentrations (average and standard deviation over 5 volunteers) for the semi-LASER acquisition in the occipital grey matter. Due to high fitting correlation between NAA and NAAG, PCr and Cr and PC and GPC, the sum of these metabolites is reported.

peak power. This indicates that the TR of 8 seconds could be shortened while remaining within SAR guidelines, particularly in areas with a high B_1^+ transmit efficiency as the RF peak power can be reduced accordingly. However, care must be taken as these SAR values are determined by models, and deviations can occur with the actual patient and MR setup.

The locally increased B_1^+ field allows for the use of short adiabatic pulses, which in combination with optimized gradient crushers lead to a semi-LASER implementation at a short echo time of 25 ms. Since this is longer than the minimal echo time achievable with a STEAM sequence (6 ms), for very short T2 components like the macromolecules a loss in signal intensity was seen, leading to a lower baseline under the metabolite resonances. Signal loss for most metabolites (which have a longer T2 relaxation time compared to the macromolecules) was not observed. Furthermore, for J-coupled spin systems like glutamate the signal loss at a 25 ms echo time is minimal due to the inherent J-coupling refocusing during the adiabatic refocusing pulses.

The experimental SNR of the semi-LASER sequence, as seen from figure 5, was approximately a factor of two higher than that of the STEAM sequence. The SPECIAL sequence shows an SNR level which is comparable to the semi-LASER for most metabolites. The macromolecular signal was highest with the SPECIAL sequence due to a combination of full signal acquisition and a short echo time.

Although not directly visible from the spectra, the chemical shift displacement artifact is a crucial factor in determining the appropriate localization scheme for an MRS study, even more so when editing techniques are being used. If single-voxel measurements of only a single uncoupled resonance are performed, chemical shift displacement artifacts might not be a problem. However if multiple resonances or coupled spin systems are studied it is of importance to acquire the signal of all resonances from the same location. When using a traditional PRESS localization the overlap of the voxels of two resonances with a frequency difference of 1 ppm is only 52%. By using the short adiabatic refocusing pulses in a semi-LASER sequence this overlap value can be improved to 87%, allowing for single-voxel spectroscopy with a high spatial correlation between the measured resonances. Furthermore, this opens the possibility to use editing techniques on coupled spin systems, which is not possible with a low spatial overlap between coupled resonances (2). In fact, with the reduced chemical shift displacement artifact of the semi-LASER sequence, the efficiency and spatial accuracy of editing techniques are expected to improve substantially considering that this displacement extends to four compartments. The relatively short duration of the localization scheme leaves room for long and very selective editing pulses, essential to some editing sequences as was shown for prostate MRS at 7T (26). Therefore, the use of accurate editing techniques therefore becomes possible at 7 T with the semi-LASER localization that provides full signal acquisition, a low chemical shift displacement artifact and echo times ≥ 25ms.

Residual lipid signals were regularly seen with the STEAM and SPECIAL sequence. They can however be suppressed by using additional outer volume suppression pulses (27). In the SPECIAL sequence the artifact was even more pronounced since small phase differences between the two averages, caused by involuntary motion or system instability, ended up as large subtraction errors of the odd and even scans. Even with the large voxel used in this study, the signal in the individual scans was a factor of 10 higher than the subtracted signal, Therefore magnetization transfer effects or motion artifacts lead to a degraded spectral quality, as seen from the residual lipid signals in figure 5. This however could be prevented, at least to some extent, by using additional outer volume suppression pulses. The semi-LASER localization showed to be much less sensitive to extra cranial lipid contaminations due to the double selection in two of the three directions and resulted in good spectral quality without the use of additional outer volume suppression in most volunteers. Some spectra however still show a slight modulation in the area around the lipid resonance. This resulted in an unreliable quantification of lactate (table 1), and could also be a source of variation in the quantification results for the other metabolites. To reduce this source of variation, especially for lactate quantification, the signal of residual lipid contaminations could be further reduced by using two additional outer volume suppression pulses in the slice selection direction since the selectivity of the excitation pulse in the semi-LASER localization is far inferior to that of the double high BW-adiabatic refocusing pulses. In conclusion, single-voxel semi-LASER localization at short echo time at 7 tesla is possible with a two channel birdcage coil, each driven with a 4 kW amplifier. Since the semi-LASER

sequence provides twice the SNR compared to the STEAM sequence, is less prone to motion artifacts compared to the SPECIAL sequence and has the lowest chemical shift displacement artifact, the semi-LASER sequence is a good candidate for studying *in vivo* metabolism, particularly at high fields.

2.5 Acknowledgements

The authors thank David Foxall from Philips Medical Systems for providing the adiabatic refocusing pulse and the Dutch technology foundation (STW, NIG-10882) and the Dutch scientific organization (NWO, VENI-DK) for financial support.

References

1. Kaiser LG, Young K, Matson GB. Numerical simulations of localized high field 1H MR spectroscopy. J Magn Reson 2008;195:67-75.
2. Lange T, Dydak U, Roberts TPL, Rowley HA, Bjeljac M, Boesiger P. Pitfalls in lactate measurements at 3T. AJNR Am J Neuroradiol 2006;27:895-901.
3. Kaiser LG, Young K, Meyerhoff DJ, Mueller SG, Matson GB. A detailed analysis of localized J-difference GABA editing: theoretical and experimental study at 4 T. NMR Biomed 2008;21:22-32.
4. Tkáč I, Andersen P, Adriany G, Merkle H, Ugurbil K, Gruetter R. In vivo 1H NMR spectroscopy of the human brain at 7 T. Magn Reson Med 2001;46:451-6.
5. Mekle R, Mlynárik V, Gambarota G, Hergt M, Krueger G, Gruetter R. MR spectroscopy of the human brain with enhanced signal intensity at ultrashort echo times on a clinical platform at 3T and 7T. Magn Reson Med 2009;61:1279-1285.
6. Ordidge RJ, Connelly A, Lohman JAB. Image-selected in Vivo spectroscopy (ISIS). A new technique for spatially selective nmr spectroscopy. J Magn Reson 1986;66:283-294.
7. Garwood M, DelaBarre L. The return of the frequency sweep: designing adiabatic pulses for contemporary NMR. J Magn Reson 2001;153:155-177.
8. Scheenen TWJ, Klomp DWJ, Wijnen JP, Heerschap A. Short echo time 1H-MRSI of the human brain at 3T with minimal chemical shift displacement errors using adiabatic refocusing pulses. Magn Reson Med 2008;59:1-6.
9. Scheenen TWJ, Heerschap A, Klomp DWJ. Towards 1H-MRSI of the human brain at 7T with slice-selective adiabatic refocusing pulses. MAGMA 2008;21:95-101.
10. Vaughan JT, Garwood M, Collins CM, Liu W, DelaBarre L, Adriany G, Andersen P, Merkle H, Goebel R, Smith MB, Ugurbil K. 7T vs. 4T: RF power, homogeneity, and signal-to-noise comparison in head images. Magn Reson Med 2001;46:24-30.
11. Van De Kamer JB, De Leeuw AAC, Hornsleth SN, Kroeze H, Kotte ANTJ, Lagendijk JJW. Development of a regional hyperthermia treatment planning system. International Journal of Hyperthermia 2001;17:207.
12. Van Leeuwen GM, Lagendijk JJ, Van Leersum BJ, Zwamborn AP, Hornsleth SN, Kotte AN. Calculation of change in brain temperatures due to exposure to a mobile phone. Phys Med Biol 1999;44:2367-2379.
13. Versluis MJ, Kan HE, Buchem MAV, Webb AG. Improved signal to noise in proton spectroscopy of the human calf muscle at 7 T using localized B1 calibration. Magn Reson Med 2010;61:207-211.
14. Matson GB. An integrated program for amplitude-modulated RF pulse generation and re-mapping with shaped gradients. Magn Reson Imaging 1994;12:1205-1225.
15. Schär M, Kozerke S, Fischer SE, Boesiger P. Cardiac SSFP imaging at 3 Tesla. Magn Reson Med 2004;51:799-806.

16. Jansen JFA, Backes WH, Nicolay K, Kooi ME. 1H MR spectroscopy of the brain: absolute quantification of metabolites. Radiology 2006;240:318-332.
17. Otazo R, Mueller B, Ugurbil K, Wald L, Posse S. Signal-to-noise ratio and spectral linewidth improvements between 1.5 and 7 Tesla in proton echo-planar spectroscopic imaging. Magn Reson Med 2006;56:1200-1210.
18. Tkáč I, Starcuk Z, Choi IY, Gruetter R. In vivo 1H NMR spectroscopy of rat brain at 1 ms echo time. Magn Reson Med 1999;41:649-656.
19. Natt O, Bezkorovaynyy V, Michaelis T, Frahm J. Use of phased array coils for a determination of absolute metabolite concentrations. Magn Reson Med 2005;53:3-8.
20. Hennig J. The application of phase rotation for localized in Vivo proton spectroscopy with short echo times. J Magn Reson 1992;96:40-49.
21. Thompson RB, Allen PS. Sources of variability in the response of coupled spins to the PRESS sequence and their potential impact on metabolite quantification. Magn Reson Med 1999;41:1162-1169.
22. Govindaraju V, Young K, Maudsley AA. Proton NMR chemical shifts and coupling constants for brain metabolites. NMR Biomed 2000;13:129-53.
23. Behar KL, Rothman DL, Spencer DD, Petroff OA. Analysis of macromolecule resonances in 1H NMR spectra of human brain. Magn Reson Med 1994;32:294-302.
24. Hetherington HP, Avdievich NI, Kuznetsov AM, Pan JW. RF shimming for spectroscopic localization in the human brain at 7 T. Magn Reson Med 2010;63:9-19.
25. Mao W, Smith MB, Collins CM. Exploring the limits of RF shimming for high-field MRI of the human head. Magn Reson Med 2006;56:918-922.
26. Klomp DWJ, Scheenen TWJ, Arteaga CS, van Asten J, Boer VO, Luijten PR. Detection of fully refocused polyamine spins in prostate cancer at 7 T. NMR Biomed 2011; 24(3) 299-306
27. Tkáč I, Gruetter R. Methodology of 1H NMR Spectroscopy of the Human Brain at Very High Magnetic Fields. Appl Magn Reson 2005;29:139-157.

Chapter 3

High field MR spectroscopy of the human brain at short TE and TR

NMR in Biomedicine 2011; 24(9):1081-8

Vincent O. Boer[1], Jeroen C.W. Siero[1], Hans Hoogduin[1], Jetse S. van Gorp[1,2], Peter R. Luijten[1], Dennis W.J. Klomp[1]

[1]*Department of Radiology, UMC Utrecht, the Netherlands*
[2]*Laboratory of Biophysics, Department of Agrotechnology and Food Sciences, Wageningen University and Research Center, The Netherlands*

Abstract

In vivo MRS of the human brain at 7 tesla allows identification of a large number of metabolites at higher spatial resolutions than currently possible at lower field strengths. However, several challenges complicate *in vivo* localization and artifact suppression in MRS at high spatial resolution within a clinically feasible scantime at 7 tesla. Published MRS sequences at 7 tesla suffer from long echo times, inherent SNR loss, large chemical shift displacement artifacts or long repetition times due to excessive RF power deposition. In this work a pulse-acquire sequence was used that does not suffer from these high field drawbacks. A slice selective excitation combined with high resolution chemical shift imaging for in-plane localization was used to limit chemical shift displacement artifacts. The pulse-acquire approach resulted in a very short echo time of 1.4 ms. A cost function guided shimming algorithm was developed to constrain frequency offsets in the excited slice, therefore adiabatic frequency selective suppression could be employed to minimize artifacts from high intensity lipids and water signals in the excited slice. The high sensitivity at a TR of 1 second was demonstrated both on a supraventricular slice as well as in an area very close to the skull in the frontal cortex at a nominal spatial resolution of 0.25 cc within a feasible scantime.

3.1 Introduction

^{1}H-MR spectroscopy (^{1}H-MRS) is an attractive method to non-invasively obtain information of metabolite contents in the human brain. Many applications of MRS have found their way into clinical research fields such as multiple sclerosis, epilepsy, Parkinson's disease, psychiatry and oncology (1-3).

The advantages of moving to a high static magnetic field are twofold. For one chemical shift dispersion increases with field strength leading to a decreased overlap between metabolite resonances, which enables the unambiguous identification of metabolites at higher accuracy (4).

Secondly the gain in signal-to-noise ratio (SNR) permits more sensitive MRS or an increased spatial resolution when the gain in SNR is exchanged for a reduction in voxel size. Several publications have shown promising results for *in vivo* high field (≥7T) MRS, however the combination of a high spectral and a high spatial resolution within a reasonable scan time has not fully been exploited for human high field MRS. In this work we present a method where high metabolic information content at high spatial resolution is acquired at 7 tesla within a clinically feasible scantime.

Traditional localization techniques employed at high field for human brain ^{1}H-MRS exhibit several drawbacks due to the limited RF peak power, increased chemical shift dispersion and specific absorption rate (SAR) limits. Therefore traditional MRS sequences suffer from long echo times, large chemical shift displacement artifacts, inherent SNR loss and/or long repetition times due to SAR safety limits. A long echo time is unfavorable since it leads to severe signal loss due to both T_2 relaxation and J-coupling evolution for coupled spin systems. Large chemical shift displacement artifacts are encountered when using slice selective excitation and refocusing with low bandwidth RF pulses leading to spatial misregistration of spins at different chemical shifts. Especially with the limited RF peak power (10-20 μT) and increased chemical shift dispersion at high field this can lead to unacceptably large voxel displacements between resonances (5). Furthermore the use of many RF pulses in outer volume suppression (OVS), water suppression and localization leads to a high RF power deposition per unit of time. Then, to remain within SAR safety limits, long repetition times have to be used leading to reduced SNR within a given scan time.

Several recent publications have countered a number of these challenges for human ^{1}H-MRS at 7 tesla, however none of them show to cope with all the restrictions, within a reasonable scan time. To be able to reliably detect a large number of metabolites at a short echo time Tkać et al have proposed the use of a local transmit/receive coil (6). The high local B_1^+ field enables the use of high bandwidth RF pulses and therefore a reduced chemical shift displacement artifact. In combination with the stimulated acquisition mode (STEAM) localization a short echo time of 6 ms can be obtained leading to reliable detection of many metabolites including J-coupled spin systems like glutamate and

glutamine. However, the stimulated echo approach inherently causes a factor of two loss in SNR. Therefore alternative methods to acquire the full signal intensity have been proposed: the localized by adiabatic selective refocusing (LASER) sequence (5) and the spin echo full intensity acquired localized (SPECIAL) sequence (7). Although the LASER sequence reduces chemical shift displacement artifacts substantially it suffers from a relatively long echo time whereas the SPECIAL sequence has a shorter echo time, but here a large chemical shift displacement artifact remains present in the refocusing direction. Also, the SPECIAL sequence requires full relaxation of the signal for a proper subtraction scheme in the localization. Furthermore the requirement of a high B_1^+ field for these sequences by using local coils limits the use to the surface of the head. To counter these high field related problems it was proposed to move away from slice selective refocusing and use the free induction decay localized by OVS (FIDLOVS) (8). Since there is no slice selective refocusing, the chemical shift displacement artifacts are minimal, and because it is a pulse-acquire method with a delayed acquisition of 6 ms, the J-coupling evolution is comparable to short echo time spin echo methods. For simplicity, we refer to the acquisition delay time as echo time (as it is an echo formed by gradient rewinding). However, as all other published methods the FIDLOVS sequence remains limited by SAR restrictions due to high RF power deposition in the OVS scheme, leading to a long repetition time (≥5 seconds) and thus a long inherent scantime. The use of long repetition times can be essential to reduce T_1 effects in absolute quantification (9); however an optimal SNR per unit of time is available at shorter repetition times. Here we present an alternative for the suppression of signals outside the region of interest that can be used at low RF power deposition. A method is proposed that is no longer hampered by long repetition times, signal loss due to either long echo times or a stimulated acquisition nor by chemical shift displacement, even with the use of a volume coil.

In general, the SAR demanding OVS is used in combination with spatial selective RF-pulses for localization in order to minimize signals generated outside the area of interest. Signal originating from these off-resonance regions such as subcutaneous lipids can cause baseline distortions in a large spectral range and hamper detection of the resonances of interest. However, by minimizing the global off-resonance effects by B_0 shimming, artifacts can be suppressed by low power frequency selective sequences (10). In this case OVS and slice selective refocusing may be omitted to reduce echo time and repetition time and therefore maximize SNR per unit time.

In this work we show the use of a cost function guided shimming algorithm to simultaneously minimize the linewidth in an ROI and maximize global B_0 homogeneity, enabling the effective use of frequency selective suppression of water and lipid signals at low RF power deposition at 7T. Combined with a slice selective pulse acquire CSI sequence, artifact free spectra can be obtained from an ROI placed in the human brain, at full signal intensity, with very short echo time, excluding substantial chemical shift displacement artifacts and without the need for OVS or full RF-localization schemes. The repetition time could therefore be minimized to 1 second leading to a maximized SNR, allowing an

increased spatial resolution for high field MR spectroscopy within a clinically feasible scan time.

3.2 Methods

Experiments were performed on a 7 tesla whole body MR scanner (Philips, Cleveland, USA). A birdcage transmit head coil was used in combination with a 16-channel receive coil (Nova Medical, Inc, Burlington, MA, USA). Written informed consent was given by all 8 volunteers prior to the exam. T_1 weighted anatomical images were obtained from all volunteers on which the slice of interest for the spectroscopy study was positioned. To demonstrate the versatility of the method, MR spectra were obtained both from a supraventricular slice in the middle of the brain as well as from a region in the frontal lobe close to the skull.

In order to control both local and global frequency offsets (ΔB_0) in the excited slice, an imaged based shimming approach was employed where an acquired B_0 field map was used in a shimming algorithm. Instead of conventional least squares minimization of the variation of the B_0 distribution in a small region of interest (ROI), a tailored cost function was constructed to compute the optimal shim settings (11). The cost function incorporates both the frequency variations inside a user-defined ROI, but also takes into account the frequency offsets outside the ROI by minimizing the number of voxels with a large frequency offset in the complete slice. The separation of water (4.7 ppm) and lipid (1.3 ppm) resonances from the nearest peaks of metabolites (4.1 ppm and 1.9 ppm, respectively) is approximately 0.6 ppm, hence the maximal allowed ΔB_0 outside the ROI was set to 180 Hz (i.e. 0.6 ppm at 7T). The cost function therefore included a term with the amount of voxels that have an offset of more than 180 Hz in order to limit the B_0 offset outside the ROI. The condition for the B_0 distribution inside the ROI was to have a minimal standard deviation to warrant a narrow spectral linewidth. In formula, the cost function C_{st} to be minimized by the algorithm was:

$$C_{st} = \sigma_{ROI} + N_{180Hz}, \qquad (1)$$

where σ_{ROI} denotes the standard deviation of the B_0 distribution inside the ROI, and N_{180Hz} is the number of B_0 field map voxels, expressed as a percentage, outside the ROI which deviate more than 180 Hz from the mean B_0 inside the ROI.

The shimming was performed in the following steps. Prior to the spectroscopy exam a B_0 field map was acquired using a 3D dual gradient echo sequence (TR = 17 ms, TE = 2.0 ms, ΔTE = 1.0 ms, FA = 13°, T_{acq} = 0.5 min, 15 slices, voxelsize = 3×3×3mm^3). The field map was masked using a 10% intensity threshold on the magnitude image and was subsequently phase unwrapped (12). An ROI of 30×30×20mm^3 was drawn onto the field map. Cost

function guided shimming calculations were performed in Matlab (The Mathworks Inc., Natick, MA) A constrained nonlinear optimization algorithm (fmincon) (13) was used to find the shim coefficients which minimize the cost functionwithin hardware shim current limits (14). The algorithm optimized up to 3rd order shim fields which were available on the MR system. The computed optimal shim currents were ported back to the acquisition software. Applying the calculated currents to the high order shim coils inevitably leads to additional contaminating fields, known as shim impurities (15). These impurities can be modeled as additional spherical harmonic terms and were measured in a 2nd B_0 map. As the higher order shims contained substantial lower order impurities, the minimization routine was performed again on an acquired B_0 map to calculate a compensation for the second and first order impurities generated by the third order shims. Finally the procedure was repeated for a third time, applying only linear shim terms.

With this shimming approach the variations in frequency of water and fat resonances in the excited slice were minimized, therefore artifacts originating from the high intensity subcutaneous lipids were confined to a limited bandwidth around the lipid frequency. Similar reasoning applies to the water signal coming from off-resonance regions. To determine if these high intensity lipids can generate artifacts in other spatial regions due to inaccuracy in the localization, simulations were performed to determine the effect of the spatial response function of the CSI sampling method. The use of a Hamming filter (16) to improve the spatial response function was analyzed. Matrix sizes from 8×8 to 32×32 were reconstructed to investigate the effect of the spatial resolution on the localization accuracy. In addition, spectroscopic imaging (CSI) measurements were obtained and the residual lipid signals were analyzed over the entire slice by integrated the spectral range from 1.9 to 0.9 ppm. Integration maps are visualized as a color map over the anatomical slice to illustrate regions with potential lipid artifacts.

Highly effective water suppression in the homogeneous ROI is required for only a narrow bandwidth, but also a reasonably effective and broadband suppression on both water and lipid is required for the complete slice. Simultaneous adiabatic water and lipid suppression was achieved by using a variation on the sequence for water suppression with adiabatic modulated pulses (SWAMP) (17). The original SWAMP method uses only single slopes of four sequential adiabatic full passage (AFP) pulses as adiabatic excitations for suppression of the water signal, here both slopes of the AFP pulses were used to generate a dual band adiabatic excitation which was set around the water and lipid resonance to achieve simultaneous adiabatic water and lipid suppression. Furthermore two AFP pulses were employed where the carrier frequency and bandwidth of these two pulses were optimized to broaden the excitation bands.

A slice selective pulse-acquire sequence was used (figure 1) consisting of an asymmetric excitation pulse with a nominal flip angle of 67 degrees, the Ernst angle (18) for a T_1 of 1500 ms (average T_1 (19) of metabolites of interest), and a repetition time of 1 second. By using the maximum B_1^+ of 20 μT of the volume transmit coil and a slice thickness of 10 mm the chemical shift displacement error during the excitation was minimized to 0.66 mm/

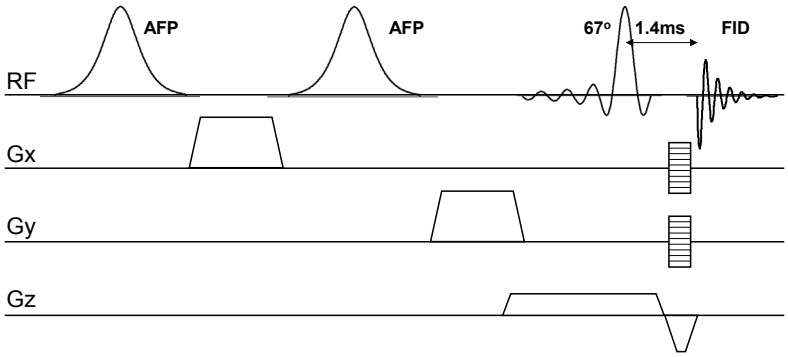

Figure 1: RF pulse sequence consisting of two AFP pulses for simultaneous water and lipid suppression followed by a pulse-acquire CSI sequence to generate a (gradient) echo at 1.4 ms echo time.

ppm. Localization in the in-plane directions was performed with chemical shift imaging (matrix 32×32) to achieve a nominal spatial resolution of 5×5×10 mm^3. A Hamming filter (16) was used to optimize the spatial response function and minimize crosstalk between voxels resulting in an effective voxel volume of 0.42 ml. Hamming weighted acquisition (16) was employed where the center of k-space is acquired once, resulting in a scan time of 12 minutes, or was acquired 6 times, resulting in a scan time of 28 minutes. The repetition time was set to 1 second.

The FID-signal was sampled with an echo time of 1.41 ms (i.e. 0.41 ms delay of the RF pulse and 1.00 ms of the phase encoding and slice refocusing gradients). The signal was sampled at a bandwidth of 4 kHz, 512ms readout time. The linear phase on the spectra caused by the delayed acquisition was compensated for in post-processing (8).

To generate a calibration signal for coil summation and a reference for quantification a fast acquisition of the water signal was performed at identical spatial resolution. The sampling time was reduced to 64 ms at a bandwidth of 4 kHz. The nominal flip angle was lowered to 1 degree to prevent saturation. By omitting the water and lipid suppression pulses the TR for this scan could be shortened to 69 ms leading to a scan duration of 56 seconds for a complete water reference file.

Complementary a B_1^+ map (20) was acquired to correct for spatial variation of the flip angle (3D FFE, TR1/TR2 = 25/125 ms, TE = 3 ms, matrix = 68×45×9, nominal FA = 20°, voxelsize = 3×3×4 mm, T_{acq} = 1.2 min).

Spectra were reconstructed from the 16 receive channels with complex weighting factors calculated from the water reference file (21). Hankel-Lanczos singular value decomposition (HLSVD) filtering (22) of residual water signal and sequential phasing of the signal, with the known first order phase and a user defined zero order phase, was performed in jMRUI (23).

In order to estimate the metabolite concentrations, LCModel based software was used

for metabolite fitting. Metabolite basis sets were simulated using the GAVA software package (24). The first 1.41 ms of the FID of the basis sets was truncated to include effects from the slight acquisition delay into the basis sets (8).

Due to the short TR the spectra become T_1 weighted, therefore instead of absolute concentrations, only apparent concentrations at the given repetition time can be reported.

The short TR also has an effect on the metabolite basis sets. For instance in the creatine molecule, the methylene resonance (3.9 ppm) has a shorter T_1 relaxation time compared to the methyl resonance (3.0 ppm). Therefore the ratio of the two creatine peaks in a steady state is different from the ratio in the fully relaxed state. In the fitting procedure this was resolved by fitting creatine with two singlets. For the remaining compounds, the difference in T_1 values is assumed to be constant at 1.5s. An estimation of the metabolite concentrations was made for the used repetition time from the ratio of the metabolite signal intensity with intensity of the water peak after multiplication with a correction factor *C* to correct for the steady state signal

$$C = \frac{\sin(\alpha_w)}{\sin(\alpha_m)} \frac{1 - E_{1w}}{1 - \cos(\alpha_w)E_{1w}} \frac{1 - \cos(\alpha_m)E_{1m}}{1 - E_{1m}}, \qquad (2)$$

where subscript *m* and *w* denote the metabolite and water scan respectively, α is the flip angle and E1 is defined as $e^{-TR/T1}$. A brain water content of 80% was assumed for grey matter.

The macromolecular (MM) baseline was measured in an additional inversion recovery experiment and used as an additional basis set in the LCModel fit (4). Identical scan parameters were used, apart from an additional inversion pulse to null signal from the

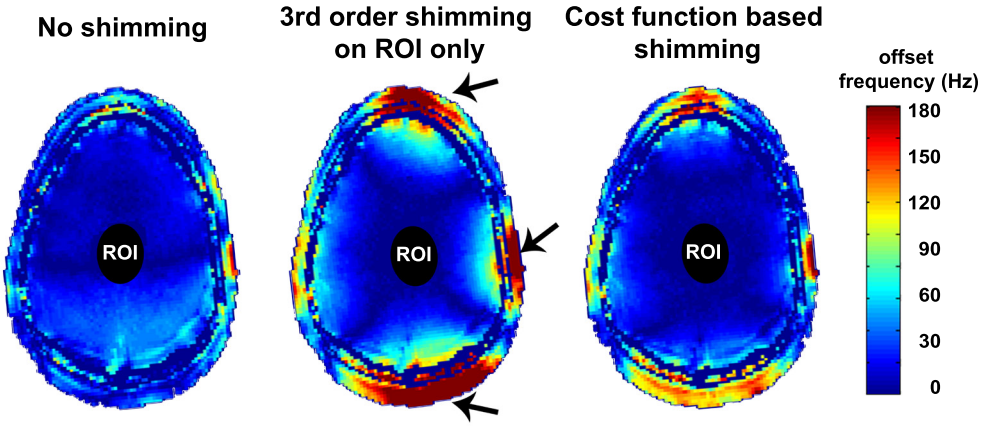

Figure 2: B_0 field maps without shimming (left), with shimming on the ROI only (middle) and with a cost function guided algorithm (right) where both the linewidth in the ROI and the frequency offsets in the slice are minimized. Note the strong off resonance areas outside the ROI (indicated by the arrows) that are substantially reduced by cost function based shimming.

metabolites (TE/TR = 1.4/2000 ms, inversion time = 689 ms). The MM signal from 16 voxels in grey matter was averaged to generate a basis set for the MM with a low noise contribution. Furthermore the MM spectrum was HLSVD filtered (22) between 1.8 and 1.0 ppm to remove resonances in this partly suppressed spectral region.

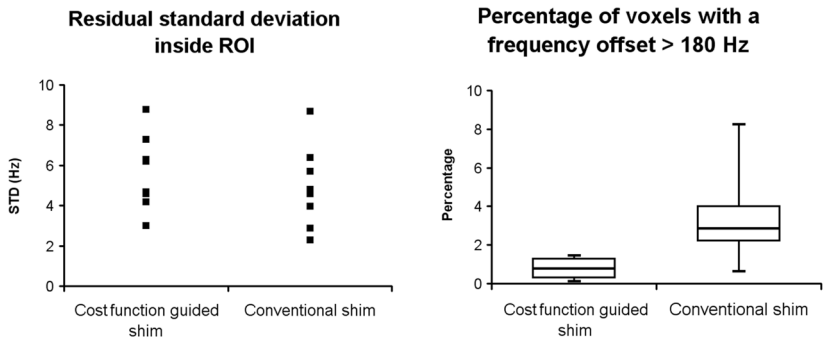

Figure 3: Analysis of the shimming results obtained in eight healthy volunteers, comparing the residual standard deviation inside the ROI (left) and the off-resonance outside the ROI expressed as N_{180Hz} (left). Although shim quality inside ROI remains unaffected, the off-resonance outside the ROI is substantially improved.

3.3 Results

The cost function based shimming algorithm was able to reduce high frequency offsets in the excited slice while simultaneously minimizing the linewidth in a selected region of interest (equation [1]). B_0 fieldmaps without shimming (σROI = 10 Hz), with traditional least squares optimization (σROI = 3 Hz) and with the cost function guided shimming (σROI = 3 Hz) are shown in figure 2. It is clear that using up to third order shims to minimize the linewidth in a ROI will lead to low residual B_0 inhomogeneities, however at the cost of large frequency offsets in the complete slice. By using the cost function based approach the frequency offsets in the slice can be controlled. An analysis of the shim results in 8 volunteers is given in figure 3. After the cost function based shimming, residual field variation (σROI) was found to be 5 Hz on average, which was similar to the traditional least squares optimization on the ROI only. Frequency offsets outside the ROI expressed as N180Hz were reduced significantly. After the cost function guided shimming the estimated experimental spectral linewidth was 10-12 Hz for NAA inside the ROI.

Simulations were performed to examine how high signals from subcutaneous lipids after shimming affect voxels in the complete slice due to inaccuracy in the CSI localization. Figure 4 shows that there is residual signal from subcutaneous lipids which decays fast with increasing distance from the skull. Comparing figure 4c with figure 4d it can be seen that, with the use of a Hamming filter, artifacts due to the pointspread function are reduced

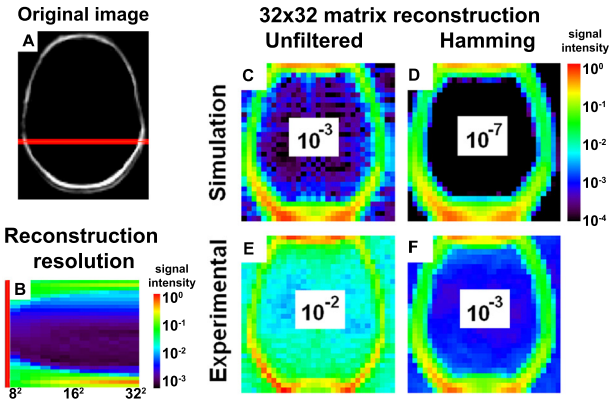

Figure 4: Simulations and experiments on pointspread signals generated by subcutaneous lipids. The original lipid image (a) was reconstructed on different resolutions (b). Lipid signal levels outside the lipid area are substantially reduced with higher resolution. Above a matrix size of 16×16, the artifact level shows to be constant. Reconstructions with a 32×32 matrix without (c) and with (d) hamming filter show a significant reduction in artifact level. Experimental results (e,f) do not show similar artifact reduction factors, but the use of a hamming filter still allows for an order of magnitude decrease in lipid pointspread signal.

below the noise level already at few voxels distant from the high intensity subcutaneous lipids. However, from the experimental data shown in figure 4e and figure 4f the same gain in localization accuracy is not observed. This may be due to additional ghosting artifacts caused by a modulation of the MR signal over the points in k-space, arising either from equipment imperfections (25) or physiological instability such as B_0 fluctuations caused by breathing (26). As shown in figure 4b the experimental artifact level is influenced by the spatial resolution: a matrix size below 12×12 shows residual lipid contaminations over large areas. Increasing the spatial resolution decreases the artifact level, and at spatial resolution above 16×16 the artifact level remains constant. For the CSI exam a resolution of 32×32 was used in which the subcutaneous lipid and water signals cause a ghosting artifact at approximately 10-3 of the initial signal intensity which could still dominate over the noise in the experiment. By applying additional frequency selective suppression (see below) the intensity of these subcutaneous lipids and thereby the ghosting signal over the whole slice is reduced further.

Frequency selective suppression was performed with a variation on the SWAMP. The bandwidth and carrier frequency of two AFP suppression pulses were optimized for simultaneous water and lipid suppression. The dual band excitation of both AFP pulses resulted in a 30 Hz suppression band around 4.7 ppm and 150 Hz band around 1.3 ppm. Bloch simulations show that perturbation of spins in the region from 4.3 ppm to 1.8 ppm was below 1% where the water suppression factor was 99% over 30 Hz (and 80% over 100 Hz) and the lipid suppression factor was 78% over 150 Hz respectively (figure 5).

Figure 6 shows several examples of spectra from gray matter from the artifact free

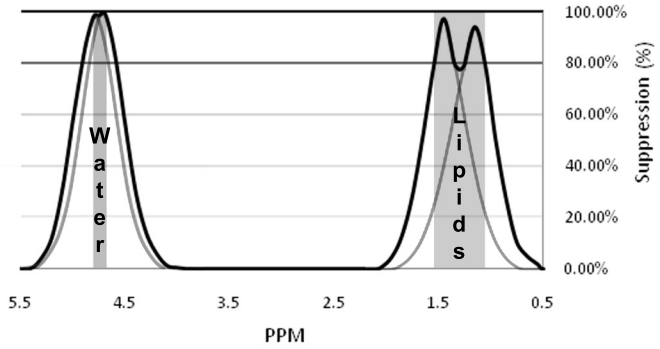

Figure 5: Suppression profile of the double AFP pulses where the bandwidths and carrier frequencies are optimized for dual band suppression resulting in 99% suppression efficiency over 30Hz (80% over 100Hz) around the water resonance and 78% suppression efficiency over 150 Hz around the lipid resonance.

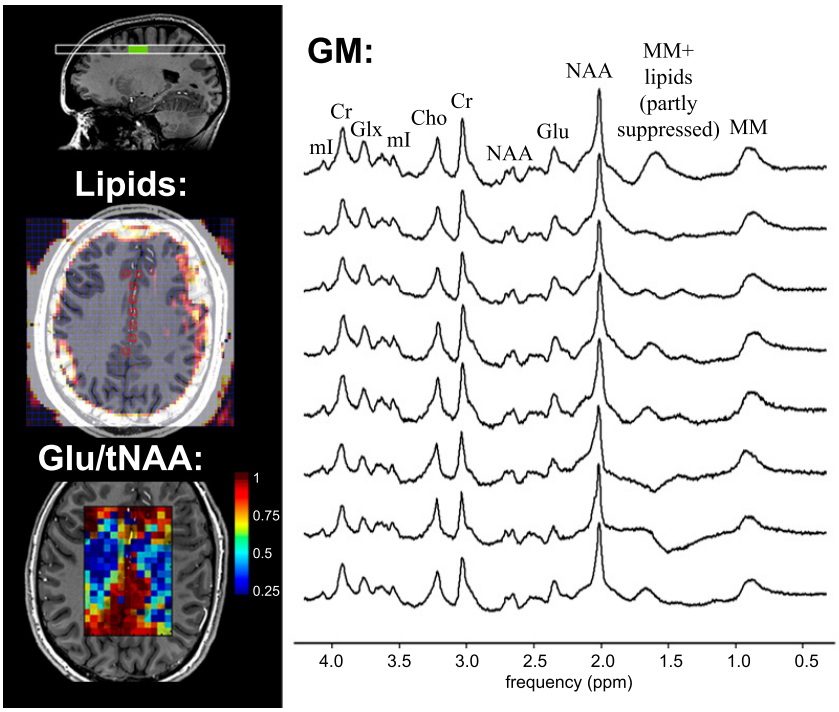

Figure 6: Results of the pulse acquire CSI sequence on a supraventricular slice. The upper color overlay indicates areas which are contaminated with high intensity lipid signals (yellow/white). The lower color overlay shows a (non-interpolated) Glu/tNAA ratio map for the artifact free area in the middle of the slice. On the right several voxels (5×5×10mm^3) from the grey matter are plotted. Acquisition was performed with Hamming weighted acquisition where central k-space points where averaged 6 times (acquisition time 28 min).

region in a high resolution CSI dataset recorded on a supraventricular slice. Also a Glu/tNAA map is shown, indicating a difference in the measured Glu/tNAA ratio for grey and white matter, as also seen from the quantification results in table 1. The complete slice, with the exception of areas less than four voxels distant from the skull, is free from lipid contaminations. A macromolecular contribution from short T_2 components can clearly be seen in the spectra demonstrating the sensitivity to short T_2 components. Apparent concentrations at 1 second TR were estimated on an average of 8 grey matter voxels, and an average of 6 white matter voxels to increase the SNR and fitting accuracy (table 1). Figure 7 shows the fit of several known metabolites to the average GM spectrum.

When an area of interest is close to the skull the contaminations from lipid signals are still severe, as shown in figure 4. However the slice orientation can be optimized to generate an artifact free region close to the skull. Figure 8 shows an example of an acquired spectrum where a double oblique slice was oriented close to the skull at the location of interest in the frontal cortex. With this slice orientation the intersection of the slice and the subcutaneous lipid signals remains several voxels away from the region of interest and an area free of lipid contamination is achieved very close to the skull.

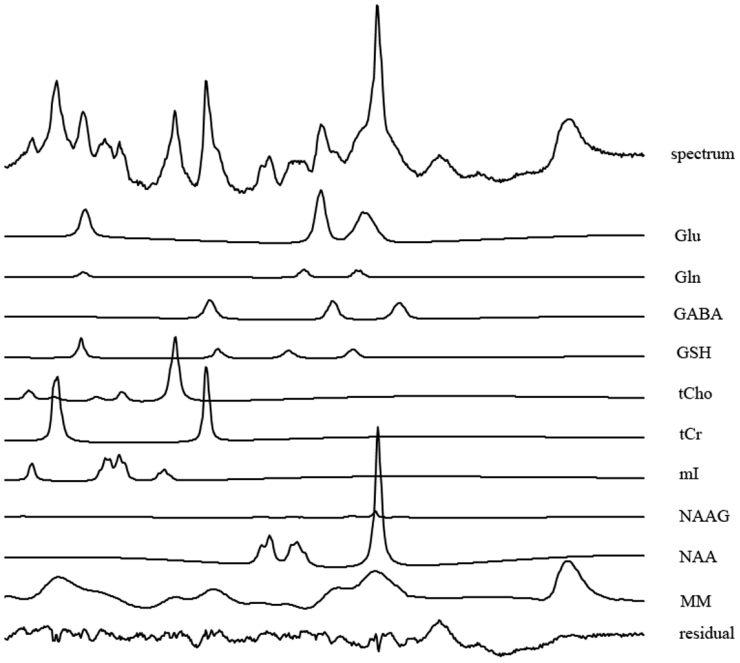

Figure 7: Metabolite fitting results on an average of 8 grey matter voxels. A constant T_1 was assumed for all resonances, apart from Cr where the methyl and methylene resonances were fitted with separate basis sets.

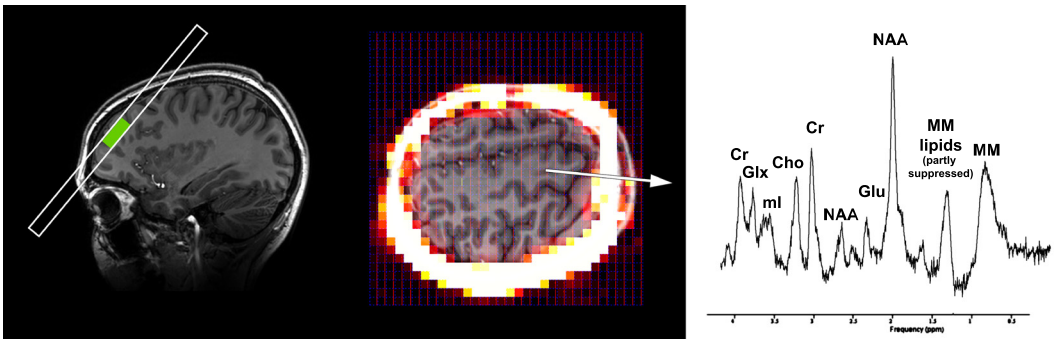

Figure 8: Results of the pulse acquire CSI sequence (5×5×10mm³) on a double oblique slice through the frontal cortex. The slice orientation allows for data acquisition close to the skull in the slice direction. All k-space data was acquired once (acquisition time 12 min).

3.4 Discussion

Advantages for ^{1}H MRS at high field are twofold; both SNR and chemical shift dispersion are increased leading to more sensitive experiments at higher spatial resolutions. In this work a method is described for MR spectroscopy at high field with very short echo time and short repetition time to acquire maximum SNR. In this way it becomes feasible to achieve spectra from a voxel size of 0.4 ml acquired in 12 minutes from the human brain.

Methods presented for MRS at high field coincide either with long echo times, large chemical shift displacement artifacts, inherent SNR loss from stimulated acquisition or long repetition times. In this work a method is described that combines several techniques, and results in a sequence that is not sensitive to signal loss due to T_2 decay or to J-modulation, has a low RF power deposition. As a concequence, a short repetition time can be uses, leading to very high SNR within a given scan time as described by Ernst et al (18). Gradient encoded localization with slice selective excitation was used instead of volume selective excitation as proposed by Henning et al (8). Therefore chemical shift displacement artifacts were only encountered in the direction of the excitation slice. As the repetition time was 1 second the Ernst angle was only 67 degrees. Using the full peak B_1^+ amplitude for the excitation pulse the bandwidth could be maximized leading to a chemical shift dispersion artifact of only 0.66 mm/ppm for a slice thickness of 10 mm.

The proposed method is insensitive to signal loss due to J-coupling evolution and T_2-dephasing since the FID was sampled directly after excitation (8). The echo time of the sequence was shortened to 1.44 ms. The delayed acquisition however causes a slight T_2^* weighting which results in an estimated signal loss of 2% based on the linewidth of NAA. The short echo time, short repetition time and increased chemical shift dispersion at high field make the sequence very sensitive to macromolecular resonances which might be used as additional biomarkers (27,28).

Since outer volume suppression and slice selective refocusing were not used in the sequence, care was taken to minimize possible baseline distortions from subcutaneous lipids or water signals which were excited in regions close to the skull. The combination of high resolution CSI with a novel cost function guided shimming algorithm prevents baseline distortions in the central ROI of the slice and allows the acquisition of artifact free spectra in the region from 1.9 to 4.1 ppm. Cost function guided shimming not only minimizes the linewidth in a user defined region of interest, of which high quality spectra can be obtained, but simultaneously minimizes frequency offsets in the complete slice, to allow for frequency selective suppression that is effective over the whole slice. By calculating the shimfields with a cost function that takes these two conflicting constraints into account, both global and local homogeneity is achieved. The size of the region of interest was chosen such that the global homogeneity did not compromise the quality of the local B_0 homogeneity (figure 3). The choice for frequency selective lipid suppression coincides with a low RF power deposition, similar as presented by Balchandani et al (10), however prevents the detection of resonances that might be clinically relevant such as lactate and macromolecules in the region around 1.3 ppm. Recent developments in the use of multiple transmit coils combined with dynamic RF shimming may be an appropriate alternative for the detection of these resonances if the MR system is equipped with multi-transmit capabilities (29).

The reduction in repetition time compared to the fully relaxed state allows for a significant gain in SNR. For several components the increase in SNR is even higher due to a shorter T_1. Using this relatively short repetition time introduces a T_1 weighting in the spectra. Absolute concentration estimation therefore becomes more difficult since a T_1 correction has to be made for every resonance. Absolute quantification is therefore not accurate since T_1 relaxation times of all metabolites *in vivo* at 7 tesla are currently not available. Even more, they may be altered in case of disease. Therefore this contrast may in itself be used to assess altered metabolism, particularly in studies that use control groups. In this study we have performed an estimation of the concentration with the incorporation of an average T_1 correction, therefore the apparent concentrations at 1 second repetition time have been reported .

The short TR can also have an influence of the ratios within a metabolite basis set. One of the most prominent effects is expected for the creatine methylene resonance, therefore only the fitting of the creatine methylene resonance was adapted. It is expected that fitting performance can be further improved by correcting ratios of individual resonances per metabolite with accurate knowledge of the T_1 values.

Due to the short TR an increased number of k-space points can be acquired in a given scan time. This was used to employ Hamming weighted k-space averaging to regain the loss in SNR caused by the Hamming filter. More complicated sampling schemes could also be used within a reasonable scantime to reduce pointspread artifacts even further (30).

The maximized sensitivity of the proposed method was traded for spatial resolution in order to show a decrease in voxel volume with an order of magnitude compared to

Apparent metabolite concentrations (mM)	Grey matter	White matter
GABA	1.3 ± 0.2	0.2 ± 0.2
Glu	8.5 ± 0.6	4.0 ± 0.3
Gln	0.3 ± 0.2	0.2 ± 0.2
GSH	1.5 ± 0.2	1.1 ± 0.1
mI	4.6 ± 0.3	4.1 ± 0.2
NAA	10.4 ± 0.4	9.1 ± 0.3
NAAG	0.3 ± 0.2	2.4 ± 0.2
PE	1.0 ± 0.3	0.9 ± 0.3
tCr	7.7 ± 0.3	7.5 ± 0.4
tCho (GPC+PC)	2.3 ± 0.1	2.9 ± 0.1
tNAA (NAA+NAAG)	10.6 ± 0.3	11.5 ± 0.3
MM (arbitrary units)	4.7 ± 0.2	3.5 ± 0.2

Table 1: Apparent metabolite concentrations for a TR of 1 second (mM ± COV) as calculated from an average spectrum of 8 voxels from the grey matter and an average spectrum of 6 WM voxels. Concentrations have been estimated assuming a T_1 value of 1500 ms.

traditional spectroscopy methods without compromising spectral quality. Because of the high spatial resolution it is possible to distinguish voxels of gray matter from white matter throughout the brain.

3.5 Conclusion

We have shown that ^{1}H-MR spectroscopy at high field is possible with limited chemical shift displacement artifacts at short echo time and short repetition time with full signal acquisition by moving away from slice selective refocusing and use slice selective excitation in combination with pulse-acquire chemical shift imaging and cost function guided B_0 shimming. Results are shown for both a supraventricular slice as for an area close to the skull in the frontal cortex.

3.6 Acknowledgements

We thank Robin A. de Graaf (Magnetic Resonance Research Center, Yale University) for providing the LCModel based fitting software.

References

1. Leary SM, Davie CA, Parker GJM, Stevenson VL, Wang LQ, Barker GJ, Miller DH, Thompson AJ. 1H Magnetic resonance spectroscopy of normal appearing white matter in primary progressive multiple sclerosis. J. Neurol. 1999;246(11):1023-1026.
2. Smith ICP, Stewart LC. Magnetic resonance spectroscopy in medicine: clinical impact. Prog Nucl Magn Spectrosc 2002;40(1):1-34.
3. Ross AJ, Sachdev PS. Magnetic resonance spectroscopy in cognitive research. Brain Res Rev 2004;44(2-3):83-102.
4. Tkáč; I, Öz G, Adriany G, Uğurbil K, Gruetter R. In vivo 1H NMR spectroscopy of the human brain at high magnetic fields: Metabolite quantification at 4T vs. 7T. Magnetic Resonance in Medicine 2009;62(4):868-879.
5. Scheenen TWJ, Heerschap A, Klomp DWJ. Towards 1H-MRSI of the human brain at 7T with slice-selective adiabatic refocusing pulses. MAGMA 2008;21(1):95-101.
6. Tkáč I, Andersen P, Adriany G, Merkle H, Ugurbil K, Gruetter R. In vivo 1H NMR spectroscopy of the human brain at 7 T. Magn Reson Med 2001;46(3):451-6.
7. Mekle R, Mlynárik V, Gambarota G, Hergt M, Krueger G, Gruetter R. MR spectroscopy of the human brain with enhanced signal intensity at ultrashort echo times on a clinical platform at 3T and 7T. Magn Reson Med 2009;61(6):1279-1285.
8. Henning A, Fuchs A, Murdoch JB, Boesiger P. Slice-selective FID acquisition, localized by outer volume suppression (FIDLOVS) for 1H-MRSI of the human brain at 7 T with minimal signal loss. NMR in Biomedicine 2009;22(7):683-696.
9. Jansen JFA, Backes WH, Nicolay K, Kooi ME. 1H MR spectroscopy of the brain: absolute quantification of metabolites. Radiology 2006;240(2):318-332.
10. Balchandani P, Spielman D. Fat suppression for 1H MRSI at 7T using spectrally selective adiabatic inversion recovery. Magn Reson Med 2008;59(5):980-988.
11. Siero JCW, Boer VO, Hoogduin J, Luijten PR, Klomp DWJ. Cost function guided 3rd order B0 shimming for MR spectroscopic imaging at 7T. In: Proceedings 17th Annual Meeting, ISMRM, Honolulu, USA, 132. 2009
12. Jenkinson M. Fast, automated, N-dimensional phase-unwrapping algorithm. Magn Reson Med 2003;49(1):193-197.
13. Powell MJD. Numerical Analysis, ed. G.A. Watson, Lecture Notes in Mathematics. 1987.
14. Wen H, Jaffer FA. An in vivo automated shimming method taking into account shim current constraints. Magn Reson Med 1995;34(6):898-904.
15. Koch KM, Rothman DL, de Graaf RA. Optimization of static magnetic field homogeneity in the human and animal brain in vivo. Prog Nucl Magn Reson Spectrosc 2009;54(2):69-96.

16. Pohmann R, von Kienlin M. Accurate phosphorus metabolite images of the human heart by 3D acquisition-weighted CSI. Magn Reson Med 2001;45(5):817-826.
17. de Graaf RA, Nicolay K. Adiabatic water suppression using frequency selective excitation. Magn Reson Med 1998;40(5):690-6.
18. Ernst RR. Application of Fourier Transform Spectroscopy to Magnetic Resonance. Rev. Sci. Instrum. 1966;37(1):93.
19. Otazo R, Mueller B, Ugurbil K, Wald L, Posse S. Signal-to-noise ratio and spectral linewidth improvements between 1.5 and 7 Tesla in proton echo-planar spectroscopic imaging. Magn Reson Med 2006;56(6):1200-1210.
20. Yarnykh VL. Actual flip-angle imaging in the pulsed steady state: A method for rapid three-dimensional mapping of the transmitted radiofrequency field. Magn Reson Med 2007;57(1):192-200.
21. Wald LL, Moyher SE, Day MR, Nelson SJ, Vigneron DB. Proton spectroscopic imaging of the human brain using phased array detectors. Magn Reson Med 1995;34(3):440-445.
22. Van den Boogaart A, Van Ormondt D, Pijnappel WWF, de Beer R, Ala-Korpela M. Mathematics and Signal Processing III. Oxford: 1994.
23. Naressi A, Couturier C, Devos JM, Janssen M, Mangeat C, de Beer R, Graveron-Demilly D. Java-based graphical user interface for the MRUI quantitation package. MAGMA 2001;12(2-3):141-152.
24. Soher BJ, Young K, Bernstein A, Aygula Z, Maudsley AA. GAVA: spectral simulation for in vivo MRS applications. J Magn Reson 2007;185(2):291-299.
25. Lerski RA, Straughan K, Williams JL. Practical aspects of ghosting in resistive nuclear magnetic resonance imaging systems. Phys Med Biol 1986;31(7):721-735.
26. van Gelderen P, de Zwart JA, Starewicz P, Hinks RS, Duyn JH. Real-time shimming to compensate for respiration-induced B0 fluctuations. Magn Reson Med 2007;57(2):362-8.
27. Mader I, Seeger U, Weissert R, Klose U, Naegele T, Melms A, Grodd W. Proton MR spectroscopy with metabolite-nulling reveals elevated macromolecules in acute multiple sclerosis. Brain 2001;124(5):953-961.
28. Graham GD, Hwang JH, Rothman DL, Prichard JW. Spectroscopic assessment of alterations in macromolecule and small-molecule metabolites in human brain after stroke. Stroke 2001;32(12):2797-2802.
29. Hetherington HP, Avdievich NI, Kuznetsov AM, Pan JW. RF shimming for spectroscopic localization in the human brain at 7 T. Magn Reson Med 2010;63(1):9-19.
30. Garwood M, Schleich T, Bendall MR, Pegg DT. Improved fourier series windows for localization in in vivo NMR spectroscopy. J Magn Reson 1985;65(3):510-515.

Chapter 4

Multi-slice ^{1}H MRSI of the human brain at 7 Tesla using dynamic B_0 and B_1 shimming

Magnetic Resonance in Medicine 2011; in press

Vincent O. Boer[1]; Dennis W.J. Klomp[1]; Christoph Juchem[2]; Peter R. Luijten[1]; Robin A. de Graaf[2]

[1.] *Department of Radiology, University Medical Center Utrecht, Utrecht, The Netherlands*
[2.] *Department of Diagnostic Radiology, Yale University School of Medicine, MR Research Center (MRRC), New Haven, Connecticut, USA*

Abstract

Proton MR spectroscopic imaging of the human brain at ultra-high field (≥7T) is challenging due to increased RF power deposition, increased magnetic field B_0 inhomogeneity and increased RF magnetic field inhomogeneity. And, especially for multi-slice sequences, these effects directly inhibit the potential gains of higher magnetic field and can even cause a reduction in data quality. However, recent developments in dynamic B_0 magnetic field shimming and dynamic multi-transmit RF control allow for new acquisition strategies. Therefore, in this work slice-by-slice B_0 and B_1 shimming was developed to optimize both B_0 magnetic field homogeneity and nutation angle over a large portion of the brain. Together with a low-power water and lipid suppression sequence and pulse-acquire spectroscopic imaging, a multi-slice MRSI sequence is shown to be feasible at 7T. This now allows for multi-slice metabolic imaging of the human brain with high sensitivity and high chemical shift resolution at ultra-high field.

4.1 Introduction

Proton MR spectroscopic imaging (MRSI) at ultra-high field strength, in principle, allows for acquisition of metabolic information with a high sensitivity and accuracy due to an increased intrinsic signal to noise ratio (SNR) and an increase in chemical shift dispersion. However, the increases in chemical shift dispersion also requires higher bandwidth (BW) radio frequency (RF) pulses in suppression and localization schemes. At the same time RF power deposition increases, putting a limit on the amount and strength of the RF pulses that can be used. In addition, the homogeneity in both static magnetic field (B_0) and transmit magnetic field (B_1^+) decreases with higher field strength, since both the magnetic susceptibility artifacts and the RF wave interference effects become more pronounced, causing severe spatial variation in spectral linewidth and the attained nutation angle. As a consequence, traditional localization and suppression sequences for (multi-slice) MRSI are not directly transferable to human ultra-high field systems such as 7T since they would lead to severe SNR loss, large chemical shift displacement artifacts, incomplete water and lipid suppression and compromised spectral linewidth. However, recent developments in B_0 shimming and RF transmit systems allow for the development of new acquisition strategies. First, the B_0 homogeneity in multi-slice imaging and spectroscopy sequences has been shown to benefit from the slice-specific, dynamic application of up to third order spherical harmonic shim fields, as to insure optimal shimming for every individual slice, a technique known as dynamic shim updating (DSU) (1-2). Secondly, for MR (spectroscopic) imaging, multi-element transmit arrays show an important advantage over volume coils or surface coils since they allow homogenization of the transmit B_1^+ field in the brain over large regions (3), or to define custom shaped B_1^+ fields for purposes of outer volume suppression (4-5), or inner volume selection (6). This is mostly performed by a person-to-person (numerical) optimization of the transmit amplitudes and phases of multiple transmit elements, so called RF shimming (or B_1^+ shimming). With these novel developments, homogenization of both the B_0 and B_1^+ field of the human brain becomes possible, thereby possibly opening the way for multi-slice spectroscopic imaging of large areas at 7T.

Several approaches for single-slice MRSI in the human brain have been shown at ultra-high field (5,7-11); however, none of these methods appears to be readily extendable to a multi-slice acquisition scheme in order to achieve coverage over a larger area of the human brain. All proposed sequences are limited with respect to RF power deposition, therefore restricting the minimum achievable repetition time (TR) and therefore the number of slices that can be acquired. Especially high BW adiabatic inversion or refocusing pulses have not been considered for multi-slice MRSI yet, due to the high duty cycle on RF power and the associated high RF power deposition (5,10). The method of Xu et al (12) does achieve 3D coverage by performing 3D phase-encoding in a PRESS-selected box. Also Scheenen et al (13) have shown a 3D acquisition, albeit with a surface coil. While these methods provide

high-quality data, it precludes the use of dynamic B_0 shimming to improve the magnetic field homogeneity.

With the FID-acquisition technique (7-8), signal is acquired immediately after slice-selective excitation and phase encoding, thereby eliminating the slice-selective refocusing pulse needed for spin echo formation. Therefore, this approach lowers the RF power deposition substantially. At the same time, such a pulse-acquire technique reduces B_1^+ sensitivity, minimizes chemical shift displacement artifacts and maximizes sensitivity, since very short echo times can be realized (e.g. in the order of a few milliseconds). The published FID-acquisition methods are not readily modified and extended for multi-slice acquisitions due to the high RF power deposition associated with the water and lipid suppression schemes.

In this work a low power multi-slice MRSI sequence is presented that allows for a short effective TR and therefore enables the acquisition of multi-slice MRSI. A B_1^+ and T_1 insensitive water and lipid suppression has been developed which is based on a limited number of low RF power pulses. The optimization of the RF powers and interpulse delays resulted in excellent water and lipid suppression over the whole volume. Slice-based B_0 and B_1^+ updating was used to improve the homogeneity of both the static magnetic field and the transmit B_1^+ field. MRSI from five slices in the human brain at 7T is presented, acquired in 18 minutes with a voxel size of $8\times8\times8mm^3$.

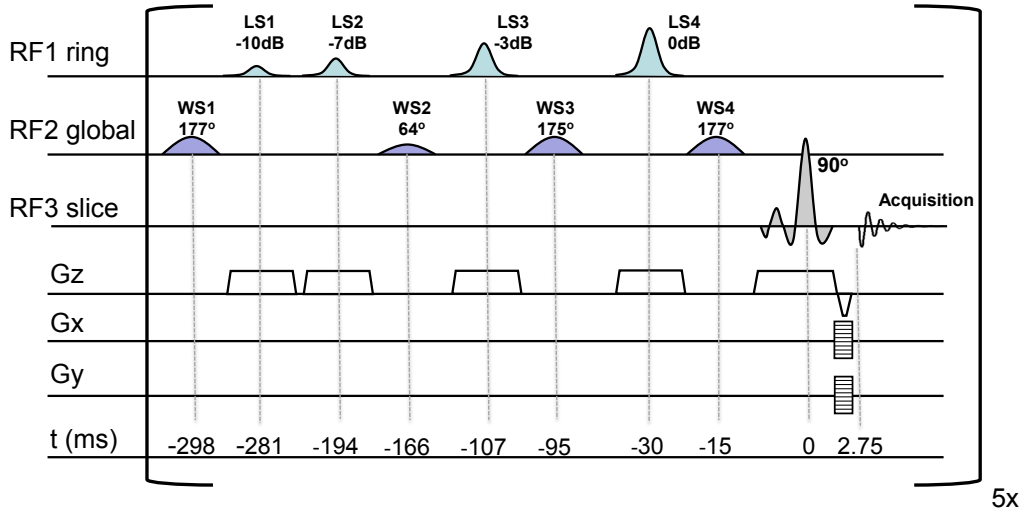

Figure 1: The multi-slice MRSI sequence consists four RF- and slice-selective lipid suppression pulses (LS1-4), four global water suppression pulses (WS1-4) and a slice-selective 90 degree excitation pulse, combined with 2-dimensional phase encoding for signal localization. This sequence was repeated every 500 ms, resulting in a TR of 2.5 s for the five-slice MRSI sequence. B_0 and RF shim settings were updated before every RF pulse. Pulse-timing is indicated in milliseconds, relative to the center of the excitation pulse. As the RF1 ring mode provides non-uniform nutation, the values are expressed in dB attenuation of the maximum RF power.

4.2 Methods

MR measurements were performed on a 7 tesla actively shielded, 68 cm inner diameter MR magnet interfaced to a Direct Drive spectrometer with 8 transmit and receive channels (Agilent, Santa Clara, CA). The asymmetric gradient system (Agilent, Santa Clara, CA) included a full set of third order shim coils equipped with preemphasis and B_0 compensation on all shim terms, which was essential for successful DSU (2). All data were acquired using an eight element cylindrical transceiver array (10) driven by an eight channel (8×1 kW) RF amplifier (CPC, Hauppauge, NY). In this study, five human subjects were scanned with the MRSI sequence on five axial slices through the brain. All subjects were studied in accordance with Yale Institutional Review Board guidelines for research on human subjects.

4.2.1 MRSI sequence

Multi-slice MRSI was performed on five axial slices with an (interleaved) slice-selective pulse-acquire MRSI sequence (figure 1). The Shinnar Le Roux optimized (14) slice-selective 90 degrees excitation pulse (BW=2.3kHz) was followed by phase encoding gradients and a refocusing gradient, resulting in a (gradient) echo time (TE) of 2.75 ms and a TR of 2500 ms (e.g. effective TR=500ms). A chemical shift displacement artifact was only present in the direction of the slice selective excitation (1 mm/ppm). MRSI data was acquired with 25×25 circular sampling of k-space over a 200×200 mm^2 field-of-view, resulting in a total acquisition time of 18 min. With a slice thickness of 8 mm, the nominal and actual voxel sizes were 512 μL and 875 μL respectively. Signal acquisition was performed for 170 ms (512 complex points over a 3 kHz spectral BW). Water and lipid suppression modules were inserted before every slice-selective excitation pulse, where the duration of the suppression module was optimized in order not to exceed the 320 ms available between the end of the signal acquisition and the next slice-selective excitation pulse.

An additional, fast MRSI scan to acquire the water signal was performed, at identical resolution, but with a shorter readout (128 points), a reduced excitation angle to prevent T_1 saturation and without water and lipid suppression (TR=260ms, scan time=10s) to estimate the required correction coefficients for coherent summation of the signals from the different receive channels (15). No receiver or intensity correction was performed on the spectra.

4.2.2 Water suppression

Global water suppression in the steady-state (effective TR=500 ms) was performed with an optimized WET scheme (16) that consisted of four frequency selective Gaussian excitation pulses (figure 1). Using the Bloch equations, and by taking the effective TR of the water suppression scheme into account, the nutation angles and delays between the four pulses were numerically optimized to maximize the suppression efficiency. This resulted in the situation where the steady-state magnetization of the water signal was effectively nulled

at the time of the excitation (figure 2a). To compensate for residual B_0 variations in the brain, the numerical optimization comprised the frequency range of +/- 20 Hz around the Larmor frequency. With this approach, the average suppression factor in the steady-state was 980 fold (figure 2b) within the range of 60% and 140% of the nominal B_1^+ and for typical T_1 values (17) of water in CSF, gray and white matter of the human brain at 7T.

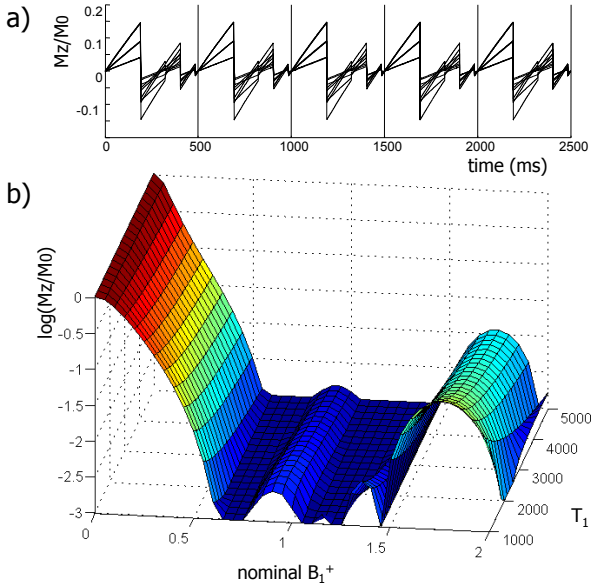

Figure 2: The steady-state water suppression was developed by minimization of the longitudinal magnetization after four suppression pulses in the steady-state. The time evolution of the longitudinal magnetization (Mz) is shown (a) for different T_1 (GM, WM, CSF) and B_1^+ (70%, 100%, 130%) values. Using the steady-state behavior, the magnetization is effectively nulled at the time of the slice-selective excitation. In (b) the suppression factor is shown for a range of T_1 and B_1^+ values at the time of the slice-selective excitation. The suppression is highly effective for a range of B_1^+ values and nearly insensitive to T_1 values of water in the human brain. For B_1^+ between 60-140% and T_1 between 1-5 seconds, the average suppression factor was 980.

4.2.3 Lipid suppression

Lipid suppression pulses were interleaved with the water suppression scheme (figure 1) and was performed for a ring shaped RF shim setting on the skull (see below). Care was taken to assure that the four slice-selective excitation pulses did not to perturb the magnetization on neighboring slices nor saturate the brain metabolites. However, since the B_1^+ transmit field in the skull close to the transmit coils was highly inhomogeneous, adequate lipid suppression demanded a method that was insensitive to a large range of B_1^+ values. For this purpose, the nutation angles and delays of a four pulse WET sequence (16)

were numerically optimized through Bloch simulations to provide a 30-fold suppression over a factor of three times the nominal B_1^+ value and T_1 values for lipids between 400 and 600 ms. Slice-selective hyperbolic secant pulses (18) were used since they provide a B_1^+ insensitive slice profile, thereby minimizing the impact on the magnetization in adjacent slices. A uniform suppression of all lipid resonances was achieved by matching the BW of the lipid suppression pulses to the BW of the slice-selective excitation pulses.

The suppression efficiency of the water and lipid suppression was measured by calculating the ratio of two images with similar scanning parameters as the MRSI sequence. One image was acquired with the suppression pulses on, and one image with the suppression pulses off. A suppression map was then calculated as the ratio of these two images.

4.2.4 B_0 shimming

Magnetic field B_0 homogenization was based on gradient echo B_0 field mapping from 15 slices with four echo times, that covered the same volume as the multi-slice MRSI sequence (TR=450ms, FOV=200×200mm^2, slice thickness=3.3mm, matrix=50×50, scan time=90 seconds). In order to accommodate the shimming requirements for both non-slice-selective and slice-selective pulse sequence elements, a global B_0 shim over the whole brain volume as well as slice-specific B_0 shims were calculated. To compensate through-plane magnetic field inhomogeneity, the slice-specific shims were calculated over three adjacent slices of the B_0 mapping dataset that covered the spatial extent of the MRSI slice. The global B_0 shim setting was employed during the water and lipid suppression. Before the slice-selective excitation and acquisition, the shims were switched to the slice-specific B_0 shim setting. Eddy currents and off resonance effects during the fast updating of high order shims were prevented by preemphasis and B_0 compensation, which was incorporated for each of the second and third order shim coils (2). No current limits were employed in the fitting of the shim fields, at maximum 20% of the dynamic range of the shim amplifiers (20A) was required for first-through-third order shimming. The effectiveness of the slice-based DSU was assessed from the B_0 maps for first through third order DSU, and compared to the results with static B_0 shimming (measured up to third order and simulated up to fourth order). In addition, water MRSI measurements with DSU and with static shimming were performed to assess the impact of third order DSU on the water linewidth. All MRSI metabolite measurements were performed with third order slice-based DSU. The spectral line width was measured by manually estimating the full width at half maximum of the creatine CH3 resonance at 3.0 ppm.

4.2.5 B_1^+ shimming

Using an eight channel transceiver array, it was possible to optimize the excitation pattern for every RF pulse. Optimization of the B_1^+ transmit field was performed by numerical optimization of the transmit amplitudes and phases, after measurement of the complex transmit B_1^+ fields. This was performed by combining phase information from gradient

echo images with B_1^+ amplitude field maps obtained by Bloch-Siegert shift B_1^+ mapping (19). The transmit phase information was measured by sequentially turning on each transmit channel in a multi-slice gradient echo acquisition (TE/TR=3.5/100 ms, FOV=200×200mm^2, 5 slices, slice thickness=8mm, matrix=50×50, total scan time=40s). From the transmit B_1^+ phase information, an RF shim setting was derived that created a constructive interference between the eight coils in the center of the brain. This RF phase-shim was used for the excitation pulse in the B_1^+ mapping sequence to generate a high overall nutation angle, and therefore high measurement sensitivity. B_1^+ amplitude mapping was performed with a five slice gradient echo sequence, employing the Bloch-Siegert B_1^+ mapping technique (TE/TR=13.5/650 ms, FOV=200×200mm^2, slice thickness=8mm, matrix=50×50, scan time=65 s per transmit channel). The off-resonant Fermi calibration pulse (8 ms duration, placed at ±1.5 kHz) was turned on for each of the eight transmit channels in consecutive measurements. Pixels with low SNR that could corrupt the phase measurement, and therefore the B_1^+ estimation, were removed from the dataset. An extrapolation of the B_1^+ map through these points was performed by 2D-polynomial fitting.

With both the phase and amplitude information of the B_1^+ field in the five slices, RF shim settings were calculated by a numerical least squares minimization of the variation of the B_1^+ field. Several RF shim settings were generated to ensure an optimal B_1^+ field for every RF pulse; a slice-specific uniform excitation, a ring shaped excitation pattern on the skull area for lipid suppression on every slice and a global uniform excitation for water suppression in all five slice. During the MRSI sequence the RF system was switched to the appropriate RF shim for every RF pulse.

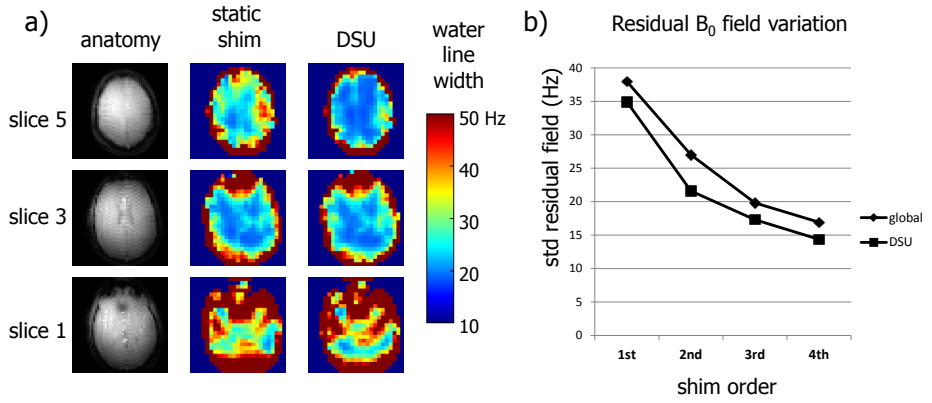

Figure 3: B_0 homogeneity for slice-based DSU compared to global B_0 shimming. The impact of DSU on the measured water linewidth with third order shimming is shown (a). Limited gain is seen in the center slice, however, the upper and lower slices show clear linewidth reductions. Severe inhomogeneities remain in the lower slice, above the nasal and ear cavities, which are not easily compensated by spherical harmonic shimming. Improvement in the B_0 homogeneity with DSU was simulated (b) for different shim orders (first through fourth order shimming).

The RF power deposition was monitored at the input power of all the individual transmit elements. RF power was mostly required for water suppression (46%) and lipid suppression pulses (43%). The localization (with slice-selective excitation) only required a small fraction of the total RF power (11%). The global RF power deposition of 2.3 ± 0.3 W/kg (mean ± SD, n = 5) was well within FDA guidelines. Local SAR values were estimated at 5 W/kg from numerical simulations (5) of the homogeneous and ring mode SAR distributions of the coil.

Water residuals were subtracted from the spectra by HLSVD filtering (20). Although no correction for acquisition delay is required to perform further spectral analysis and metabolite fitting (7), a correction for the missing first points was performed for display purposes. To this end, an HSVD fit of the time domain signal was performed, and the first 8 missing data points were extrapolated before Fourier transform.

4.3 Results

Optimization of the uniformity of the static B_0 magnetic field on a slice-by-slice basis showed an improved homogeneity compared to a global optimization strategy. Figure 3a shows the effect of slice-specific DSU on the water linewidth in one volunteer, as determined by the fast MRSI measurement without water suppression. The slice-based B_0 optimization led to improved B_0 magnetic field homogeneity compared to a global optimization, especially in the upper and lower slices. However, close to the nasal cavity, large residual B_0 inhomogeneities remained which could not be compensated with the third order spherical

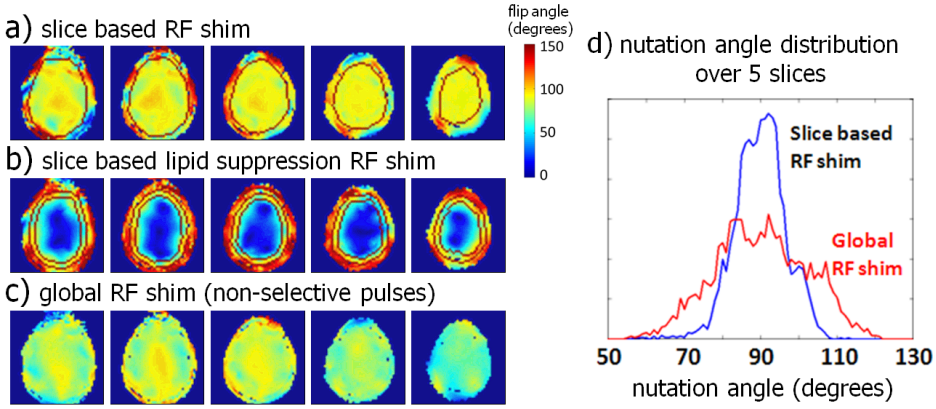

Figure 4: RF shimming over five slices; a slice-by-slice optimization was used for the slice-selective excitation pulses (a), a slice-by-slice ring mode was used for lipid suppression (b) and a global optimization was used for the water suppression (c). The histogram of the nutation angle (d) demonstrates the improvement in overall nutation angle homogeneity with a slice-based B_1^+ optimization.

harmonic fields. The outcome of slice-specific DSU was analyzed in the five subjects by means of the average residual B_0 field inhomogeneity (figure 3b). For the slice positions and coverage used in this study, slice-based DSU improved the B_0 magnetic field homogeneity compared to a global optimization by approximately one order of spherical harmonic fields (e.g. third order DSU is comparable with full fourth order static shimming).

Pulse specific RF shimming was performed by calculating three sets of RF shim settings. Firstly, slice-specific RF shims (figure 4a) were calculated for slice-selective excitation by finding the optimal combination of transmit phases and amplitudes which maximized the nutation angle homogeneity over the brain. Secondly, slice-specific lipid suppression RF shims (figure 4b) were calculated by maximizing the excitation on the skull while simultaneously minimizing the excitation over the brain, resulting in a excitation of the skull only (figure 4b). Thirdly, a global excitation RF shim for non-slice-selective pulse sequence elements was calculated (figure 4c), by minimizing the variation of the field in the brain volume over all slices. Figure 4d displays the nutation angle distribution over the five slices and shows how the slice-by-slice optimization of the B_1^+ magnetic field leads to a more homogeneous distribution of the excitation nutation angles over the whole volume, compared to a single RF shim for optimization of the B_1^+ field on the center slice.

The efficiency of water and lipid suppression was quantified as the ratio of MRI images acquired with and without suppression pulses (figure 5). The optimized four pulse water suppression sequence in the steady-state was very effective, leading to suppression factors

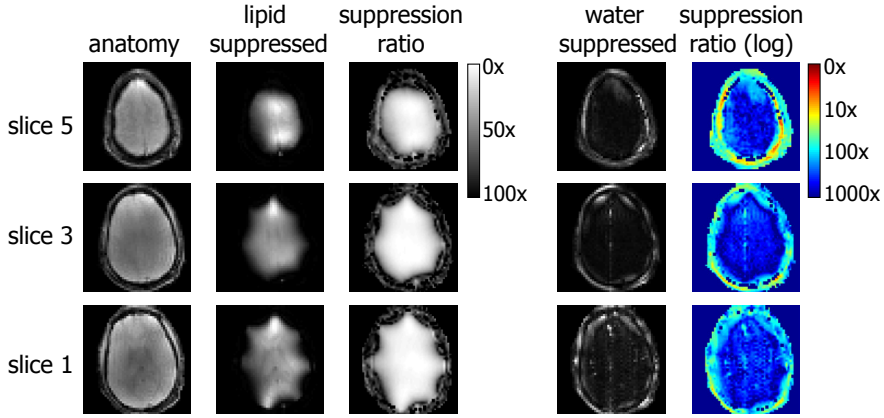

Figure 5: Evaluation of the water and lipid suppression quality in the human brain at 7T. On the left the original anatomical image, the second column shows an anatomical image with the lipid suppression pulses on and the third column shows the division of the original image and an image acquired with the lipid suppression. On the right an image acquired with water and lipid suppression is shown, together with the ratio (suppression factors) on a logarithmic scale. Water signal in the brain is suppressed by >300 fold, signal in the skull is suppressed >30 fold.

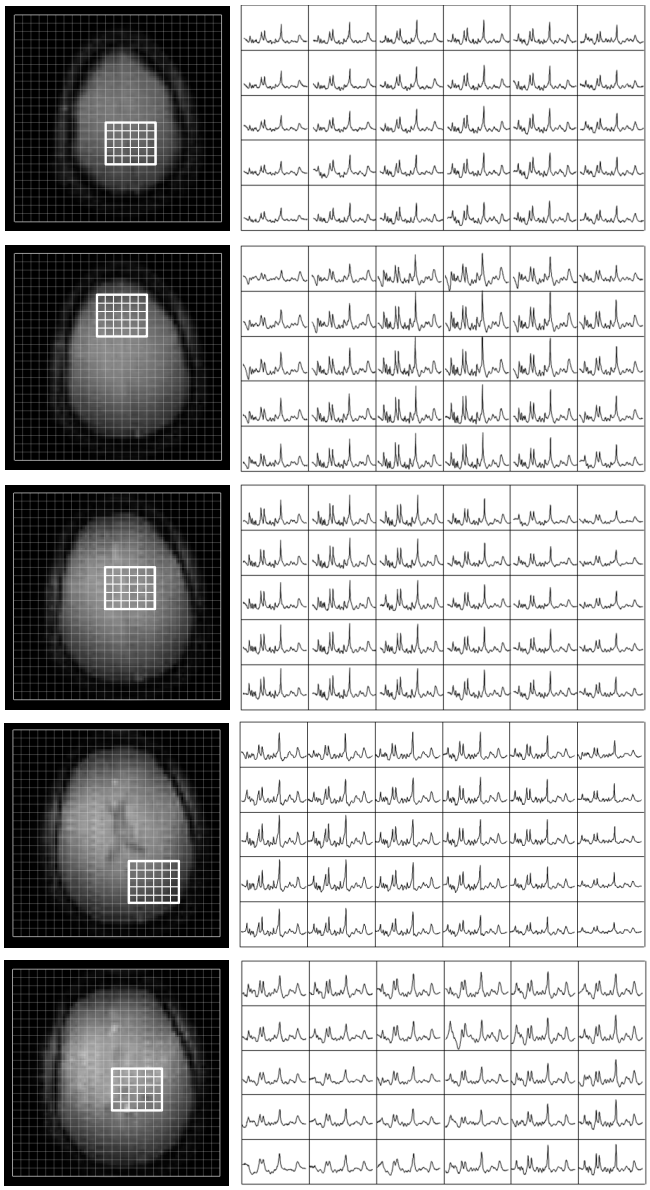

Figure 6: Five slice MRSI dataset of a healthy volunteer. For every slice 6×5 spectra out of the 20×20 matrix are shown. No linear prediction to improve the baseline or intensity correction or normalization was performed. High SNR and a narrow linewidth are apparent over large parts of the brain. Despite the short TE of 2.75 ms the absence of lipid signals is noticeable.

>300 fold in the brain. The lipid suppression led to a suppression of approximately 30 fold on the skull without perturbing large areas of brain tissue. However, the outer part of the cortex was still partially excited by the ring mode. Since the lipid suppression was slice-selective, this lead to a uniform signal loss over the spectrum for voxels close to the skull.

Several selected 5×6 areas from the 20×20 matrix from all five slices in the MRSI dataset are shown in figure 6. High overall SNR and spectral quality are apparent. The stable macromolecular (MM) signal indicates a good lipid suppression over all slices. Intensity variation of the metabolites as seen over the slices is caused by inhomogeneous linewidth (figure 3), by a spatially varying receiver sensitivity, partial volume effects and partly by undesired saturation in the transition zone of the lipid suppression pulses (figure 5). The average (± standard deviation) line widths of the 3.0 creatine resonance of the MRS voxels in the brain over the five slices was 14.2±5.5 Hz. On the individual slices, the average and standard deviation of the creatine line width were (from bottom slice to top slice) 23.6±6.2 Hz, 16.0±4.0 Hz, 12.8±2.8 Hz, 12.5±3.2 Hz and 10.6±2.0 Hz.

Two representative spectra from the white (WM) and gray matter (GM) (figure 7) show excellent spectral resolution and sensitivity. Clear differences in metabolite content, i.e. decreased glutamate (Glu) and increased N-acetylaspartylglutamate (NAAG) in the parietal white matter compared to occipital gray matter, as well as differences in the ratio of choline (Cho) and creatine (Cr).

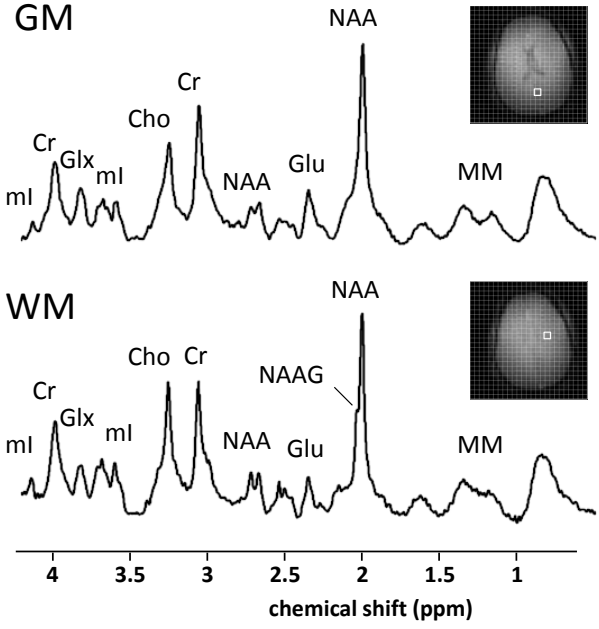

Figure 7: Two example spectra (875 µL, processed with HSVD baseline correction) from frontal white matter (WM) and parietal gray matter (GM) show differences in Glu concentration as well as Cho/Cr ratio and NAAG concentrations between gray and white matter.

4.4 Discussion

Proton MR spectroscopic imaging, and especially multi-slice MRSI, of the human brain at ultra-high field (≥7T) is challenging due to increased RF power deposition, increased magnetic field B_0 inhomogeneity and increased RF magnetic field inhomogeneity. Many of these effects directly inhibit the potential gains of higher magnetic field and can even cause a reduction in data quality due to increased chemical shift displacement artifacts, incomplete water and lipid suppression and a decrease in spectral resolution. In addition, traditional multi-slice spectroscopic imaging cannot be directly translated to ultra-high magnetic fields due to the increased RF power deposition. However, recent developments in dynamic magnetic field shimming and dynamic RF control with multi-element transmit coils allow for novel acquisition strategies.

Several groups have shown promising results with 2D/3DMRSI at ultra-high field, where various acquisition strategies as well as suppression techniques for water and lipid signals have been employed. These methods include highly selective lipid suppression with several slice-selective saturation pulses (7), spectrally (9) or spatially selective inversion recovery (5,10), spectral saturation of water and/or lipids (7-8) and spectrally selective refocusing (5,10-11) of the metabolites of interest. Unfortunately, methods that employ such non-selective RF pulses for excitation or refocusing do not allow direct extension to multi-slice acquisition as they perturb the magnetization in adjacent slices. Also, the chemical shift displacement artifacts associated with localization at ultra-high field makes the use of traditional refocusing pulses undesired, adiabatic (13)or spatial-spectral pulses (11-12) might overcome this issue, however only with long pulse durations, leading to long echo times. In addition, the significant RF power deposition associated with refocusing and water and lipid suppression for these 2D/3D methods does typically prevent the extension to multiple interleaved slices due to SAR concerns. This is especially true when high-BW adiabatic inversion or refocusing pulses are used for suppression or localization.

Therefore, in this work low-power water and lipid suppression was developed and combined with a pulse-acquire MRSI acquisition to minimize the number of RF pulses, and to allow for a short effective TR as required for multi-slice MRSI. The SNR of the measurement was maximized by using a pulse acquire acquisition with a very short echo time and a multi-element transceiver array. Multi-slice MRSI of the brain was shown to be feasible within a reasonable scan time and with minimal chemical shift displacement artifacts by using dynamic B_0 and B_1^+ optimization. MRSI was performed on five axial slices, where both the B_0 and B_1^+ fields were optimized on a slice-by-slice basis. All B_0 and B_1^+ settings were switched to the appropriate values during the sequence before every RF pulse.

Third order dynamic updating of the B_0 shim fields has been shown to improve the magnetic field homogeneity over the five slices compared to a global optimization strategy, to a degree that is comparable to static fourth order shimming. Slice based shim

updating was applied in a multi-slice sequence, and can be extended to more slices or be combined with multi-stack 3D acquisitions. It is however limited to sequences where multiple volumes are simultaneously examined. But even if a single volume is excited, dynamic shim updating allows for optimization of the B_0 and B_1 field for water or lipid suppression pulses, independent of the excitation. After slice based shim updating in certain regions, the B_0 magnetic field homogeneity is still not perfect. Especially above the nasal cavity, considerable B_0 magnetic field residuals remained. These distortions could not be compensated with the shallow zero-through-third order spherical harmonic fields, and more sophisticated shim systems are required to also improve field homogeneity in these regions (21-22). However, slice-based DSU maximizes the usefulness of conventional spherical harmonic shim systems.

Bloch-Siegert B_1^+ mapping in combination with short TE gradient echo images was used for RF shimming on a slice-by-slice basis. The high accuracy and large dynamic range of this method allowed for reproducible B_1^+ mapping and RF shimming. However, as the current B_1^+ mapping method required up to 10 minutes of acquisition time, image acceleration techniques might be employed to reduce the calibration time of the transmit settings. Slice-based RF shimming improved the overall homogeneity of the nutation angle distribution as compared to a single-slice RF shim optimization. Especially the lower and upper slices of the volume benefited significantly from a slice-based optimization strategy. Further gain is expected when the slice coverage is increased to approach the physical dimensions of the RF transceiver array.

For optimization of the water suppression, a fixed effective TR of 500 ms was used which represents a reasonable compromise between T_1 saturation and experiment duration for the typical brain metabolites (TR=5×500ms). A further reduction of the effective TR is possible, but requires a re-optimization of the delays and powers of the water suppression pulses. In addition, less conservative settings for RF power deposition might be applied since the local heat hotspots may be distributed more than was assumed here because of the differences in RF shim settings used for the different slices (23). Careful assessments of these calculations, along with an *in vivo* validation, as well as more advanced TX array coil design or RF shimming strategies with simultaneous SAR minimization might further increase the number of slices that can be acquired per unit of time.

Lipid suppression was performed with an RF shimmed ring-mode, where the extra-cranial lipids in the slice were saturated with only a single low power RF pulse, relieving much of the RF power deposition which is usually required for lipid suppression. To make the lipid suppression less sensitive to the steep drop off in B_1^+ close to the transmit coils, four pulses were used with optimized delays and RF powers. However, as with most lipid suppression techniques, there is a tradeoff between adequate lipid suppression and saturation of the metabolites in the outer part of the cortex. Future development of transmit arrays (e.g. more than eight elements) will potentially allow for an even sharper transition zone between extra cranial lipids and brain tissue in the slice. Suppression maps (figure 5) were measured, and can be used retrospectively for data normalization or data rejection.

The acquisition delay, which is inherent to a pulse-acquire approach, is known to cause a first-order phase over the spectra in the frequency domain. The acquisition delay does not pose a problem for spectral quantification, since it can be incorporated into the metabolite basisset as prior knowledge (7). However, for displaying purposes a correction was applied by making an HSVD fit to the time domain signal and consecutive back extrapolation of the missing first data points. The remaining baseline that is seen in the spectra is due to the very short T_2 components mainly originating from macromolecules (24) since this short echo time sequence significantly enhances these resonances. For accurate quantification of the metabolite concentrations, a reliable estimation of this macromolecular baseline is essential (25), especially since at ultra-high field these macromolecules are very well resolved from one another (26). This macromolecular baseline can be included in the quantification algorithm, as is readily done for short TE single-voxel MRS either by simulation or measurement of these macromolecular compounds. Measurements of the macromolecular compounds has been shown to be more accurate than mathematical modeling (27) and these measurements are generally performed by inserting an additional (preferably adiabatic) inversion pulse prior to the excitation in order to null the metabolite signals. However, inserting such a high BW inversion pulse into the multi-slice MRSI sequence would greatly increase the power deposition, rendering it a multi-slice application at short TR impossible. A different strategy for macromolecular estimation must therefore be developed before accurate metabolic fitting can be performed, which is beyond the scope of this paper.

In conclusion, multi-slice MRSI of the human brain has been demonstrated at ultra-high field. B_0 and B_1^+ homogeneity was optimized on a slice-by-slice basis with slice-based DSU and pulse specific RF shimming with an eight channel transceiver array. Low-power lipid suppression based on RF shimming and low-power water suppression in the steady-state were employed in a five slice MRSI sequence for metabolic profiling of large areas of the human brain at ultra-high field within a reasonable scan time.

4.5 Acknowledgements

This research was supported by NIH grants R01 EB000473, R42 RR031457 and P30 NS052519.

References

1. Koch KM, McIntyre S, Nixon TW, Rothman DL, de Graaf RA. Dynamic shim updating on the human brain. J Magn Reson 2006;180:286-296.
2. Juchem C, Nixon TW, Diduch P, Rothman DL, Starewicz P, de Graaf RA. Dynamic Shimming of the Human Brain at 7 Tesla. Concepts Magn Reson 2010;37B:116-128.
3. Mao W, Smith MB, Collins CM. Exploring the limits of RF shimming for high-field MRI of the human head. Magn Reson Med 2006;56:918-922.
4. Boer VO, Voogt I, van de Bank BL, Kroeze H, van den Berg CAT, van Lier AL, Raaijmakers A, Luijten PR, Klomp DWJ. Ultra high field 1H-MRS: outer volume suppression by local excitation. In: Proceedings of the ESMRMB. Antalya, Turkey; 2009. p 74.
5. Hetherington HP, Avdievich NI, Kuznetsov AM, Pan JW. RF shimming for spectroscopic localization in the human brain at 7 T. Magn Reson Med 2010;63:9-19.
6. Katscher U, Börnert P, Leussler C, van den Brink JS. Transmit SENSE. Magn Reson Med 2003;49:144-150.
7. Henning A, Fuchs A, Murdoch JB, Boesiger P. Slice-selective FID acquisition, localized by outer volume suppression (FIDLOVS) for 1H-MRSI of the human brain at 7 T with minimal signal loss. NMR Biomed 2009;22:683-696.
8. Boer VO, Siero JC, Hoogduin H, van Gorp JS, Luijten PR, Klomp DW. High-field MRS of the human brain at short TE and TR. NMR Biomed 2011. In press, DOI 10.1002/nbm.1660
9. Balchandani P, Spielman D. Fat suppression for 1H MRSI at 7T using spectrally selective adiabatic inversion recovery. Magn Reson Med 2008;59:980-988.
10. Avdievich NI, Pan JW, Baehring JM, Spencer DD, Hetherington HP. Short echo spectroscopic imaging of the human brain at 7T using transceiver arrays. Magn Reson Med 2009;62:17-25.
11. Balchandani P, Pauly J, Spielman D. Interleaved narrow-band PRESS sequence with adiabatic spatial-spectral refocusing pulses for 1H MRSI at 7T. Magn Reson Med 2008;59:973-979.
12. Xu D, Cunningham CH, Chen AP, Li Y, Kelley DA, Mukherjee P, Pauly JM, Nelson SJ, Vigneron DB. Phased array 3D MR spectroscopic imaging of the brain at 7 T. Magn Reson Imaging 2008;26:1201-1206.
13. Scheenen TW, Heerschap A, Klomp DW. Towards 1H-MRSI of the human brain at 7T with slice-selective adiabatic refocusing pulses. MAGMA 2008;21:95-101.
14. Pauly J, Le Roux P, Nishimura D, Macovski A. Parameter relations for the Shinnar-Le Roux selective excitation pulse design algorithm. IEEE Trans Med Imaging 1991;10:53-65.
15. Natt O, Bezkorovaynyy V, Michaelis T, Frahm J. Use of phased array coils for a determination of absolute metabolite concentrations. Magn Reson Med 2005;53:3-8.
16. Ogg RJ, Kingsley PB, Taylor JS. WET, a T1- and B1-insensitive water-suppression method for in vivo localized 1H NMR spectroscopy. J Magn Reson B 1994;104:1-10.

17. Rooney WD, Johnson G, Li X, Cohen ER, Kim SG, Ugurbil K, Springer CS, Jr. Magnetic field and tissue dependencies of human brain longitudinal 1H2O relaxation in vivo. Magn Reson Med 2007;57:308-318.
18. Silver MS, Joseph RI, Hoult DI. Highly selective [pi]/2 and [pi] pulse generation. Journal of Magnetic Resonance 1984;59:347-351.
19. Sacolick LI, Wiesinger F, Hancu I, Vogel MW. B1 mapping by Bloch-Siegert shift. Magn Reson Med 2010;63:1315-1322.
20. van den Boogaart A, van Ormondt D, Pijnappel WWF, de Beer R, Ala-Korpela M. Mathematics and Signal Processing III. McWhirter JG, editor. Oxford: Clarendon Press; 1994.
21. Juchem C, Nixon TW, McIntyre S, Rothman DL, de Graaf RA. Magnetic field homogenization of the human prefrontal cortex with a set of localized electrical coils. Magn Reson Med 2010;63:171-180.
22. Juchem C, Nixon TW, McIntyre S, Boer VO, Rothman DL, de Graaf RA. Dynamic Multi-Coil Shimming of the Human Brain at 7 Tesla. Journal of Magnetic Resonance 2011 In Press. doi:10.1016/j.jmr.2011.07.005
23. Tang L, Hue YK, Ibrahim TS. Studies of RF Shimming Techniques with Minimization of RF Power Deposition and Their Associated Temperature Changes. Concepts Magn Reson Part B Magn Reson Eng 2011;39B:11-25.
24. Behar KL, Rothman DL, Spencer DD, Petroff OA. Analysis of macromolecule resonances in 1H NMR spectra of human brain. Magn Reson Med 1994;32:294-302.
25. Pfeuffer J, Tkac I, Provencher SW, Gruetter R. Toward an in vivo neurochemical profile: quantification of 18 metabolites in short-echo-time 1H NMR spectra of the rat brain. J Magn Reson 1999;141:104-120.
26. Otazo R, Mueller B, Ugurbil K, Wald L, Posse S. Signal-to-noise ratio and spectral linewidth improvements between 1.5 and 7 Tesla in proton echo-planar spectroscopic imaging. Magn Reson Med 2006;56:1200-1210.
27. Gottschalk M, Lamalle L, Segebarth C. Short-TE localised 1H MRS of the human brain at 3 T: quantification of the metabolite signals using two approaches to account for macromolecular signal contributions. NMR Biomed 2008;21:507-517.

Chapter 5

Direct B_0 field monitoring and real-time B_0 field updating in the human breast at 7T

Magnetic Resonance in Medicine; in press

V.O. Boer[1]; B.L. vd Bank[1], G. van Vliet[2], P.R. Luijten[1], D.W.J. Klomp[1]

[1.] *Department of Radiology, University Medical Center Utrecht, The Netherlands*
[2.] *Image Science Institute, University Medical Center Utrecht, The Netherlands*

Abstract

Large dynamic B_0 fluctuations are observed in the human body during MR scanning, compromising image quality and detection sensitivity in several MR imaging and spectroscopy sequences. Partially, these dynamic B_0 fluctuations are due to physiological motion such as breathing, but also other sources of temporal B_0 field fluctuations are present in the MR system (e.g. eddy currents). Especially at ultra high field (≥7T) the increased susceptibility effects lead to large B_0 field variations over time. Direct measurement and correction of these temporal field variations of up to 70 Hz will lead to a significant reduction of artifacts and improved measurement stability/reproducibility. For direct measurement of the temporally changing B_0 field, a simple field probe was developed, that was placed in proximity to the tissue of interest. In this work it is shown how such a field probe system can be used to monitor temporal B_0 field variations in the human body during MRI and MRS. Furthermore, it is shown how the acquired temporal B_0 field information can drive a dynamic shim module to directly correct the B_0 magnetic field in real-time.

5.1 Introduction

B_0 field variations, and the resulting phase and frequency variations during MRI and MRS sequences, can lead to a range of artifacts, including ghosting, signal loss, phase corruption and line broadening. Several sources of dynamic field variations during routine MRI scanning can be identified, and are either attributed to scanner instability (e.g. eddy currents and drift) or motion of the body, and the consequently changing susceptibility distribution in the magnet. Expansion of the chest during breathing causes severe artifacts in tissue close to the chest, such as the breast (1), but it also affects imaging in body parts at further distance. In fact, breathing induced phase changes are currently a limiting factor in high resolution imaging of the brain (2). However, breathing is not the only source of these spatio-temporal field variation. Also cardiac pulsation (3) and motion of the extremities (4) can be a limiting factor in accurate MR image acquisition. Since susceptibility effects scale with field strength, extreme field variations are expected at ultra high field (≥7T) resulting in uncontrolled frequency alterations. B_0 field variations of several hertz in the brain (2,5) and up to 40 Hz in the breast have been reported (6,7) at ultra high field. If not corrected for, these B_0 fluctuations lead to problems with localization and non-Lorentzian line broadening in MRS (8), and can cause severe signal loss or ghosting artifacts, for example in susceptibility weighted imaging (2,4), fMRI (9), temperature measurements (3), phase based perfusion imaging (10), spectroscopic imaging or spectral editing.

Several strategies have been reported for correction of dynamic B_0 field shifts, including triggering/gating on the respiration, correcting using a pre-calibrated respiratory belt (2), navigator acquisitions in the sequence (11,12) and retrospective spectral alignment in ^{1}H MRS based on residual water signal (13). However, the use of triggering or gating will in general lengthen the scan time, while additional navigator acquisitions require careful sequence design, can interfere with data acquisition and influence the steady state signal. Breathing monitoring with a respiratory belt can be used to correct for breathing induced field variation, however it does not allow for correction of field variations caused by cardiac motion, scanner drift or eddy currents. Also a calibration procedure is required for respiratory compensation, and changing breathing patterns or any other type of motion might compromise the ability to correct the local resonance frequency. Retrospective correction based on an internal reference signal in the spectrum can be a good option for single-voxel ^{1}H MRS, provided that sufficient SNR is available in every acquisition, as was shown by Bolan et al in the human breast using the (residual) water signal (8). This is however not an option for spectroscopic imaging or for MRS of low sensitivity nuclei (such as ^{31}P), where no reference signal is observable in each shot. Also it cannot be extended to correct for B_0 shim variations during scanning. A general and direct B_0 measurement, independent of the MRI or MRS sequence, that can monitor the temporal B_0 field variations during scanning similar to a field-frequency lock on high resolution NMR systems (17) is therefore preferable for several MR sequences applied in the human body.

Recently, external field probes have been proposed as a way to monitor spatio-temporal magnetic fields in an MR scanner for gradient calibrations and eddy current corrections (14). This work extends that concept, in order to use external field monitoring to measure temporal field variation in the human body during MR experiments to correct for the varying B_0 magnetic field resulting mainly from physiological motion. By using a simple field probe in close proximity to the human breast we show how it is possible to perform dynamic B_0 field corrections and demonstrate the dramatic line shape improvement for ^{1}H MR spectroscopy in the human breast. Also, by incorporating a dynamic shim control module into the system, it is shown how the B_0 field information can be used to correct the B_0 field in real-time.

5.2 Methods

Experiments were performed with a whole body 7T MRI system (Philips, Cleveland, OH, USA), using a home-build dedicated unilateral breast trancieve coil consisting of two perpendicular loops (figure 1) which were both double tuned to the ^{1}H and ^{31}P frequency to allow for both ^{1}H and ^{31}P imaging and spectroscopy (15). The two perpendicular loop coils were driven in quadrature mode. A regular pressure band was used to monitor the breathing pattern during experiments. The subjects were positioned in a prone, head first

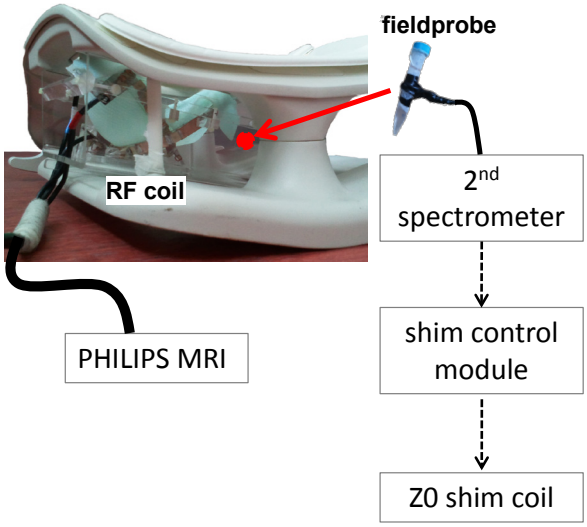

Figure 1: MR setup with the unilateral breast coil and the field probe, which was interfaced to a 2nd spectrometer. For the real-time field correction the 2nd MR-spectrometer was interfaced to a hardware shim control unit that was able to update the Z0-coil current.

position. All measurements were carried out in compliance with the local institutional medical ethics committee guidelines.

To investigate the spatio-temporal field variations that are present in the breast at 7T, a series of fast 2D gradient echo scans was performed on a coronal slice through the human breast (TR = 10 ms, TE = 1.97 ms, matrix = 64×48). The B_0 field offset (ΔB_0) was calculated from the temporal phase information ($\phi(t)$):

$$\Delta B_0 = \frac{\phi(t) - \phi(0)}{\gamma TE}$$

The impact of B_0 field correction with the Z0 shim field on these temporal B_0 field maps was simulated by subtracting the average B_0 field from every field map.

To monitor B_0 field fluctuations during MR measurements with a B_0 field probe, a small NMR transceiver coil was placed medially next to the breast coil. This B_0 field probe was designed as a Helmholtz pair wound on a 1 cm diameter cylinder containing 2,2,2 trifluoroethanol. The field probe was tuned to the ^{19}F frequency for 7T and interfaced to a separate spectrometer to allow for independent field monitoring during MRI/MRS scanning. Although the 2,2,2 trifluoroethanol resonance results in a multiplet, the signal was considered as a single frequency since J-coupling evolution during the short readout is very small.

The field variation during the MR measurements was monitored with the B_0 field probe by fast, non-localized pulse-acquire measurements on the ^{19}F resonance frequency. 32 complex data points were acquired at a 4 kHz bandwidth (8 ms readout) directly after a 200 μs hard pulse. A least squares fit of the phase of the FID in the time domain was performed to estimate the local frequency (f) according to $f = d\phi/dt$.

B_0 field correction was performed in two ways; retrospectively and in real-time. The field probe system was either continuously probing the B_0 field (TR=10ms), or at discrete time intervals as dictated by the MRI system via a TTL pulse. Data was discarded if the X,Y,Z gradients of the system were switched on. Data was stored to disk either to be used for retrospective correction, or for real-time B_0 field updating of the MR system. In order to correct for B_0 field variations during the measurement in real-time, the second spectrometer was interfaced to a hardware shim control module ('Load & Go Real Time Shims RTS', Resonance Reasearch Inc., Billerica, MA, USA) which was interfaced to the shim coils in the MR system. Since information of a single field probe was available, only the current in the Z0 coil was adapted for real-time field control, independent of the MR system. Directly after data acquisition on the field probe, the complex MR data was saved to disk, and processed with a MATLAB (The Mathworks, Natick, MA, USA) routine that performed a fit of the frequency and send the updated current to the shim control module over RS232. Switching the Z0 coil during MR measurements might cause additional eddy currents which compromise the field correction approach proposed here. Therefore a measurement of the eddy currents induced by switching of the Z0 coil was performed similar to the method described by Juchem et al. (16), leading to the observation that no

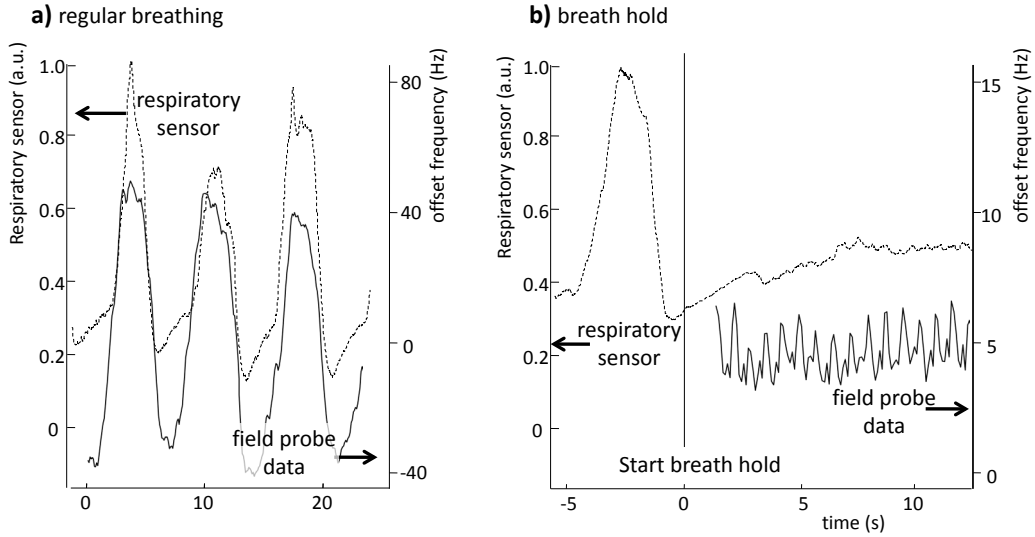

Figure 2: Field measurement from the ^{19}F field probe (solid line) data during regular breathing (a) shows large variations in the measured offset field, however this does not correspond one-on-one to signal from the respiratory belt (dotted line). During a breath hold (b) smaller and faster field variations, which are possibly caused by cardiac pulsation.

eddy currents of longer than 5 ms were present in the system while switching the actively shielded Z0 shim coil.

To demonstrate the B_0 field correction based on the independent field probe, localized single-shot ^1H MRS experiments (STEAM, TE = 7 ms, voxelsize = 1 cm^3, TR = 2 s) were performed in the glandular tissue in the human breast. Static shimming was performed with second order spherical harmonic terms, which were calculated as a least squares fit to a B_0 field map in the voxel of interest (TR/TE1/TE2 = 5.2/3.0/4.0 ms, FOV = 240×180×60 mm^3, voxel size = 3×3×3 mm^3, scan duration = 16.3 s). To separate possible effects of motion of the breast from non-local susceptibility effects caused by breathing etc, healthy female as well as male subjects were scanned, where in the latter case a water phantom was placed in the coil. In this way there was no direct contact between the male subject and the phantom, and the resulting observed B_0 field variation were therefore attributed to non-local susceptibility effects as caused by physiologic motion and scanner instabilities.

5.3 Results

Field monitoring with a field-probe resulted a high SNR reference signal for data correction and real-time updating of the B_0 field. The signal-to-noise ratio of the acquired FID on the ^{19}F frequency was typically >500 for all data points of the FID. The measurement accuracy was assessed from a series of static measurements (no subject in the bore) to be 0.17 Hz (standard deviation). With the ^{19}F field probe unit, the B_0 field could be measured during regular breathing (figure 2a) and shows to correlate to some extent with the signal from the respiratory belt. Even more rapid field variations, possibly caused by cardiac motion can be observed during a breath hold (figure 2b).

B_0 field variations measured in the human breast showed to reach up to 70 Hz over time (figure 3a), but can be reduced by an order of magnitude with field correction (figure 3b). In ^1H MRS measurements on a water phantom, with a male subject lying on the coil, field variations of up to 100 Hz were observed during regular breathing (figure 4b) reducing the water resonance peak to a broad hump (figure 4c). The male subject was not touching the

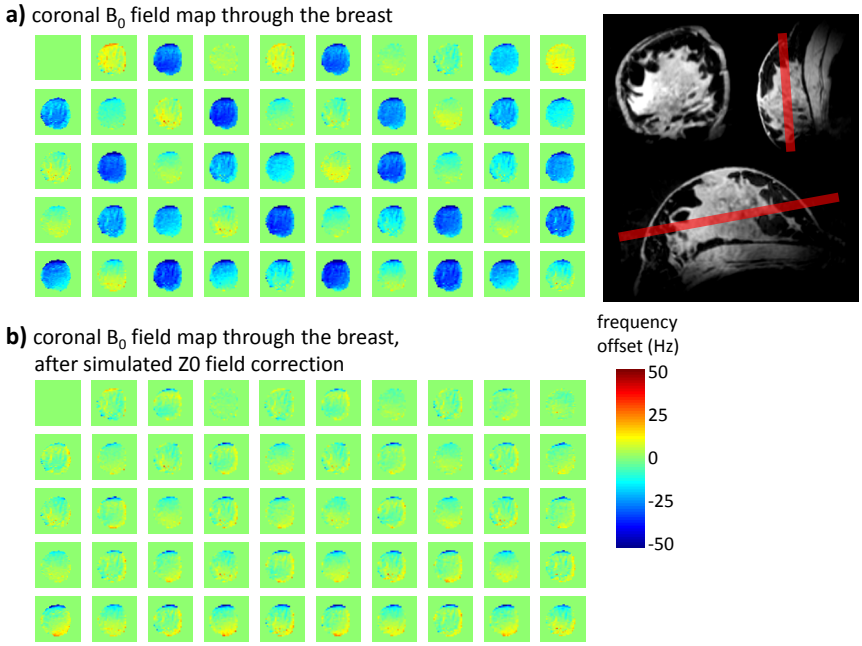

Figure 3: Observation of the B_0 field fluctuations in the human breast as measured by fast 2D MR imaging (scan interval = 480 ms). Field fluctuations show to easily exceed 50 Hz (a) over short time intervals. By subtracting the mean frequency variation over the slice, the residual B_0 field variations can be greatly reduced (b), indicating that retrospective or real-time frequency correction of the Z0 field can greatly improve the B_0 field stability in the human breast.

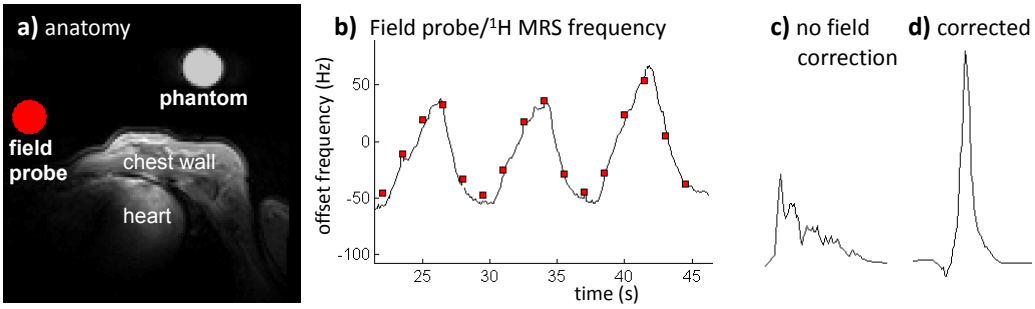

Figure 4: Retrospective frequency correction of the signal from a water phantom placed under the chest of a male subject lying on the breast coil (a). Large frequency variations are seen in the water signal from the phantom due to non-local effects caused mainly by breathing and cardiac pulsation. Field probe data was acquired continuously (b, continuous line), and 32 short TE ^{1}H MRS measurements were performed (b, red squares). The ^{1}H MRS spectra were saved individually and retrospective frequency corrected with the field-probe data (d) leading to a large SNR gain compared to the non-corrected spectrum (c).

phantom, indicating that the field variations are indeed caused by non-local physiological effects such as breathing. During ^{1}H MRS in the glandular tissue in the human breast, B_0 field deviations were observed up to 70 Hz (figure 5b), which exceeded the water line width, leading to significant SNR loss and even to a splitting of the water peak (figure 5c).

Retrospective field correction of the ^{1}H MRS data was performed by simultaneous, continuous measurement of the B_0 field with the ^{19}F field probe. Retrospective correction shows to greatly improve signal intensity and restore the expected line shape of the water signal (figure 4c).

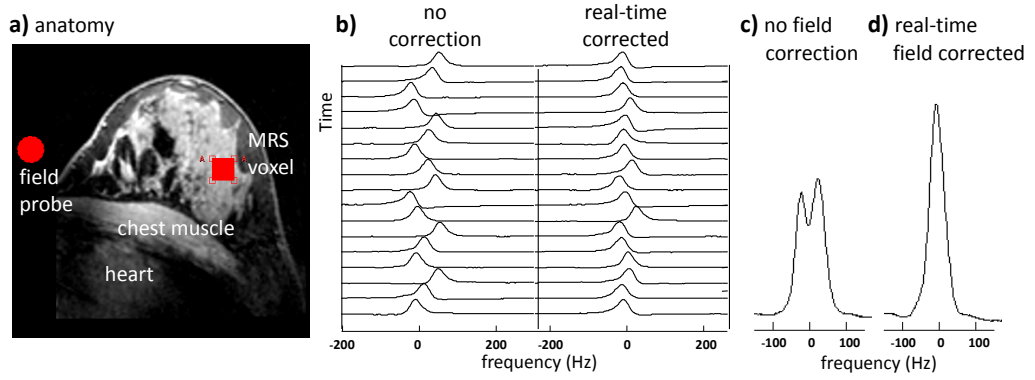

Figure 5: Real-time in vivo frequency correction in the glandular tissue in the human breast. Real-time correction of the B_0 field shows a large improvement in frequency stability (b). The summed result (d) shows a significant line shape and SNR improvement over the uncorrected data (c).

Real-time correction of the B_0 field was performed by triggering a B_0 field update, which measures the B_0 field on the field probe and controls the Z0 shim field, starting a measurement 200-150 ms before the ^{1}H MRS acquisition. This delay was required for signal acquisition (8 ms), data storage and reading on the console (100 ms), data processing (20 ms) and RS232 communication (10 ms) between the console and the shim control module. Since no eddy currents of more than 5 ms were observed with the Z0 channel, eddy current compensation of this channel was not applied. Real-time field correction on a phantom with a male subject on the coil showed to reduce field variations from 50 Hz to 8 Hz (data not shown). Real-time field correction with the field probe measurements and Z0 updating reduced the uncontrolled field variance, leading to a better defined signal and significant SNR increase in single voxel ^{1}H MRS measurement in the glandular tissue of a healthy female subject (figure 5c).

5.4 Discussion

A temporally changing B_0 magnetic field can lead to a range of artifacts in MR imaging and spectroscopy, if not corrected for. In this work the temporally changing B_0 magnetic field, which is mainly caused by physiological motion and hardware instabilities, was analyzed. During MR scanning, the B_0 magnetic field was directly monitored by means of an external B_0 field probe operating at the ^{19}F frequency. This allowed for the direct, fast and independent acquisition of B_0 field information and consequently enabled retrospective or even real-time field correction.

To demonstrate the use of a B_0 field probing and updating system, an application to the human breast at 7T was shown. Uncontrolled magnetic field fluctuations measured in the human breast at 7T showed to greatly exceed the variations measured previously in the human brain at 7T (2) due to the close proximity to the lungs. As expected, these fluctuations are increased compared to measurements performed in the breast at 4T (10) due to increased susceptibility effects at higher static B_0 magnetic field. The dynamic field variations were shown to correlate partially with data from a respiratory sensor, however the breathing pattern observed by the sensor is a sum of several components, with at least two degrees of freedom of the diaphragm and the intercostals. Therefore the resulting B_0 field variation is difficult to characterize with information from a respiratory sensor alone. In addition, B_0 field variation in the breast might also be caused by the heartbeat and possibly also from magnetic field instabilities that are subject-independent (e.g. eddy currents). The observed B_0 field variations cause field fluctuations of up to 70-100 Hz in the breast and seem to be mainly caused by respiration, which, if not corrected for, can lead to a range of artifacts depending on the MRI/MRS sequence. In this work the improvement on line shape in ^{1}H-MR spectroscopy has been shown, but B_0 field correction is expected to be beneficial in any MRI or MRS sequence that is sensitive to the local resonance frequency,

such as sequences with lipid or water suppression, multi-shot EPI, or long TE gradient echo sequences such as susceptibility weighted imaging.

Various ways of B_0 field correction have been reported in literature, including interleaved navigator acquisitions, respiratory induced B_0 field compensation using a respiratory belt, and various ways of triggered or gated data acquisition. Unfortunately, navigator acquisitions can interfere with the MR sequence, might increase scan time and/or saturate the signals of interest. Furthermore they require complex pulse sequence design for every individual sequence. Respiratory monitoring for B_0 field correction does not interfere with the MR measurement, however it requires a subject-specific calibration measurement, where the frequency as a function of belt expansion is recorded with fast MR imaging. This makes it an indirect correction technique, and apart from a changing breathing pattern after calibration, it does not allow for correction of other sources of B_0 field variations such as eddy currents or scanner drift. Also triggering or gating of the data acquisition allows for artifact free data acquisition, however it increases scan time and compromises steady state acquisitions.

Monitoring the B_0 field variations over time with a field probe does allow for a direct and independent way of monitoring the B_0 field during any MRI sequence. Both retrospective and real-time correction of the MR signal show to greatly improve the stability of the MR acquisition. Applications are found in sequences which are sensitive to the resonance frequency, such as ^{1}H MRS and long TE imaging where both real-time corrections and post-processing techniques can be used for signal recovery and artifact reduction. Especially in the case when frequency selective RF pulses are used, such as in chemical shift selective suppression or editing, a stable Larmor frequency is essential, and real-time B_0 field corrections may be the only way of achieving that goal.

The B_0 field in the breast was monitored with a field probe placed medially to the breast, which was operating at the ^{19}F frequency and was interfaced to a separate spectrometer. Therefore the field monitoring system had minimal interaction with the ^{1}H and ^{31}P RF paths of the original MR system.

Real-time correction of the B_0 field was performed by triggering the field correction system before ^{1}H MRS acquisition. A delay of approximately 150-200 ms was required for data acquisition, data handling and Z0 updating where data handling on the additional MR console was the slowest step in the process. No further attempts were made to speed up data handling since the method was at this point fast enough to compensate the slowly varying fields as caused by breathing. Fast varying fields, possibly caused by cardiac motion, were not corrected for in real-time here due to the delay between the B_0 field measurement and Z0 field update. The residual field variation over time (figure 5) after real-time correction was caused by alterations in the magnetic field that exceeded the temporal resolution of the real-time interface, but also by the spatial mismatch between the field probe and the voxel of interest. The first effect can be minimized by hardware and software optimization to speed up the correction protocol. At this point, 150-200 ms was required, mainly caused by software restriction in data transfer between the spectrometer and the Matlab routine.

However this might be optimized to a point where data acquisition is the slowest step in the process. To correct for the latter effect, which is caused by a spatially changing magnetic field over time, real-time higher order dynamic shimming will be required. At 4T it was shown that there is a linear term that changes over time during breathing, especially close to the chest wall and in the muscle tissue (8). Therefore the next step in real-time field updating will be to correct temporally and spatially varying B_0 fields with first, and possibly second or third order shimming. The method described here for updating the Z0 shim coil with a single field probe, can be readily extended by employing multiple field probes on specific points in space (17) in combination with hardware eddy current pre-emphasis on all shim channels on the MR system (16) or perhaps by using software compensation of high order eddy currents (18).

Retrospective, as well as real-time correction of ^{1}H-MR spectroscopy data in a voxel placed close to the chest showed a significant improvement in SNR and line shape using the data obtained from a single field probe. Using Z0 field corrections only, temporal field variations of up to 100 Hz could be significantly reduced, even in real-time. Therefore, field probed control of the B_0 magnetic field stability can be used to improve stability and performance in MR acquisitions.

5.5 Acknowledgements

We would like to thank dr. Barmet of the ETH in Zurich for helpful discussion on building the field probe. In addition, the Dutch Scientific Organization (NWO 40-00506-98-11001, VENI-DK-916.10.163) is acknowledged for financial support.

References

1. Haddadin IS, McIntosh A, Meisamy S, Corum C, Styczynski Snyder AL, Powell NJ, Nelson MT, Yee D, Garwood M, Bolan PJ. Metabolite quantification and high-field MRS in breast cancer. NMR Biomed 2009;22:65-76.
2. van Gelderen P, de Zwart JA, Starewicz P, Hinks RS, Duyn JH. Real-time shimming to compensate for respiration-induced B0 fluctuations. Magn Reson Med 2007;57:362-368.
3. Peters NHGM, Bartels LW, Sprinkhuizen SM, Vincken KL, Bakker CJG. Do respiration and cardiac motion induce magnetic field fluctuations in the breast and are there implications for MR thermometry? J Magn Reson Imaging 2009;29:731-735.
4. Versluis MJ, Peeters JM, van Rooden S, van der Grond J, van Buchem MA, Webb AG, Osch MJP. Origin and reduction of motion and f0 artifacts in high resolution T2*-weighted magnetic resonance imaging: application in Alzheimer's disease patients. Neuroimage 2010;51:1082-1088.
5. Van de Moortele P-F, Pfeuffer J, Glover GH, Ugurbil K, Hu X. Respiration-induced B0 fluctuations and their spatial distribution in the human brain at 7 Tesla. Magn Reson Med 2002;47:888-895.
6. Bolan PJ, Snyder CJ, DelaBarre LJ, Bolinger L, Garwood M, Vaughan JT. Preliminary experience with breast 1H MRS at 7 Tesla. In: Proceedings of the 14th Annual Meeting of ISMRM, Seattle, USA, 2006. p 580.
7. Bank BL van de, Boer VO, Luttje MP, Wijnen JP, van Vliet G, Hoogduin JM, Luijten PR, Klomp DWJ. Frequency correction for MR Spectroscopy in the human breast at 7 Tesla with external field monitoring. In: Proceedings of the 19th Annual Meeting of ISMRM, Montreal, Canada. 2011. p 646
8. Bolan PJ, Henry P-G, Baker EH, Meisamy S, Garwood M. Measurement and correction of respiration-induced B0 variations in breast 1H MRS at 4 Tesla. Magn Reson Med 2004;52:1239-1245.
9. Reese TG, Heid O, Weisskoff RM, Wedeen VJ. Reduction of eddy-current-induced distortion in diffusion MRI using a twice-refocused spin echo. Magn Reson Med 2003;49:177-182.
10. Korporaal JG, van den Berg CAT, van Osch MJP, Groenendaal G, van Vulpen M, van der Heide UA. Phase-based arterial input function measurements in the femoral arteries for quantification of dynamic contrast-enhanced (DCE) MRI and comparison with DCE-CT. Magn Reson Med 2011; Epub ahead of print. DOI: 10.1002/mrm.22905
11. Henry PG, van de Moortele PF, Giacomini E, Nauerth A, Bloch G. Field-frequency locked in vivo proton MRS on a whole-body spectrometer. Magn Reson Med 1999;42:636-642.
12. Thiel T, Czisch M, Elbel GK, Hennig J. Phase coherent averaging in magnetic resonance spectroscopy using interleaved navigator scans: compensation of motion artifacts and magnetic field instabilities. Magn Reson Med 2002;47:1077-1082.

13. Helms G, Piringer A. Restoration of motion-related signal loss and line-shape deterioration of proton MR spectra using the residual water as intrinsic reference. Magn Reson Med 2001;46:395-400.
14. De Zanche N, Barmet C, Nordmeyer-Massner JA, Pruessmann KP. NMR probes for measuring magnetic fields and field dynamics in MR systems. Magn Reson Med 2008;60:176-186.
15. Klomp DWJ, van de Bank BL, Raaijmaker A, Korteweg MA, Possanzini C, Boer VO, van de Berg CAT, van de Bosch MAAJ, Luijten PR. Phosphorus MRSI and proton MRS at 7 Tesla: initial results in human breast cancer. NMR Biomed 2011; Epub ahead of print. DOI: 10.1002/nbm.1696
16. Juchem C, Nixon TW, Diduch P, Rothman DL, Starewicz P, De Graaf RA. Dynamic shimming of the human brain at 7 T. Concepts Magn Reson 2010;37(B):116-128.
17. Barmet C, De Zanche N, Wilm BJ, Pruessmann KP. A transmit/receive system for magnetic field monitoring of in vivo MRI. Magn Reson Med 2009;62:269-276.
18. Sengupta S, Avison MJ, Gore JC, Brian Welch E. Software compensation of eddy current fields in multislice high order dynamic shimming. J Magn Reson 2011;210:218-227.

Chapter 6

Efficient spectral editing at 7T: GABA detection with MEGA-sLASER

Magnetic Resonance in Medicine; in press

A. Andreychenko[1,2], V.O. Boer[1], C.S. Arteaga de Castro[1,2], P.R. Luijten[1], D.W.J. Klomp[1]

[1.] *Department of Radiology, University Medical Center Utrecht, Utrecht, The Netherlands*
[2.] *Department of Radiotherapy, University Medical Center Utrecht, Utrecht, The Netherlands*

Abstract

At high field (7T) spectral editing of γ-Aminobutyric acid (GABA) with MEGA-point-resolved spectroscopy (MEGA-PRESS) is inefficient due to the large chemical shift displacement error (CSDE). In this paper, a new pulse sequence is designed which has minimal CSDE to perform an efficient spectral editing of the GABA 3.0 ppm resonance at 7T. The sequence consists of the conventional MEGA editing pulses and a semi-localized by adiabatic selective refocusing sequence (sLASER). Phantom and *in vivo* measurements demonstrated an efficient detection of GABA. Using ECG triggering, excellent *in vivo* performance of the MEGA-sLASER provided well-resolved GABA signals in 27 ml volumes in the human brain at an echo time (TE) of 74 ms within a relatively short acquisition time (5 min). Furthermore, the high efficiency of the MEGA-sLASER was demonstrated by acquiring small volumes (8 ml) at an echo time (TE) of 74 ms, and long TE measurements (222 ms in 27 ml volume).

6.1 Introduction

The *in vivo* detection of some metabolites in the human brain with ^{1}H MRS is challenging due to low SNR and overlap with more concentrated metabolites (i.e. choline, creatine, NAA) and macromolecules. However, the J-coupling behavior can be used for several less concentrated molecules to distinguish their signals from overlapping non-coupled signals. Several techniques have been proposed to separate the dominant signals from the signal of interest. These techniques include: echo-time optimization (1), spectral editing (2-3), homonuclear transfer (4), 2D MRS (5-6), multiple quantum filters (7-8), and using prior knowledge in data processing like LCModel as shown in CSI experiments (9-10). All of these techniques require a high efficiency as the signals from the target metabolites are low. In addition, most of these techniques rely on subtraction or phase encoding, which data include high signals from other metabolites, therefore, are prone to potential artifacts. An efficient and stable measurement setup is required to achieve a robust *in vivo* quantification of the weak target signals. In this work we focus on J-difference spectral editing at high field (7T) for detection of the 3.0 ppm resonance of γ-Aminobutyric acid (GABA). GABA is the dominant inhibitory neurotransmitter in the human brain, and a variety of neurological and psychiatric disorders is believed to be associated with changes of GABA concentration levels (11). However, the robust *in vivo* detection of GABA levels in the human brain is challenging due to the low concentration (1-2 mM) and the overlap of all GABA resonances with more intense compounds, such as creatine (4.5-10.5 mM), glutamate (6-12.5 mM), NAA (7.5-17 mM) and several macromolecules, making direct detection difficult (12-13).

The GABA molecule has three CH_2 groups which resonate at 1.9, 2.3 & 3.0 ppm. The 3.0 and 1.9 ppm resonances couple to each other (J≈7 Hz) so that at 3.0 ppm a peak shape similar to a triplet (14) is visible in the MR spectrum, whose side peaks are modulated during the J-coupling evolution. The J-difference spectral editing technique to separate the coupled GABA resonance from overlapping singlets (e.g. creatine) is based on a subtraction of two spectra with a fixed echo time: one spectrum where the 3.0 ppm GABA pseudo-triplet underwent undisturbed J-coupling evolution and a second spectrum where the J-coupling evolution was refocused by applying a selective refocusing pulse to the coupled 1.9 ppm resonance. Thus, the resulting spectrum contains only the edited GABA signal at 3.0 ppm whereas the 3.0 ppm singlet resonances are eliminated.

Other signals might be present in the edited spectrum. First, co-edited signals will appear from spins with similar J-couplings (≈7Hz) to the spins, which chemical shifts are within the refocusing bandwidth of the selective refocusing pulse. In case of the spectral editing of the 3.0 ppm GABA resonance the refocusing pulse aimed at 1.9 ppm also affects part of the 2.1 ppm glutamate/glutamine, the 1.7 ppm macromolecule (MM) and the 1.9 ppm homocarnosine (dipeptide consisting of histidine and GABA) resonance. Therefore, the edited spectrum also contains easily resolved signals at 3.7-3.8 ppm because of the similar couplings (6-7.5 Hz) between 3.7-3.8 and 2.1 ppm glutamate/glutamine resonances.

However, the coupling partner of the 1.7 ppm MM (J=7.8 Hz) has a resonance at 3.0 ppm which overlaps the 3.0 ppm GABA signal (15). To minimize the MM contamination, a selective refocusing pulse can be applied in both experiments, which is symmetric around the 1.7 ppm MM resonance(16). In this way the MM contamination in the edited spectrum is eliminated.

The contribution of the homocarnosine molecule is inevitable in spectral editing experiment and thus, the reported 3.0 ppm signal is actually the sum of free GABA and homocarnosine. Second, the singlet signals can also appear in the edited spectrum (e.g. NAA) if their chemical shift overlaps with the refocusing bandwidth of the selective refocusing pulse.

Spectral editing of GABA at high field (7T) is expected to benefit from an increased SNR (17-18), despite its potentially shorter T_2 relaxation time (19). Another advantage for spectral editing at high field is the increased chemical shift dispersion, which, for the editing pulses, results in a shorter pulse duration with an equal spectral selectivity.

On the other hand, due to the low peak B_1^+ values that can be obtained in humans at high field, the bandwidth of traditional refocusing pulses is severely compromised. Therefore, slice selective refocusing leads to an increased chemical shift displacement error (CSDE) at high field and consequently, to a hampered accuracy in voxel localization (20). Due to the low bandwidth refocusing pulses, the observed signal in a localized editing technique is originating from four compartments that, apart from the spatial misalignment of the voxel, can reduce the edited GABA signal by 20-25% already at a field strength of 3T (21). At higher fields (7T), even with the use if an efficient head coil, the loss could still become 30% due to increased CSDE for the low bandwidth refocusing pulses (22). Recently, a semi-localized by adiabatic selective refocusing sequence (sLASER (20,23)) was shown to enable ^{1}H-MRS of the human brain at 7T with minimal CSDE because of the use of high bandwidth adiabatic refocusing pulses in combination with a dual-transmit setup with a volume head coil. This sequence is an ideal candidate for the efficient spectral editing because of the low chemical shift displacement artifact reached with the high bandwidth refocusing pulses.

In this study, we have combined an sLASER sequence with two dual-banded editing pulses (MEGA-sLASER) for the 3.0 ppm GABA detection. In this way, a spatially accurate and time efficient spectral editing sequence is shown to be feasible for GABA detection *in vivo* in the human brain at 7T.

6.2 Methods

MRS measurements were performed with a 7T MR scanner (Achieva, Philips, Cleveland, OH, USA) interfaced to a dual-channel volume transmit head coil (Nova Medical, Inc., Burlington, MA, USA) and a 16 or 32 channel receiver array (Nova Medical, Inc.,

Burlington, MA, USA). RF focusing (23) with two transmit channels (max 2×4kW) was used to generate a B_1^+ field of 20 μT in the selected volume of interest, which was verified by local power optimization (24). Spectral editing with the MEGA-sLASER technique was performed in a water phantom containing 10 mM of GABA for sequence optimization, as well as in several healthy volunteers. Written informed consent was given by all subjects prior to examination.

Two dual-banded refocusing pulses (MEGA1 and MEGA2, both 10 ms long in order to fit them in a sLASER sequence) were created for simultaneous water suppression

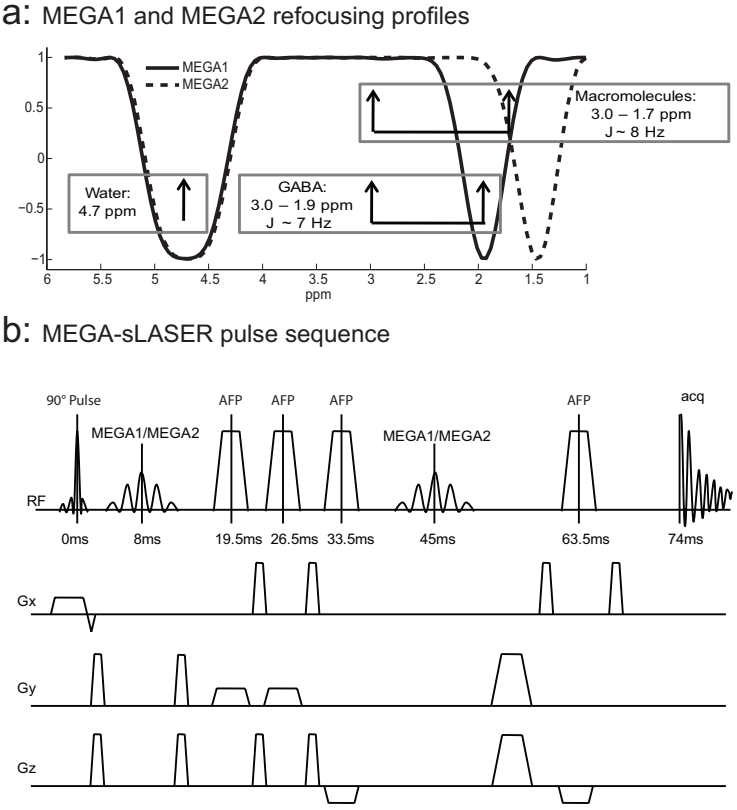

Figure 1. a: Refocusing profiles of the MEGA1 and MEGA2 pulses used in the odd and even acquisitions, respectively. Both pulses refocus water signal at 4.7 ppm. MEGA1 refocuses J-coupling evolution of the 3.0 ppm GABA resonance. MEGA2 does not refocus the 1.9 ppm GABA resonance and in addition eliminates macromolecule co-editing by affecting the 1.7 ppm macromolecule resonance in a similar way as the MEGA1. The 3.0 ppm GABA and macromolecule resonances have similar J-coupling values: approximately 7 and 8 Hz, respectively; b: The MEGA-sLASER sequence consists of an asymmetric slice selective excitation pulse, two pairs of slice selective adiabatic refocusing pulses and two MEGA spectral editing pulses. MEGA1 and MEGA2 pulse shapes were used in alternating experiments.

and J-difference editing, by merging broad and narrow banded Shinnar-Le Roux (SLR) refocusing pulses (25). Both the MEGA1 and MEGA2 pulses had one broad refocusing band (FWHM = 230 Hz, full width at 95% maximum (FW95%M) = 77 Hz) at 4.7 ppm for water suppression. The narrow refocusing band of the first (MEGA1) pulse (FWHM = 130 Hz, FW95%M = 22 Hz) was centered at 1.9 ppm for refocusing of the J-coupling evolution of the 3.0 ppm GABA resonance. The second (MEGA2) pulse had a similar narrow refocusing band centered at 1.5 ppm in order not to refocus the 1.9 ppm GABA resonance, but to affect the 1.7 ppm MM resonance in a similar way as the MEGA1 pulse (Figure 1a). Both refocusing pulses were surrounded by optimized crusher gradients to spoil unwanted coherence pathways. In summary, editing with the MEGA1,2 pulses had the following goals: J-coupling of the 3.0 ppm GABA resonance was refocused in the odd acquisitions whereas it evolved in the even acquisitions; the MM signal was affected similarly in both even and odd acquisitions and was therefore eliminated in the edited spectrum; simultaneous water suppression was performed with the MEGA1,2 pulses. No additional water pre-saturation or inner/outer volume suppression was used.

A sLASER voxel localization was used with an asymmetric excitation pulse (BW of 3.6 kHz) and four 5 ms adiabatic refocusing pulses (BW of 6 kHz). Crusher gradients were manually optimized for optimal spoiling of unwanted coherences. Quantum mechanical simulations of the MEGA1-sLASER and MEGA2-sLASER pulse sequence were performed for the coupled 1.9 and 3.0 ppm GABA resonances and coupled 1.7 and 3.0 ppm macromolecule resonances with TopSpin 2.0 (Bruker Biospin, Billerica, MA, USA). The J-coupling values were approximated to 7Hz using the average of the different J-coupling values reported for GABA in literature (12-14,26). The shapes of the adiabatic and MEGA pulses were loaded into TopSpin, the carrier frequency was set to 4.7 ppm. The spectral width of the simulations was set to 10 ppm. The simulated GABA and macromolecule spin systems also included a singlet in order to normalize the results of individual simulations. The MEGA-sLASER sequence was simulated for a number of echo times (68, 70, 74 and 78 ms). Then, the edited 3.0 ppm GABA and co-edited macromolecule signal intensities were compared for each echo time. The echo time of 74 ms was chosen because the ratio of the edited GABA signal over the co-edited macromolecule signal had its maximum. The MEGA-sLASER sequence was run with alternating MEGA1 and MEGA2 pulses (Figure 1b). The MEGA1-sLASER sequence refocused the J-coupling of the 3.0 ppm GABA resonance and preserved the in-phase 3.0 ppm GABA pseudo-triplet, whereas the MEGA2-sLASER sequence allowed for J-coupling evolution and at an echo time (TE) of 74 ms, the two side peaks of 3.0 ppm GABA pseudo-triplet were inverted with respect to the central peak. Thus, after the subtraction only the two side peaks of the 3.0 ppm GABA pseudo-triplet were preserved and the overlapping resonances were eliminated.

However, the intensity of the creatine resonance at 3.0 ppm is one order of magnitude higher than the edited GABA signal. Therefore, any phase difference or B_0 drift between the odd and even acquisitions would lead to a significant residual creatine signal in the edited spectrum. To improve the phase and frequency stability, the MEGA1-sLASER

and MEGA2-sLASER acquisitions were performed in an interleaved manner and cardiac triggering was used. ECG triggering was used with careful placement of the leads on the chest to minimize ECG signal distortion in the 7T MR bore. The use of cardiac triggering to increase phase and frequency stability was assessed by estimating the suppression factor in the edited spectrum from a series (N=64) of *in vivo* measurements of the water signal. Cardiac triggering was performed in all the GABA editing experiments. Retrospective phase and frequency alignment (27) was performed on all data sets as the SNR of the single shots was high enough (minimum SNR of 4) to estimate a reliable phase/frequency correction.

MEGA-sLASER spectra were acquired in the grey matter of the occipital lobe (TR = 4100, 64 acquisitions) with TE = 74 ms in 27 ml voxels (five subjects) and an 8 ml voxel (one subject). In one subject an additional MEGA-sLASER spectrum was acquired with a TE of 222 ms in a 27 ml voxel.MR spectra corresponding to the even acquisitions were subtracted from the odd spectra. In the edited spectrum the residual water signal was filtered by HLSVD fitting in jMRUI (28). All the edited spectra obtained with a TE of 74 ms in 27 ml voxels were normalized to the integrated 3 ppm creatine peak to test reproducibility

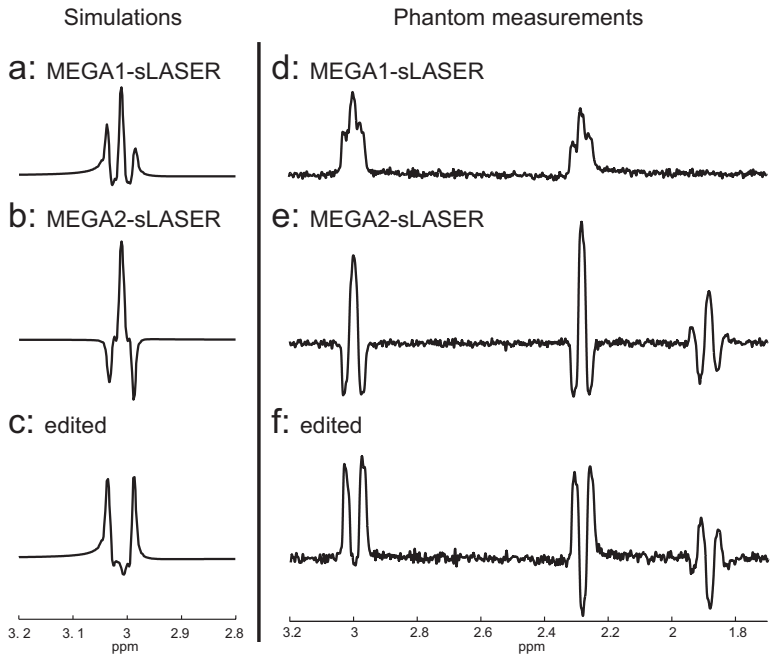

Figure 2. The simulated 3.0 ppm GABA resonances: MEGA1-sLASER (a), MEGA2-sLASER (b) and the edited spectrum (c) and measured MEGA1-sLASER (d) and MEGA2-sLASER (e) spectra obtained in a GABA phantom, and the edited spectrum (f). The measured shapes of the 3.0 ppm GABA resonance correspond well to the simulations. The editing efficiency was 0.52, determined as a peak area ratio of the edited and the J-coupling refocused 3.0 ppm GABA signal in the phantom spectra.

between the subjects. To demonstrate the MM elimination that was reached by using the MEGA2 pulse shape, similar measurements were performed where in the odd experiments the refocusing pulse was shifted far from the 1.5 ppm region and the intensities of the edited 3.0 ppm resonances were compared.

6.3 Results

Phantom measurements were performed to evaluate editing performance of the MEGA-sLASER sequence and compared with the simulated spectra (Figure 2). The edited spectrum clearly showed the two side peaks of the 3.0 ppm GABA pseudo-triplet. The editing efficiency was 0.52, determined as a peak area ratio of the edited and J-coupling

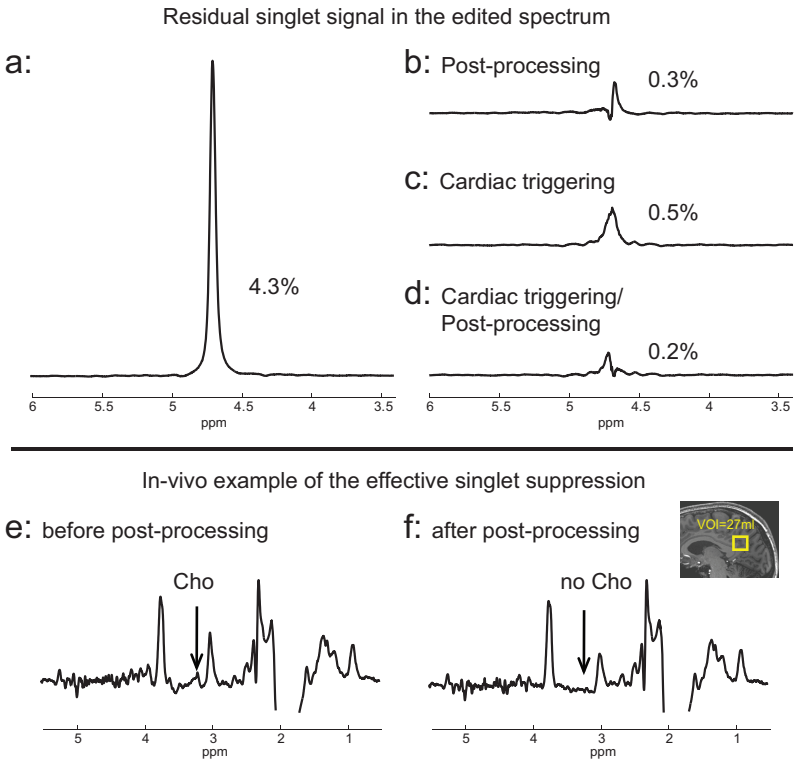

Figure 3. Residual singlet signal in the edited spectrum as assessed from a non-water suppressed scan. The spectra were acquired without water suppression (MEGA pulses were turned off) to evaluate effect of cardiac triggering (c,d) and post-processing (b,d) on the singlet suppression in the edited spectra i.e. creatine and choline An in vivo example of the improved singlet suppression with post-processing in the edited MEGA-sLASER spectrum is shown. In the edited spectrum the residual 3.2 ppm choline signal is present prior phase/frequency correction (e) and effectively eliminated with post-processing (f).

refocused 3.0 ppm GABA signals in the phantom spectra.

In vivo water measurements showed that subtraction of the odd water scans from the even scans without cardiac triggering or without retrospective phase and frequency alignment led to a factor 23 suppression of the singlet signal. Performing cardiac triggering improved the suppression factor to 200 (Figure 3 a-d). Retrospective frequency and phase alignment was possible for these spectra because of the high SNR and it increased the suppression factor to 330 fold without and to 500 fold with cardiac triggering. An *in vivo* example of effective suppression of residual singlet signal (e.g. choline) with post-processing in the edited MEGA-sLASER spectrum is shown in Figure 3 e,f.

The chemical shift displacement error of the coupled 1.9 and 3.0 ppm GABA resonances in the MEGA-sLASER sequence was only 6 % in both refocusing directions. After subtraction of the even MR spectra (Figure 4a) from the odd MR spectra (Figure 4b) the five edited *in vivo* MR spectra showed well-distinguishable signals (SNR ~ 17) for GABA at

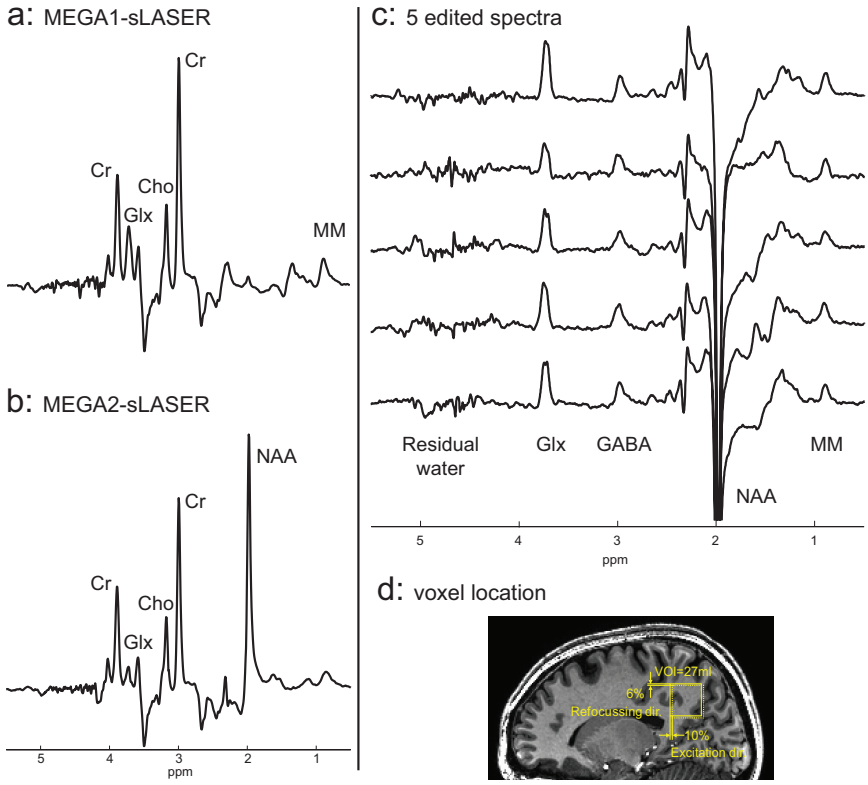

Figure 4. Summed MEGA1-sLASER(a), MEGA2-sLASER(b) spectra obtained in vivo in one subject, and five in vivo edited spectra (c) obtained in the occipital lobe (d). The 3.0 ppm GABA signal as well as the co-edited glutamine and glutamate signals are clearly visible. As well as the NAA singlet at 2.0 ppm, since that is only present in the even spectra and is not subtracted in the edited spectrum. No choline (3.2 ppm) residual is seen, indicating a good suppression of non-edited resonances.

3.0 ppm (Figure 4c). The co-edited Glx resonances at 3.7 ppm were also present in the edited spectrum. The absence of any residual signal of the choline singlet at 3.2 ppm indicated good singlet suppression and, therefore, a reliable editing performance. The average peak area ratio of the edited GABA in five volunteers to Cr was 0.066 with a standard deviation of only 7%.

The well-resolved 3.0 ppm GABA resonance (SNR = 8) was present in the edited spectrum obtained in the 3-fold smaller voxel (8 ml) which showed high efficiency of the MEGA-sLASER editing sequence (Figure 5a). The edited spectrum obtained with the three times longer echo time of 222 ms also demonstrates the high efficiency of the MEGA-sLASER sequence (Figure 5b). The 3.0 ppm GABA resonance was 3-fold higher than the noise level, the co-edited MM resonance at 0.9 ppm was hardly visible because of its much shorter transverse relaxation time.

The edited spectrum acquired without the MEGA2 pulse contained a 3/2-fold higher signal at 3.0 ppm than with the MEGA2 pulse, indicating that the MM contribution at 3.0 ppm was successfully eliminated (Figure 5c).

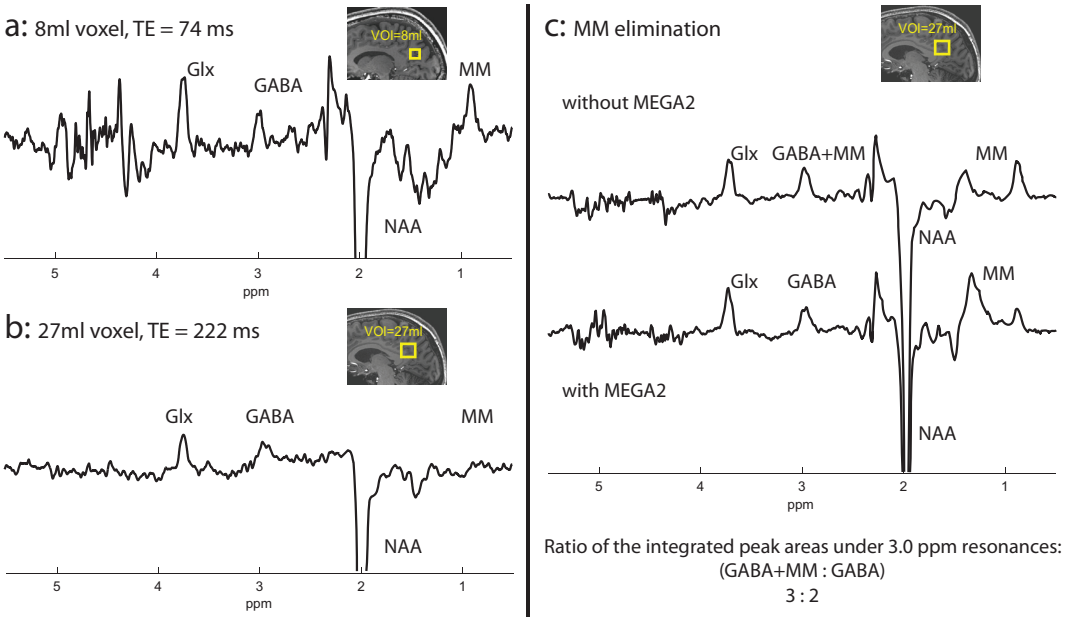

Figure 5. Edited in vivo spectra, acquired in the occipital lobe within acquisition times of 5 minutes each. At a TE of 74 ms, the GABA signal could be obtained from a small voxel of only 8ml (a). Even at a TE of 222 ms (b) the GABA signal could be obtained from a voxel size of 27 ml. When comparing two edited in vivo spectra (TE=74ms, voxel of 27ml), acquired without and with macromolecule elimination (c) the ratio of the integrated peak areas under 3.0 ppm resonances (GABA+MM : GABA) is 3:2, which confirms the considerable co-editing of the macromolecule resonance without MEGA2 pulses.

6.4 Discussion

Stable detection of GABA levels in the human brain is generally hampered by low detection sensitivity, phase and frequency instabilities and overlap of the GABA resonance with the high intensity signals of creatine and macromolecules. GABA detection at high field (7T and above), could benefit from a potentially increased SNR. In addition, at high field the use of shorter selective pulses can be applied because of the increased chemical shift dispersion, which enabled incorporation of these pulses in a sLASER technique while remaining within the optimal echo-time required for GABA editing. Using the broadband slice selective adiabatic refocusing pulses of the sLASER technique combined with B_1^+ focusing with a dual-channel birdcage coil, the generally unacceptable high chemical shift displacement errors (CSDE) at 7T could be reduced significantly. Therefore, in this study we could detect GABA in the occipital lobe with a high efficiency. The MEGA-sLASER technique might be as well applied to other locations in the human brain unless the maximum achievable B_1^+ field is below 20 μT, e.g. the cerebellum does not have a sufficiently high B_1^+ field with the dual-channel birdcage coil (23).

From quantum mechanical simulations it was seen that the optimal echo time of the MEGA sLASER sequence for the spectral editing of the 3.0 ppm GABA resonance was 74 ms, which is slightly longer than the conventionally used echo time of 68 ms (2-3,29). This can be explained by the partial spin-locking of the 3.0 ppm GABA resonance due to the relatively high duty cycle of RF pulses in the echo time. Consequently, the effective echo time is extended in comparison with a MEGA-PRESS editing techniques that contain only two refocusing pulses.

Elimination of CSDE and phase disturbances in the subtracted MR spectra with the interleaved MEGA-sLASER method enabled efficient *in vivo* GABA detection; an SNR of 17 in a 27 ml voxel was acquired within an acceptable measurement time of 5 min. To improve phase stability during the measurement, both interleaved scanning and cardiac triggering were performed, since cardiac activity had a significant influence on the phase and frequency in these measurements at relatively long TE (74ms) (30). It has been shown how cardiac triggering improved phase and frequency stability of the acquisition. From the retrospective spectra correction it was seen that the frequency variations had a major impact on the edited spectrum quality. Using the MEGA-sLASER with cardiac triggering and retrospective frequency and phase alignment resulted in only a 7% standard deviation of the GABA to creatine ratio in 5 subjects.

The elimination of the individual spectra's post-processing effort can have a significant importance for the spectral editing in small voxels or MRSI, where the SNR of individual acquisitions is too low to be able to perform a reliable phase and frequency correction or individual shots are not available for phase/frequency correction, as with MRSI. Therefore, it can be recommended to use cardiac triggering together in these types of MRS experiments in order to perform a reliable spectral editing measurement.

The intrinsic co-editing of the MM resonance is minimized with a second pair of dual-banded refocusing pulses (MEGA2-sLASER), whereas, similar to MEGA-point-resolved spectroscopy (MEGA-PRESS) (29,31), the absence of the MEGA2 pulse shape would lead to an increase of the observed edited 3.0 ppm signal, indicating a significant contribution of the MM resonance. The relatively high SNR of the GABA signal in the long echo time MEGA-sLASER experiment shows that this long echo time experiment may be used to determine GABA T_2 relaxation time.

Despite the promising increase of SNR and spectral dispersion there has been only limited number of GABA studies at 7T (29). It would be possible to eliminate MM contamination with MEGA-PRESS editing technique at 7T as the editing MEGA pulses of the same length become more selective at higher fields. However, at high field MEGA-PRESS is hampered by a large CSDE because of the limited bandwidth of the refocusing pulses and only a small part of the selected volume gives a desirable edited GABA signal (21). To compensate for this effect the number of averages and, thus, acquisition time should be increased substantially or inner volume saturation has to be used (21). The MEGA-sLASER sequence proposed here contains adiabatic refocusing pulses that effectively reduce CSDE and a high SNR GABA signal is detected from the selected volume without a need to increase number of averages or use inner volume saturation.

Recently, a MEGA-SPECIAL technique was successfully demonstrated for GABA editing at 3T. Because of only a single slice selective refocusing pulse the signal is less affected by CSDE than with MEGA-PRESS and more selective editing pulses can be applied to eliminate MM contamination. However, in one dimension the CSDE remains substantial. In addition, the technique relies on subtraction of four acquisitions to extract the GABA edited signal, instead of two as in MEGA-PRESS or MEGA-sLASER. As a consequence, MEGA-SPECIAL demands outer volume suppression due to greater motion sensitivity, and in one dimension inner volume suppression to overcome the CSDE.

Next to spectral editing, GABA signal can be extracted from a short TE spectrum by metabolite fitting (17). The robust extraction of the weak GABA signal from other metabolites resonances is difficult with this approach. The fitting basis set of all resonances should be known at given field strength together with their T_1, T_2 relaxation times which can differ in healthy and non-healthy tissues. Particularly in MRS acquisitions at short echo time the MM baseline should be determined, possibly for every subject/patient to minimize fitting errors. All these factors make a reliable GABA quantification highly challenging as any slight error will strongly affect fitting results for the weak GABA signal.

MR spectroscopic imaging (MRSI) of GABA may even be a valuable tool in many diseases studies. Several methods have been proposed to perform GABA MRSI including editing (10), double-quantum filtering (32) and two-dimensional spectroscopy (5). These methods demand a high homogeneity of B_0 and B_1 fields in the selected volume to assure effective detection of the low SNR GABA signal over the entire volume. Moreover, these experiments are generally time consuming and single shot reference signal for every voxel is absent, disabling phase/frequency correction. The single voxel MEGA-sLASER in

combination with cardiac triggering might be extendable to 2D or 3D GABA MRSI with high efficiency.

To sum up, the presented MEGA-sLASER method demonstrated a highly efficient and accurately localized GABA signal detection with short acquisition times (5 min) at high fields (7T). Excellent efficiency of this method allowed GABA detection in small voxels (8 ml) at short echo times (74ms) but also at much longer echo times (222 ms) that make the method very promising to assess absolute GABA concentration in the human brain at 7T.

References

1. Hu J, Yang S, Xuan Y, Jiang Q, Yang Y, Haacke EM. Simultaneous detection of resolved glutamate, glutamine, and gamma-aminobutyric acid at 4 T. J Magn Reson 2007;185(2):204-213.
2. Rothman DL, Petroff OA, Behar KL, Mattson RH. Localized 1H NMR measurements of gamma-aminobutyric acid in human brain in vivo. Proc Natl Acad Sci U S A 1993;90(12):5662-5666.
3. Mescher M, Merkle H, Kirsch J, Garwood M, Gruetter R. Simultaneous in vivo spectral editing and water suppression. NMR Biomed 1998;11(6):266-272.
4. Pan JW, Avdievich N, Hetherington HP. J-refocused coherence transfer spectroscopic imaging at 7 T in human brain. Magn Reson Med 2010;64(5):1237-1246.
5. Jensen JE, Frederick BD, Wang L, Brown J, Renshaw PF. Two-dimensional, J-resolved spectroscopic imaging of GABA at 4 Tesla in the human brain. Magn Reson Med 2005;54(4):783-788.
6. Jensen JE, Frederick Bde B, Renshaw PF. Grey and white matter GABA level differences in the human brain using two-dimensional, J-resolved spectroscopic imaging. NMR Biomed 2005;18(8):570-576.
7. Keltner JR, Wald LL, Frederick BD, Renshaw PF. In vivo detection of GABA in human brain using a localized double-quantum filter technique. Magn Reson Med 1997;37(3):366-371.
8. Wilman AH, Allen PS. Yield enhancement of a double-quantum filter sequence designed for the edited detection of GABA. J Magn Reson B 1995;109(2):169-174.
9. Zhu H, Edden RA, Ouwerkerk R, Barker PB. High resolution spectroscopic imaging of GABA at 3 Tesla. Magn Reson Med 2011;65(3):603-609.
10. Shen J, Shungu DC, Rothman DL. In vivo chemical shift imaging of gamma-aminobutyric acid in the human brain. Magn Reson Med 1999;41(1):35-42.
11. McCormick DA. GABA as an inhibitory neurotransmitter in human cerebral cortex. J Neurophysiol 1989;62(5):1018-1027.
12. Govindaraju V, Young K, Maudsley AA. Proton NMR chemical shifts and coupling constants for brain metabolites. NMR Biomed 2000;13(3):129-153.
13. Graaf Rad. In Vivo NMR Specroscopy. Principles and Techniques John Wiley & Sons Ltd.; 2007. 570 p.
14. Kaiser LG, Young K, Meyerhoff DJ, Mueller SG, Matson GB. A detailed analysis of localized J-difference GABA editing: theoretical and experimental study at 4 T. NMR Biomed 2008;21(1):22-32.
15. Behar KL, Rothman DL, Spencer DD, Petroff OA. Analysis of macromolecule resonances in 1H NMR spectra of human brain. Magn Reson Med 1994;32(3):294-302.
16. Henry PG, Dautry C, Hantraye P, Bloch G. Brain GABA editing without macromolecule contamination. Magn Reson Med 2001;45(3):517-520.

17. Tkac I, Oz G, Adriany G, Ugurbil K, Gruetter R. In vivo 1H NMR spectroscopy of the human brain at high magnetic fields: metabolite quantification at 4T vs. 7T. Magn Reson Med 2009;62(4):868-879.
18. Mangia S, Tkac I, Gruetter R, Van De Moortele PF, Giove F, Maraviglia B, Ugurbil K. Sensitivity of single-voxel 1H-MRS in investigating the metabolism of the activated human visual cortex at 7 T. Magn Reson Imaging 2006;24(4):343-348.
19. Otazo R, Mueller B, Ugurbil K, Wald L, Posse S. Signal-to-noise ratio and spectral linewidth improvements between 1.5 and 7 Tesla in proton echo-planar spectroscopic imaging. Magn Reson Med 2006;56(6):1200-1210.
20. Scheenen TW, Heerschap A, Klomp DW. Towards 1H-MRSI of the human brain at 7T with slice-selective adiabatic refocusing pulses. MAGMA 2008;21(1-2):95-101.
21. Edden RA, Barker PB. Spatial effects in the detection of gamma-aminobutyric acid: improved sensitivity at high fields using inner volume saturation. Magn Reson Med 2007;58(6):1276-1282.
22. Edden RA, Barker PB. If J doesn't evolve, it won't J-resolve: J-PRESS with bandwidth-limited refocusing pulses. Magn Reson Med 2011;65(6):1509-1514.
23. Boer VO, van Lier AL, Hoogduin JM, Wijnen JP, Luijten PR, Klomp DW. 7-T (1) H MRS with adiabatic refocusing at short TE using radiofrequency focusing with a dual-channel volume transmit coil. NMR Biomed 2011.
24. Versluis MJ, Kan HE, van Buchem MA, Webb AG. Improved signal to noise in proton spectroscopy of the human calf muscle at 7 T using localized B1 calibration. Magn Reson Med 2010;63(1):207-211.
25. Matson GB. An integrated program for amplitude-modulated RF pulse generation and re-mapping with shaped gradients. Magn Reson Imaging 1994;12(8):1205-1225.
26. de Graaf RA, Chowdhury GM, Behar KL. Quantification of high-resolution (1)H NMR spectra from rat brain extracts. Anal Chem 2011;83(1):216-224.
27. Waddell KW, Avison MJ, Joers JM, Gore JC. A practical guide to robust detection of GABA in human brain by J-difference spectroscopy at 3 T using a standard volume coil. Magn Reson Imaging 2007;25(7):1032-1038.
28. Naressi A, Couturier C, Castang I, de Beer R, Graveron-Demilly D. Java-based graphical user interface for MRUI, a software package for quantitation of in vivo/medical magnetic resonance spectroscopy signals. Comput Biol Med 2001;31(4):269-286.
29. Terpstra M, Ugurbil K, Gruetter R. Direct in vivo measurement of human cerebral GABA concentration using MEGA-editing at 7 Tesla. Magn Reson Med 2002;47(5):1009-1012.
30. Van de Moortele PF, Pfeuffer J, Glover GH, Ugurbil K, Hu X. Respiration-induced B0 fluctuations and their spatial distribution in the human brain at 7 Tesla. Magn Reson Med 2002;47(5):888-895.
31. Near J, Simpson R, Cowen P, Jezzard P. Efficient gamma-aminobutyric acid editing at 3T without macromolecule contamination: MEGA-SPECIAL. NMR Biomed 2011.
32. Choi IY, Lee SP, Merkle H, Shen J. In vivo detection of gray and white matter differences in GABA concentration in the human brain. Neuroimage 2006;33(1):85-93.

Chapter 7

Double Quantum MRS editing for lactate detection at 7T

Magnetic Resonance in Medicine; provisionally accepted

V.O.Boer , P.R.Luijten, D.W.J.Klomp

Department of Radiology, University Medical Center Utrecht, Utrecht, The Netherlands

Abstract

Lactate is an important marker for anaerobic glucose metabolism, and it is therefore of particular interest in for example cerebral ischemia, skeletal muscle disorders and in the monitoring of oncology treatments. However, the *in vivo* detection of lactate with MR spectroscopy is complicated by the overlap of the low intensity lactate methyl resonance with lipid signal. Therefore double quantum filters have been employed to dephase the overlapping lipid signal, since they allow for a very high lipid suppression efficiency. For reliable lactate detection in lipid rich environment, very large crushing gradients have to be employed to dephase the lipid signal under the noise level. Double quantum filters are generally associated with signal loss of the metabolite of interest. For lactate, half of the signal is lost by selecting either the double or zero quantum coherences. Moreover, due to incomplete refocusing, traditional double quantum filters with very large crusher gradients exhibition additional loss of the already low lactate signal. In this work a refocused double quantum filter is described, which does not suffer from this source of additional signal loss. Therefore it becomes possible to detect lactate at lower concentrations, or in lipid rich environments. Lactate measurements are shown in the human calf muscle at 7T.

7.1 Introduction

Lactate is used as a biomarker of anaerobic glucose metabolism, therefore the *in vivo* measurement of lactate is interesting in many clinical areas, like oncology. Several preclinical studies have shown the use of lactate as a biomarker for tumor aggressiveness (1), response to chemotherapy (2) and radiation therapy (3). Lactate can be a marker for tissue viability in cerebral ischemia (4) and it is also involved in skeletal muscle deceases in patient with mitochondrial disorders (5). However, the *in vivo* detection of lactate is hampered by the spectral overlap of the methyl (CH_3) group of lactate and the methylene (CH_2) group of lipids, since both resonate at a frequency of 1.3 ppm. For instance, many tumors are located in areas where lipids are abundant, or they tumor may contain lipids (6). Also in muscle tissue, and particularly in diseased muscle (7) diffuse lipid tissue can be substantial. Therefore, to unambiguously distinguish the lactate from lipid signal, spectral editing has been employed, where the J-coupling behavior of the lactate methyl resonance can be used to discriminate the coupled lactate resonance from the singlet lipid resonance at 1.3 ppm. Because of the J-coupling of the lactate methyl to methine (CH) group, the lactate methyl resonance appears as an inverted doublet at an echo time of 144 ms (1/J) in a spin-echo sequence.

J-difference editing is a technique with which the lactate signal can be separated from the overlapping singlet resonances (8). Two (series of) spectra are acquired, where in the one case the J-modulation is allowed to evolve and is measured at an echo time of 1/J, and in the second case the J-coupling is refocused by selective refocusing of the coupling partner. This leads to one spectrum where the lactate signal is inverted, and one spectrum where the lactate signal is positive, while all overlapping singlet resonances will appear similar in both spectra as long as they are not perturbed by the additional refocusing pulses. Subtraction of the two spectra will yield a spectrum with only lactate, and addition of the two spectra will show only the singlet resonances. However, since the typical lactate signal intensity is several orders of magnitude lower than the overlapping lipid signal intensity, this technique is prone to subtraction artifacts, since small differences between the two spectra (e.g. caused by motion or other system instabilities) will lead to an incorrect assignment of the subtraction residual to lactate. Especially in environments with high lipid concentrations, such as certain types of tumors or fatty tissues, and in organs where the spectral quality is far from perfect due to physiological instability, the detection of lactate with J-refocused spectral editing is severely hampered, and much higher lipid suppression factors are required.

In these cases, multiple quantum filters might be more applicable since these allow for gradient dephasing of the overlapping singlet signals and hence can specifically detect lactate within a single shot (9). A multiple quantum filter typically transforms the lactate system into zero quantum (ZQ) and double quantum (DQ) states, where the double quantum state is twice as sensitive to an applied dephasing gradient (10). Therefore, after transforming

the system back to a single quantum state, a rephasing gradient of twice the area is needed for rephasing of the lactate signal. With these unbalanced gradients the lactate signal is recovered, however all non-coupled resonances (e.g. overlapping lipids) will remain in a single quantum state en experience a spin echo with unbalanced gradients, leading to a very effective dephasing of the lipid signal. However, since with this approach only the signal is observed that was in a double quantum state during the dephasing gradient, the signal that was in a zero quantum state is lost, and at maximum 50% of the lactate signal is observable.

Several multiple quantum coherence (MQC) filters have been proposed for the detection of lactate (9,11-18), but unfortunately these double quantum filters are always associated with undesired signal loss of the metabolite of interest. First, at least 50% of the lactate signal is lost by selecting the double-quantum coherence pathway, however this cannot be avoided since restoring the full signal will also cause the lipid signal to be rephased (12). Additional signal loss in traditional double quantum filters is caused by the evolution of the spin system during the multiple quantum period. Depending on the length of the multiple quantum period, complete loss of the signal of interest can occur (12). As the duration of this multiple quantum time is mainly determined by the duration of the crusher gradient and the RF pulses during this period, the duration should be minimized in order to prevent a severe loss of sensitivity, but it has to be maximized in order to improve crushing performance for lipid signal suppression (17), and to allow time for a sharp and therefore selective RF pulse profile (19). However, the required *in vivo* crushing strength might be more demanding in areas with low lactate concentrations, where residual signals need to be suppressed below the noise level. More importantly, the required gradient dephasing will be dependent the local B_0 field gradients that are present in the tissue which can counteract the applied dephasing. Therefore, the required dephasing will depend on the local susceptibility distributions (e.g. tissue composition), and B_0 field strength, since susceptibility effects scale with the static magnetic field. Unlike in a homogeneous phantom, local susceptibility transitions in tissue can lead to very sharp local B_0 field gradients which, especially at high field, will push the requirement for much stronger dephasing gradients areas. Since the detection sensitivity drops severely with such long crushing gradients for traditional double quantum filters, the unambiguous detecting of lactate *in vivo* remains challenging with these sequences and one may question if higher magnetic field can benefit the detection of lactate at all.

In this work we present a refocused DQ filter which prevents the source of additional signal loss during the multiple quantum period by refocusing both the chemical shift and J-coupling evolution. The required crushing strength is investigated in the human calf muscle at 7T, and double quantum filtered lactate measurements are shown from the human calf muscle. With the refocused DQ-filter, crusher gradients can be maximized for optimal lipid suppression, without a severe SNR penalty, therefore allowing detection of lactate at low concentration and in lipid rich environments.

Experiments are performed to establish the minimally required gradient dephasing for lipid suppression *in vivo* in the human calf muscle. Lactate detection was confirmed by on observed increase in the signal at 1.3 ppm during exercise of the calf muscle (20).

7.2 Theory and Methods

Experiments were performed on a whole body 7T MRI system (Philips, Cleveland, OH, USA), using a volume birdcage coil (Nova Medical, Inc, Burlington, MA, USA). Experiments were performed on phantoms and in the calf muscle of healthy volunteers. All measurements were carried out in compliance with the local institutional medical ethics committee guidelines.

In traditional multiple quantum filters like the SEL-MQC filters (12), the lactate methyl magnetization is allowed to evolve under J-evolution for 1/2J. At this point a selective excitation pulse on the methine group at 4.1 ppm, the mixing pulse, converts the magnetization into zero and double quantum coherences. The double and zero quantum coherences evolve for a certain period (t1) during which the double quantum selection gradients are employed. This is followed by another 90 degree pulse on the methine group, the read pulse, to convert the magnetization back to a single quantum state, which can be observed after a rephasing gradient of twice the area and a second delay of 1/2J. Two versions of this sequence were proposed by He et al, where either a soft (SSEL) or a hard (HSEL) refocusing pulse was inserted in the t1 period to refocus the chemical shift on the methyl group. With the soft refocusing pulse on the methyl group, the chemical shift is not fully refocused, since this pulse interchanges the double and zero quantum states. Before this soft refocusing pulse, the observed signal was in a zero quantum state for a period of t1/2, and after the pulse it was in a double quantum state for the same duration. However, the chemical shift evolution is different during a double or a zero quantum state, leading to a shift of the spin echo shift away from the point where the J-coupling is refocused, and therefore leads to signal loss with a factor of $\cos(\pi*J*t1)$. To fully refocus the chemical shift during the t1 period, the soft refocusing pulse was interchanged with a hard refocusing pulse which refocuses both the methyl and methine group. This prevents the interchange of zero and double quantum states, and shows a symmetric chemical shift evolution around the refocusing pulse. However, since lactate is not an AX system but an AX3 system, the J-coupling evolution during the t1 period is now no longer refocused, leading to signal loss with $\cos^2(\pi*J*t1)$.

Instead of using a single hard or soft pulse, where either the chemical shift, or the J-coupling evolution is refocused, multiple refocusing pulses can be incorporated in the t1 delay to ensure refocusing of both the chemical shift and the J-coupling evolution. For the refocused double quantum filter, a selective refocusing on the 1.3 ppm resonance was combined with a double spin echo on the 4.1 ppm resonance, therefore three refocusing

pulses were used during the multiple quantum time t1, the first one on the 4.1 ppm methine, the second one on the 1.3 ppm methyl frequency and the third one again on the 4.1 methine frequency (Figure 1). After conversion to zero and double quantum states by the mixing pulse, the double and zero quantum states are interchanged by every selective refocusing pulse. Therefore the double quantum selection gradient that can be used is 0:-1:0:+1 with a rephasing gradient after the read pulse of -4. Alternatively the other pathway can be selected with -1:0:+1:0 with a rephasing gradient of -4.

The refocused DQ filter was implemented as a single slice sequence with all gradient slopes set to 250 μs, and a gradient strength of at maximum 30 mT/m. The first excitation pulse was an asymmetric slice selective sinc pulse (BW = 3.0 kHz), all other RF pulses were sinc-gaussian shaped RF pulses of 5.5 ms duration (BW = 300 Hz).

Signal loss as a function of the t1 time for different double quantum filters was assessed from measurements on a high concentration lactate phantom. The DQ filtered signal intensity as a function of the t1 time was measured with a single soft (SSEL) or hard (HSEL) refocusing pulse in the t1 time, as well as with the novel refocused DQ filter with three refocusing pulses. Signal intensity as a function of the multiple quantum time t1 was compared with the theoretical expected signal loss of the refocused double quantum filter (exponential T2 decay (E2)), $\cos(\pi*J*t1)*E2$ for the SSEL and $\cos^2(\pi*J*t1)*E2$ for the

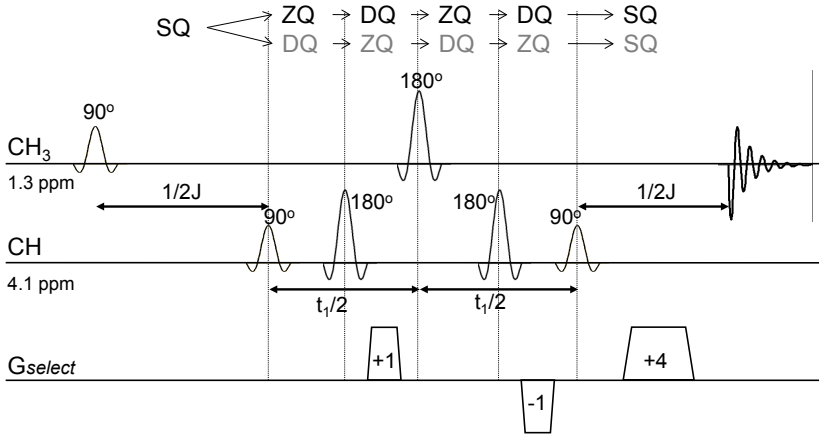

Figure 1: refocused double quantum filter sequence for single shot lactate detection. After the preparation period of 1/2J (e.g. 72 ms), the lactate coherence is converted to a zero and double quantum state by the 90° mixing pulse on the CH resonance (4.1 ppm). The selective refocusing pulses during the t1 period refocus both the J-coupling and chemical shift during the multiple quantum period. A double quantum selection gradient (Gselect) is applied during the period where the lactate is in a double quantum state. After the second 90° read pulse on the CH frequency (4.1 ppm) lactate is converted back to an observable single quantum state. A gradient with double area is applied to rephrase the lactate signal. Overlapping singlet signals at the CH3 (1.3 ppm) resonance experience a spin echo sequence with unbalanced gradients, leading to efficient signal cancellation. 50% of the lactate signal is lost since the zero quantum coherences do not experience the selection gradients.

HSEL. The T2 of lactate in the phantom was determined in a series of J-refocused spin echo experiments to be 320 ms.

Frequency and B_1 dependence of the refocusing double quantum filter was assessed from a phantom measurements where the carrier frequency as well as the RF power was varied in a series of experiments with the refocused DQ filter.

The required dephasing strength for complete *in vivo* lipid suppression was measured *in vivo* in the calf muscle of a healthy volunteer. The refocused double quantum filter was used, where the double quantum read pulse (last 90 degree pulse at 4.1 ppm) was turned off to investigate the lipid residual signal at 1.3 ppm. A 2 cm thick transverse slice through the calf muscle was selected (TR = 2 s, t1 = 50 ms, 32 averages). The gradient strength was increased until the lipid signal was suppressed to below the noise level. Then the double quantum read pulse was turned on to allow for the conversion of lactate back to observable magnetization.

An additional experiment was performed to verify that the observed signal at 1.3 ppm was indeed originating from lactate by exercising the calf muscle (20). The volunteer was placed in the scanner with the calf muscle in the volume coil. A 2 cm thick transverse slice through the calf muscle was selected (TR = 2 s, t1 = 50 ms, 32 averages). A pedal was placed under the foot, and a pulling force of approximately 700 Nm force was applied to the top of the pedal while the volunteer pushed the pedal back, in order to put strain on the calf

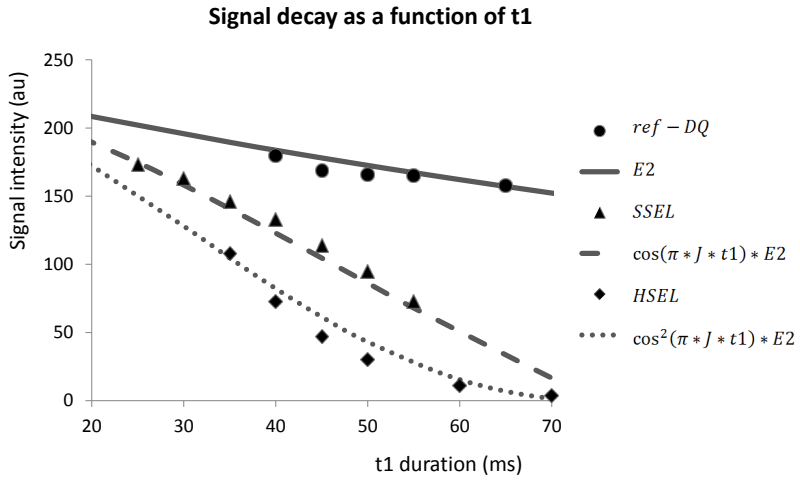

Figure 2: signal loss dependent on the double quantum time (t1) for several double quantum filters as measured in a lactate phantom at 7T (data points) and the theoretical prediction (lines). The SSEL contains a single soft refocusing pulse in the t1 time, the HSEL a single hard refocusing pulse in the t1 time, and the refocused double quantum filter contains three selective refocusing pulses in the t1 time. The refocused double quantum filter shows only exponential T2 decay (E2), where the other two methods show severe additional signal loss for longer t1 times.

muscle. After 6 minutes of rest, this exercise was performed for 3 minutes, followed by 10 minutes of rest, another 5 minutes of exercise and 6 minutes of rest while continuous lactate measurements were performed with the refocused double quantum filter.

7.3 Results

Since the large crushers, required for *in vivo* crushing of the lipid signal, require a long t1 time in the sequence, the detection sensitivity as a function of t1 time for three multiple quantum filters was assessed. The conventional SSEL and HSEL double quantum filters as well as with the proposed refocused DQ filter were tested on a phantom with increasing t1 time. Total signal intensity of the lactate resonance at 1.3 ppm is shown in Figure 2. The refocused filter is only sensitive to T2 decay where both the SSEL and HSEL DQ filters show severe additional signal loss dependent on the multiple quantum evolution time t1. A good correlation between the expected exponential T2 decay for the refocused double quantum filter, and the additional $\cos(\pi*J*t1)$, and $\cos^2(\pi*J*t1)$ dependent signal loss for SSEL and HSEL double quantum filtering is seen.

Dependence of the proposed refocused double quantum filter on the B_1 field and the offset frequency was assessed from phantom simulations. Figure 3a shows that the maximum signal intensity was retained for an approximately 0.8 ppm broad range around 1.3 ppm. Full signal was retained for B_1 values between +/- 10% of the nominal B_1 value.

The minimum required gradient crushing for *in vivo* lipid suppression was determined before an actual lactate measurement in the human calf muscle, by turning off the double quantum read pulse. By varying the dephasing area of the double quantum selection gradients, the lipid signal was reduced to below the noise level for dephasing areas above 120 ms*mT/m (Figure 4). Sequentially the double quantum read pulse (at 4.1 ppm) was

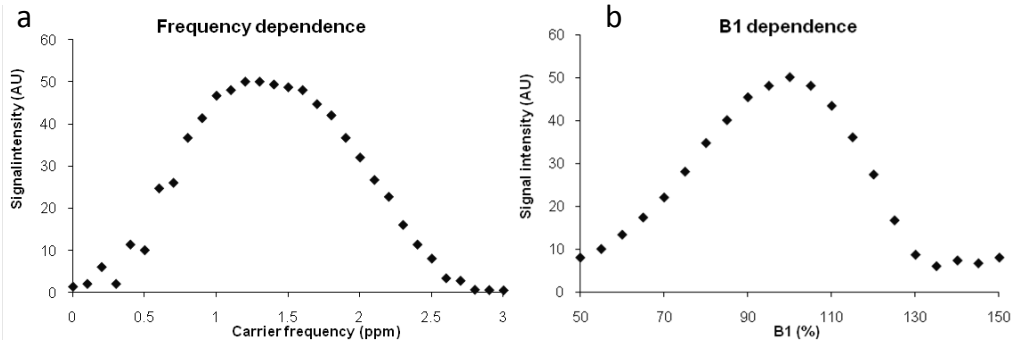

Figure 3: Frequency (a) and B_1 (b) dependent signal loss for the refocused double quantum filter as measured in a phantom.

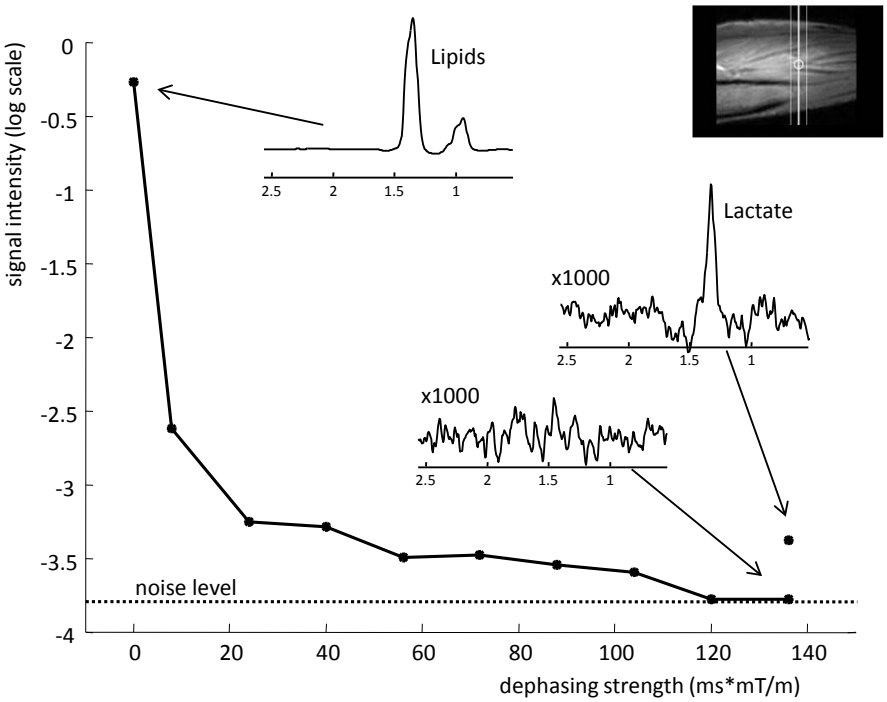

*Figure 4: In vivo lactate measurements in the human calf muscle. A transverse slice was excited through the muscle tissue. The double quantum read pulse was turned off so no that no lactate signal was detectable, and a series of experiments was performed to determine the required gradient crushing strength to dephase all lipid signal. When a sufficient dephasing efficiency, here at 136 ms*mT/m, was achieved, the DQ read pulse was turned back on to allow for the detection of lactate signal in the human calf muscle.*

turned on to revert the lactate double quantum coherences to observable signal (Figure 4).

The presence of lactate was confirmed with an exercise to stress the calf muscle. A clear increase in the observed lactate signal was seen during exercise, with a slow return to baseline level and an even higher increase during the second exercise (Figure 5).

7.4 Discussion

The unambiguous detection of lactate *in vivo* is complicated by the overlap with lipid signals. J-difference editing sequences can be employed for lactate detection if a very stable system and physiology are at hand. If not, subtraction errors might cause the wrong assignment of signal to the lactate resonance. Multiple quantum filters offer the advantage of single shot lactate detection with very good suppression of overlapping signals. The actual suppression efficiency does not so much depend on system stability, but more on the

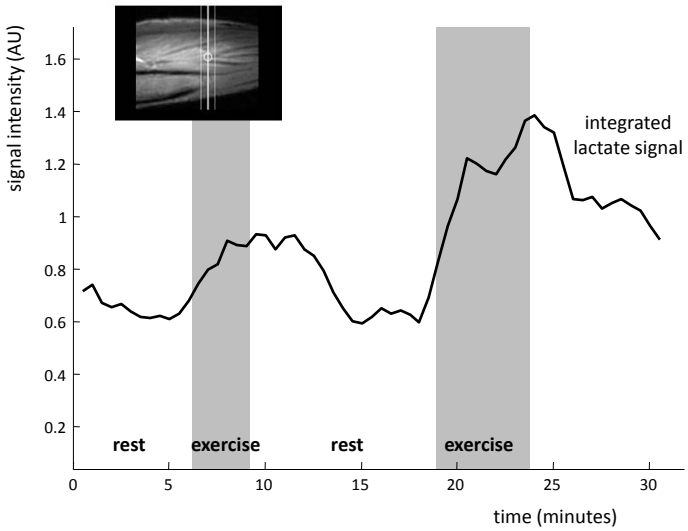

Figure 5: continuous lactate double quantum filtered measurements during rest and exercise. The signal was averaged for 1:04 minute (32 averages, TR = 2 s) and integrated between 1.0 and 1.5 ppm and a temporal average filter of 3 points was applied. Strain was put on the calf muscle by pulling on the pedal positioned below the foot for two blocks, one of 3 and one of 5 minutes. A clear increase in lactate signal was seen, with a slow decay back to baseline.

ability to dephase the overlapping lipid signals. This is performed by bringing the lactate signal into a double quantum state where it is twice as sensitive to the dephasing gradient as the lipid signals which remain in a single quantum state. After bringing the double quantum lactate coherences back into an observable single quantum state with a read pulse, a double rephasing gradient is applied for restoring the lactate signal. Overlapping singlet resonances experience a spin echo with asymmetric gradients and are dephased leading to highly efficient lipid suppression.

However, the *in vivo* requirements for these crusher gradients very much depends on the local anatomy. Local variations in susceptibility can lead to large local B_0 field gradients in the tissue, for example on the interface of tissue and air or lipids. Especially at high field these susceptibility effects increase, and put higher requirements on the dephasing gradient area. The minimum required dephasing gradient area was investigated by Mellon et al at 3T on a homogeneous safflower seed oil phantom, where a factor of 1500 lipid suppression was reached with relatively small 7.8 ms*mT/m DQ-selection gradients (14). Here it is shown, that for the *in vivo* situation in the human calf muscle at 7T, at least 120 ms*mT/m selection gradients are required to fully suppress the lipid signal (>1600 fold suppression). The effective crushing that is required for the unambiguous detection of lactate therefore greatly depends on the concentration of lactate which is to be detected, the composition of the tissue in the excited slice, static magnetic field strength, and possibly also on fast physiological fluctuations such as heartbeat.

Traditional double quantum filters such as the SSEL or HSEL do not allow for the incorporation of very long dephasing gradients. Since the *in vivo* gradient strengths are limited, long gradient crushers have to be incorporated for sufficient lipid dephasing, leading severe additional signal loss, which is due to the fact that either chemical shift or the J-coupling is not refocused over the t1 period with these methods. In the human calf muscle already a gradient dephasing of 120 ms*mT/m was required. With 30 mT/m gradients this leads to a t1 time of 18 ms (10 ms RF and 2×4 ms gradients) for the SSEL or HSEL method, leading to 10% and 20% signal loss respectively. In cases where more lipid crushing is required, as in diseased muscle tissue, or other organs like the breast or liver, the signal loss of the lactate resonance will increase dramatically (Figure 2) for the traditional double quantum filters.

In this work we have demonstrated a refocused double quantum filter, by incorporating multiple selective refocusing pulses in the t1 period to refocus both chemical shift and J-coupling evolution, thereby cancelling the term of additional signal loss and increasing the measurement sensitivity for DQ filters close to the theoretical 50%. Especially when high crushing gradients are required for lipid dephasing the t1 period can become relatively large compared to the J-coupled evolution, stressing the need for a refocused double quantum filter even more. The method was demonstrated *in vivo* by a measurement of baseline lactate level in the human calf muscle. An increase in lactate signal was observed during exercise, with a slow decay back to baseline levels.

With higher gradient dephasing areas, the lactate measurement becomes more diffusion weighted, which can be used for assessing the diffusion properties of lactate *in vivo* (21). The applied diffusion gradients required for dephasing of the lipid signal also cause some signal loss, the b-value of the sequence used to measure the lactate resonance in the human calf muscle with 136 ms*mT/m dephasing gradients (Figure 1) was 283 s/mm^2.

Although the requirement for gradient dephasing at lower field will be less stringent, the required selectivity of the RF pulses will still require relatively long t1 times, dependent on the area of interest. Therefore a refocused double quantum filter might also be interesting for low field applications.

In conclusion, a refocused double quantum filter has been shown, that allows for the incorporation of large crusher gradients into a double quantum selection filters in order to perform lactate detection in situations where very high lipid crushing efficiency is required.

7.5 Acknowledgement

We would like to express our thanks to Noah Klomp for the development and construction of the non-magnetic pedal used during the exercises. The Dutch Scientific Organization (VENI-DK-916.10.163) and the Dutch cancer society (KWF-UU2009-4500) are acknowledged for financial support.

References

1. Yaligar J, Thakur SB, Bokacheva L, Carlin S, Thaler HT, Rizwan A, Lupu ME, Wang Y, Matei CC, Zakian KL, Koutcher JA. Lactate MRSI and DCE MRI as surrogate markers of prostate tumor aggressiveness. NMR in Biomedicine 2011:n/a-n/a.
2. Lee SC, Huang MQ, Nelson DS, Pickup S, Wehrli S, Adegbola O, Poptani H, Delikatny EJ, Glickson JD. In vivo MRS markers of response to CHOP chemotherapy in the WSU-DLCL2 human diffuse large B-cell lymphoma xenograft. NMR Biomed 2008;21(7):723-733.
3. Lee SC, Poptani H, Pickup S, Jenkins WT, Kim S, Koch CJ, Delikatny EJ, Glickson JD. Early detection of radiation therapy response in non-Hodgkin's lymphoma xenografts by in vivo 1H magnetic resonance spectroscopy and imaging. NMR Biomed 2010;23(6):624-632.
4. Liu YJ, Chen CY, Chung HW, Huang IJ, Lee CS, Chin SC, Liou M. Neuronal damage after ischemic injury in the middle cerebral arterial territory: deep watershed versus territorial infarction at MR perfusion and spectroscopic imaging. Radiology 2003;229(2):366-374.
5. Hanisch F, Muller T, Muser A, Deschauer M, Zierz S. Lactate increase and oxygen desaturation in mitochondrial disorders--evaluation of two diagnostic screening protocols. J Neurol 2006;253(4):417-423.
6. Delikatny EJ, Chawla S, Leung DJ, Poptani H. MR-visible lipids and the tumor microenvironment. NMR Biomed 2011;24(6):592-611.
7. Torriani M, Townsend E, Thomas B, Bredella M, Ghomi R, Tseng B. Lower leg muscle involvement in Duchenne muscular dystrophy: an MR imaging and spectroscopy study. Skeletal Radiology:1-9.
8. Star-Lack J, Spielman D, Adalsteinsson E, Kurhanewicz J, Terris DJ, Vigneron DB. In vivo lactate editing with simultaneous detection of choline, creatine, NAA, and lipid singlets at 1.5 T using PRESS excitation with applications to the study of brain and head and neck tumors. J Magn Reson 1998;133(2):243-254.
9. Trabesinger AH, Meier D, Boesiger P. In vivo 1H NMR spectroscopy of individual human brain metabolites at moderate field strengths. Magn Reson Imaging 2003;21(10):1295-1302.
10. Bax A, De Jong PG, Mehlkopf AF, Smidt J. Separation of the different orders of NMR multiple-quantum transitions by the use of pulsed field gradients. Chem Phys Lett 1980;69:567–570.
11. de Graaf AA, Luyten PR, den Hollander JA, Heindel W, Bovee WM. Lactate imaging of the human brain at 1.5 T using a double-quantum filter. Magn Reson Med 1993;30(2):231-235.
12. He Q, Shungu DC, van Zijl PC, Bhujwalla ZM, Glickson JD. Single-scan in vivo lactate editing with complete lipid and water suppression by selective multiple-quantum-coherence transfer (Sel-MQC) with application to tumors. J Magn Reson B 1995;106(3):203-211.

13. He Q, Bhujwalla ZM, Glickson JD. Proton detection of choline and lactate in EMT6 tumors by spin-echo-enhanced selective multiple-quantum-coherence transfer. J Magn Reson B 1996;112(1):18-25.
14. Muruganandham M, Koutcher JA, Pizzorno G, He Q. In vivo tumor lactate relaxation measurements by selective multiple-quantum-coherence (Sel-MQC) transfer. Magn Reson Med 2004;52(4):902-906.
15. Melkus G, Morchel P, Behr VC, Kotas M, Flentje M, Jakob PM. Short-echo spectroscopic imaging combined with lactate editing in a single scan. NMR Biomed 2008;21(10):1076-1086.
16. Pickup S, Lee SC, Mancuso A, Glickson JD. Lactate imaging with Hadamard-encoded slice-selective multiple quantum coherence chemical-shift imaging. Magn Reson Med 2008;60(2):299-305.
17. Mellon EA, Lee SC, Pickup S, Kim S, Goldstein SC, Floyd TF, Poptani H, Delikatny EJ, Reddy R, Glickson JD. Detection of lactate with a hadamard slice selected, selective multiple quantum coherence, chemical shift imaging sequence (HDMD-SelMQC-CSI) on a clinical MRI scanner: Application to tumors and muscle ischemia. Magn Reson Med 2009;62(6):1404-1413.
18. Thakur SB, Yaligar J, Koutcher JA. In vivo lactate signal enhancement using binomial spectral-selective pulses in selective MQ coherence (SS-SelMQC) spectroscopy. Magn Reson Med 2009;62(3):591-598.
19. Lei H, Peeling J. Off-resonance effects of the radiofrequency pulses used in spectral editing with double-quantum coherence transfer. J Magn Reson 2000;144(1):89-95.
20. Meyerspeer M, Kemp GJ, Mlynarik V, Krssak M, Szendroedi J, Nowotny P, Roden M, Moser E. Direct noninvasive quantification of lactate and high energy phosphates simultaneously in exercising human skeletal muscle by localized magnetic resonance spectroscopy. Magn Reson Med 2007;57(4):654-660.
21. de Graaf RA, Rothman DL. In vivo detection and quantification of scalar coupled 1H NMR resonances. Concepts in Magnetic Resonance 2001;13(1):32-76.

Chapter 8

Summary and discussion

MR Spectroscopy at ultra-high field in humans

MR spectroscopy (MRS) has gained an important place in fundamental research as well as in clinical research. *In vivo* MR spectroscopy provides a unique window to measure the concentration of chemical compounds (metabolites) inside the human body without the need for a chirurgical intervention or puncture. It obviates the need for tissue excisions or biopsies and provides direct tissue biomarkers, rather than indirect parameters derived from blood, plasma or urine samples. MR signals from tissue volumes of less than 1 ml and metabolite concentrations below 1 mM can be detected. Therefore MR spectroscopy is applicable to study normal and pathological metabolism inside the human body. However, for many research purposes and especially for clinical practice, the sensitivity and specificity of the MRS measurement is still a limiting factor.

The sensitivity is limited by the low concentrations in the body, which make it difficult to detect these signals above the noise. This puts a restriction on the spatial resolution that can be obtained and leads to long measurement times. Also the specificity of MR spectroscopy is often a limiting factor, as the spectral resolution is not much higher than the difference in chemical dispersion between some resonances. The overlap in the MR spectrum between different compounds makes it hard to separately detect metabolites. For example, the resonances of glutamate and glutamine show significant overlap, and are difficult to detect individually.

The recent development of ultra-high field magnets for human use offers a platform where both the sensitivity and the specificity of MRS are substantially increased. The intrinsic signal-to-noise ratio (SNR) of the MRS measurements increases approximately linear with the static magnetic field strength. MR experiments at a field strength of 7 tesla therefore show a more than twofold increase in the intrinsic SNR, as compared to a 3T MR scanner. In addition, the chemical shift separation between resonances is increased, leading to a more reliable discrimination between metabolites in the MR spectrum. These two effects show potential for a next step in the evolution of *in vivo* MR spectroscopy. Before the increased sensitivity and specificity can be utilized in practice, several technical impediments will have to be overcome when performing MRS in the human body at ultra-high field.

The most important challenges that ultra-high field MRS applications impose are the decreased homogeneity in the static magnetic field (B_0) and the transmit field (B_1), a demand for higher gradient strengths, altered relaxation times and an increased power deposition in the body. This theses describes several studies and new methods to counter these challenges, and shows how high quality MRS data can be acquired at ultra-high field in humans.

Sensitivity

The most significant advantage of MR spectroscopy at ultra-high field is increased SNR, which would allow for higher spatial resolution, both in so-called single-voxel spectroscopy as well as in spectroscopic (chemical shift resolved) imaging. The first technical challenge that comes with voxel or slice selection approaches for spatial localization is the increase in chemical shift dispersion with field strength. The lack of an additional, commensurate increase in RF power (e.g. pulse bandwidth) and, to a lesser extent, the lack of gradient strength causes the RF pulses at ultra-high field to have a lower bandwidth, rather than a higher bandwidth, compared to lower field. Particularly refocusing pulses cover a very restricted spectral width, resulting in a chemical dispersion dependent shift of the location of the slice or voxel. To reduce this chemical shift displacement artifact, the stimulated echo acquisition (STEAM) has been proposed in literature for human MRS at ultra-high field. The use of a stimulated echo for localizing the signal in the human body does not require refocusing pulses, but it leads to an intrinsic and unacceptable loss of the available signal of 50%. To overcome this shortcoming, a localization sequence was developed that acquires a full spin echo with a sensitivity of close to 100%. Adiabatic refocusing pulses with a high bandwidth were used in a semi adiabatic sequence (sLASER). This enabled fast and robust single-voxel measurements of 8 ml volume with only 16 averages, which showed a low chemical shift displacement artifact between the detected metabolites (Chapter 2).

Alternatively, a pulse-acquire approach can be used, where slice selective excitation is used with gradient encoding to localize the signal in a two dimensional matrix, also with almost 100% sensitivity. This relieves the demand for refocusing pulses altogether and circumvents a severe chemical shift displacement artifact. Without the need for refocusing pulses, sensitive and time efficient sequences were developed, and consequently the spatial resolution could be increased. This allowed mapping of the metabolite concentrations in two dimensions over multiple slices in the human brain. MR spectroscopic imaging experiments were performed where several metabolites could be detected with voxel sizes down to 0.25 ml acquired in measurement times between 12 and 30 minutes (Chapter 3 and 4).

At ultra-high field, macromolecular (MM) signals underlying the metabolites in ^{1}H MR spectroscopy are better resolved from the baseline compared to low field MR spectroscopy. Even though these signals overlap with the signals from the metabolites, metabolite quantification at 7T is feasible after a measurement of this MM baseline, based on the significant differences in T_1 relaxation times (Chapter 2 and 3). In fact, an accurate description of the MM baseline might not only be a prerequisite for metabolic fitting, but since the MM baseline is quite well resolved at ultra-high field, the composition of the MM baseline might be an interesting target for future research, as the appearance of these large molecules in the MR spectrum has been linked to various disorders in literature.

Homogeneity: B_0 field

With higher magnetic field, the degree of magnetization of the human body is increased. This on one hand leads to more detectable spins, however it also leads to the effect that the absolute difference between the magnetization of different tissue types is enlarged. This means that the static magnetic field (B_0) shows more distortion due to tissue variation on for example tissue-air interfaces (magnetic susceptibility effects). Therefore additional effort must be invested at ultra-high field for the homogenization of the magnetic field (e.g. B_0 field shimming). The MR system is equipped with up to third order magnetic field (room temperature) shim coils, that can generate spatially varying magnetic fields to counteract the induced B_0 magnetic field inhomogeneity. Prior to single-voxel MR spectroscopy one can measure the field inhomogeneity with B_0 field mapping techniques. Sequentially, after proper calibration procedures, the optimal way of steering the shim coils can be calculated and applied, resulting in well resolved spectra (Chapter 2, 6 and 7).

Optimizing the magnetic field homogeneity on a small region in space though, will lead to problems with water and lipid suppression outside the region of interest that are improperly suppressed due to their large frequency offsets. Therefore a novel cost function shimming approach can be used where both the region of interest and other brain and skull regions are taken into account. This scheme can be used to ensure a good homogeneity over a whole slice to ensure efficient water and lipid suppression, without compromising the B_0 field homogeneity in the region of interest. The increased magnetic field homogeneity allows for efficient water and lipid suppression, which in turn enables the acquisition of very high spatial resolutions (Chapter 3). This approach can be taken one step further, when an optimal B_0 shim is determined for every individual RF pulse. During water and lipid suppression pulses, the B_0 field can be homogenized for large areas, where during slice selective excitation and readout, the B_0 shim can be switched to optimal settings for that specific slice (Chapter 4). For the fast switching of higher order (room temperature) shim coils however, the eddy currents on the higher order shims in the MR system have to be sufficiently compensated. Alternatively, actively shielded shim coils might be developed, which show significantly less eddy current interactions, facilitating a straightforward calibration of the system.

Not only the spatial B_0 homogeneity, but also the temporal B_0 field stability at ultra-high field is severely compromised by the increased magnetic susceptibility effects. Breathing effects for example, cause B_0 field (and thus frequency) fluctuations in the brain of up to several hertz. In the human breast, these field instability can be as high as 70 Hz over a period of several seconds. For stable and robust MR spectroscopy of the human body, these field variations have to be monitored, and ideally immediately compensated. For this purpose, a B_0 field monitoring system can be used, equipped with real-time data processing and interfaced to the B_0 field shim coils, in order to measure and correct for the magnetic field variation in a direct way (Chapter 5). It was demonstrated as a proof-of-principle that the global offset frequency can be corrected for in real-time in the human breast. The temporal

field instabilities can therefore be reduced, resulting in significantly improved spectral line shapes. On top of the global frequency, also a strong time varying linear term from anterior-to-posterior was observed, as well as smaller higher order time varying fields. For future applications, this field correction principle is readily extendable to a multi-channel field camera, so that up to third order spatial terms can be corrected for in real-time. This might not only be beneficial for correcting breathing induced instability in organs close to the chest, but also for correcting cardiac induced fluctuations and artifacts originating from accidental motion in any other part of the body.

As demonstrated in this thesis, these techniques to compensate for B_0 field variations are indispensable for high quality MR spectroscopy in man at ultra-high field strength. For many imaging applications, similar requirements on field homogeneity and drift compensations are valid. This renders these solutions useful for many other high field applications outside the field of MRS as well.

Homogeneity: B_1 field

The RF energy required to manipulate nuclear spins at higher field increases, leading to substantial interactions of the RF field (B_1 field) with the human body. At a Larmor frequency of 300 MHz, the reduced wavelength of approximately 12 cm in the human body leads to interference effects in the body, and severe signal dropouts are seen in the body when traditional excitation concepts are used. The use of a multi-transmit coil can counteract these effects, where multiple RF transmitters are used to manipulate the B_1 field. After measurement of the spatial distribution of every transmit coil the optimal drive settings for the array can be determined (B_1 shimming). With this approach, the B_1 field of multiple coils can be focused in a region to allow for the use of high bandwidth adiabatic pulses to improve detection sensitivity and localization performance (Chapter 2 and 6). Even more so, the field can be directed to a certain region, for example on the skull to allow for efficient single-pulse lipid suppression. Furthermore, the B_1 field can be made homogeneous over large areas of the brain. Fast switching between all these drive settings for the array is possible, and allows for dynamic pulse-specific RF field optimization that substantially increases the degrees of freedom for advanced spin dynamics (Chapter 4).

Suppression efficiency

As the water and lipid resonances will also show an increased SNR, ultra-high field puts a higher demand on the quality of the water and lipid suppression schemes that are used. Traditional water and lipid suppression sequences have to be reevaluated, taking into account the increased power deposition at ultra-high field (Chapter 3 and 4).

The increased temporal field instability can be a significant source of unsuppressed signal. In breast measurements, real-time field updating is shown to be almost essential to ensure a proper frequency reference for suppression (Chapter 5). Also in the brain significant instabilities can occur. For example, the cardiac cycle shows to have an important influence

in editing acquisitions for the detection of γ-aminobutyric acid (GABA) in the human brain, possibly due to pulsation of the brain. Cardiac triggering in this case showed to resolve most of these instability, boosting the suppression efficiency of creatine, which overlapped with the GABA resonance, from an (insufficient) 25 fold to more than 200 fold (Chapter 6).

Furthermore, the crushing of unwanted excitation, as for example caused by refocusing pulses in a localization sequence, has to be enhanced at higher fields. The local jumps in the magnetic susceptibility can cause very high local gradients at 7T, especially on the interface of tissue and air or lipids. This might counteract most of the dephasing which is applied with the crushing gradients. These large local gradients can therefore lead to rephasing of unwanted coherences. Also for the gradient dephasing of water and lipid signals, larger gradient areas are required. For lactate detection in the human calf muscle, a refocused double quantum filter was designed to allow for such high crusher gradients, and ensure full lipid signal dephasing (Chapter 7).

In this thesis, it is shown how efficient MR spectroscopy can be performed at ultra-high field in humans. Both single-voxel as well as two-dimensional and multi-slice experiments were performed, and demonstrated high quality MR spectroscopic data. In addition, effective editing schemes have been designed that resolve low concentration metabolites. GABA was resolved from overlapping macromolecules and creatine in the human brain, and lactate was resolved from the overlapping lipid resonances in the human calf muscle.

Future directions

This thesis studied and described the application of new RF pulse sequences to obtain high quality MR spectra in humans at 7T. The different approaches presented for MR spectroscopy at ultra-high field allow for fast, robust measurements of the metabolism in humans at high spatial and spectral resolution.

Although the techniques described have proven to result in high quality data, their direct application in clinical practice remains challenging. Streamlining of scanning protocols will be required, as well as optimization of the reconstruction and processing pipeline for the acquired MRS data. To really benefit from the increased signal-to-noise ratio at ultra-high field and increase the sensitivity and specificity for MRS applications, multi-transmit arrays will be an absolute necessity. The acquisition of MR spectra with a multi-transmit RF coils adds a degree of freedom, but will concomitantly increase the complexity of the technology. From a practical implementation point of view, the success of these techniques will depend on fast and high quality person-to-person B_1 field calibration of the coil elements, for which operator independent procedures will have to be developed. Novel developments in on-coil amplifiers and coil design technology may further improve the performance of the RF system, and accelerated B_1 field mapping sequences, combined with automatic image processing are being developed to reduce the duration of the calibration steps as much as possible. Also the *dynamic* use of multi-coil transmit arrays and B_0 shim

systems leverages the potential of ultra-high field systems, as B_0 and B_1 homogeneity can be tuned for every part of the MR sequences individually.

Countering temporal instability of the B_0 field using a B_0 field monitoring system with direct field correction was shown to be beneficial for breast MR spectroscopy at 7T, but is expected to be an asset to future improvement of stability in MR spectroscopy and MRI, in other parts of the human body and at both lower and higher field strengths. Such a system shows potential to be fully integrated and user-independent, to allow for a stable magnetic field despite subject motion, breathing and possible magnet instabilities.

In conclusion, ultra-high field offers a next step in spatial and spectral resolution for MR spectroscopy. Spectra can be obtained at unprecedented spatial resolutions for metabolites that could not reliable be measured before at lower field strengths. This thesis demonstrates the technical feasibility and real potential of ultra-high field MR spectroscopy for the study of normal and pathological metabolism in humans.

Chapter 9

Samenvatting en discussie

MR Spectroscopie op ultrahoogveld in de mens

MR spectroscopie (MRS) heeft een belangrijke plaats veroverd in fundamenteel wetenschappelijk en in klinisch onderzoek. Het gebruik van *in vivo* MRS biedt namelijk de mogelijkheid om concentraties van verschillende moleculen te meten in het menselijk lichaam. Daarmee kunnen biochemische processen in het lichaam worden onderzocht. De kracht van de techniek ligt in de unieke eigenschap dat deze stofwisseling (het metabolisme) bestudeerd kan worden in het weefsel zelf, zonder daarvoor operatief of via een punctie weefsel te moeten verwijderen. Hiermee kan men, in tegenstelling tot metingen aan bloed, plasma, urine of andere lichaamsstoffen, zonder verdere interventies biomarkers in eventueel aangedaan weefsel direct bepalen. Verschillende moleculen (metabolieten) kunnen worden gedetecteerd in volumes kleiner dan 1 ml en in concentraties onder de 1 mM. MRS is daardoor uitermate geschikt om de gezonde en afwijkende stofwisseling in het menselijk lichaam te bestuderen. Echter, de gelimiteerde gevoeligheid en specificiteit van deze techniek verhinderen het succes van veel studies. Dit resulteerde tot nu toe in een zeer beperkte toepassing in de klinische praktijk.

De gevoeligheid in MRS is gelimiteerd door de lage concentraties van de metabolieten in het menselijk lichaam. Dit maakt het moeilijk om de signalen boven het ruisniveau te detecteren. Het gevolg is dat grote detectievolumina en lange meettijden nodig zijn.

Ook de specificiteit van MRS is gelimiteerd: het onderscheidend vermogen in het spectrale domein (spectrale resolutie) dat kan worden behaald met *in vivo* MRS is niet veel groter dan de scheiding tussen de resonanties van de verschillende moleculen. De overlap van resonanties maakt het daardoor in de praktijk moeilijk om metabolieten van elkaar te onderscheiden. Bijvoorbeeld de resonanties van glutamaat en glutamine laten een significante overlap zien, en zijn daardoor moeilijk los van elkaar te detecteren.

De recente ontwikkeling van ultrahoogveld-MR magneten voor toepassing in mensen biedt een platform waarmee zowel de gevoeligheid als de specificiteit van de MRS metingen kan worden verhoogd. De gevoeligheid van de metingen gaat omhoog omdat de signaal-ruisverhouding (SNR) van de metingen ongeveer lineair met de veldsterkte toeneemt. Daardoor is er op een veldsterkte van 7 tesla meer dan twee keer zoveel SNR beschikbaar als op een MR-scanner met een veldsterkte van 3 tesla.

Daarnaast biedt ultrahoogveld-MR een verhoogde specificiteit, omdat de absolute afstand tussen de resonanties in het spectrum is vergroot. Hierdoor zijn de verschillende resonanties beter van elkaar te onderscheiden. Door deze twee effecten kan *in vivo* MRS op ultrahoogveld nieuwe inzichten bieden in het menselijk metabolisme. Echter, voordat de potentie van ultrahoogveld kan worden omgezet in een toepasbare verbetering van MRS in het menselijk lichaam, moeten verschillende technische obstakels overwonnen worden.

De belangrijkste uitdagingen in ultrahoogveld MRS zijn de verslechterde homogeniteit van het statische magneetveld (B_0) en het zendveld (B_1), de gelimiteerde sterkte van de gradiënten, veranderende relaxatietijden en een verhoogde energiedepositie in het menselijk lichaam.

In dit proefschrift worden nieuwe methoden beschreven die een adequate aanpak bieden voor deze problemen. Tevens wordt gedemonstreerd hoe MRS data van hoge kwaliteit kunnen worden verkregen.

Gevoeligheid

Verhoogde SNR is misschien wel het belangrijkste voordeel dat ultrahoogveld biedt. Deze kan namelijk worden ingezet om de spatiële resolutie te verhogen in zowel MRS metingen van een enkele locatie, als in MRS metingen met een spatiële codering waarbij veel spectra van verschillende gebieden tegelijk worden verkregen.

Het eerste obstakel dat we tegenkomen bij het aanslaan van een enkele plak, of het exciteren van een volume, is de grote scheiding tussen de frequentie van verschillende moleculen op ultrahoogveld. Deze vergrote scheiding zou gepaard moeten gaan met een gelijke verhoging van de bandbreedte van de radiofrequente (RF) pulsen die gebruikt worden voor de manipulatie van de spins. Echter, doordat het piekvermogen van de RF op ultrahoogveld eerder lager dan hoger is, hebben de RF pulsen niet voldoende bandbreedte om de verhoogde scheiding tussen de resonanties als verwaarloosbaar te beschouwen. Dit leidt, vooral bij refocuseringspulsen, tot een frequentieafhankelijke verschuiving van de locatie van de plak of het volume. Om deze verschuiving te minimaliseren is het gebruik van een gestimuleerde acquisitie (STEAM) voorgesteld in de literatuur. Deze techniek maakt geen gebruik van refocuseringspulsen waardoor 50% van het signaal verloren gaat. Om toch gebruik te kunnen maken van de verhoogde SNR op ultrahoogveld is een methode ontwikkeld waar een volle spin echo gebruikt kan worden, op bijna 100% gevoeligheid. Hiervoor zijn frequentiegemodelleerde pulsen geïmplementeerd in een semi-adiabatische sequentie (sLASER). Hiermee kunnen snelle en robuuste volume metingen van 8 ml worden opgenomen, in slechts 16 middelingen en met minimale verschuiving tussen de metabolieten (hoofdstuk 2).

Als alternatief is een methode ontwikkeld waar plakselectie wordt gecombineerd met lokalisatie door middel van gradiëntcodering. Twee dimensionale rasters van MR spectra kunnen zo worden verkregen. Doordat de lokalisatie wordt gerealiseerd door de gradiëntcodering, zijn geen refocuseringspulsen nodig, en wordt het verschuivingseffect grotendeels omzeild. Zonder de noodzaak voor refocuseringpulsen kunnen gevoelige en efficiënte metingen worden gedaan op verhoogde spatiële resoluties. MRS experimenten zijn gedemonstreerd van tweedimensionale rasters op meerdere plakken tegelijk in het menselijk brein. Volumina die zo klein waren als 0.25 ml konden worden gemeten in scantijden tussen de 12 en 30 minuten (hoofdstuk 3 en 4).

In de basislijn onder het spectrum van de metabolieten is een aantal macromoleculaire (MM) resonanties te zien. De signalen van deze grote moleculen overlappen met de meeste andere metabolieten. Om goed onderscheid te kunnen maken is daarom een onafhankelijke meting van deze signalen nodig (hoofdstuk 2 en 3). Dit kan door de signalen te filteren op hun T_1-relaxatietijd, omdat de macromoleculaire signalen een veel kortere T_1-relaxatietijd

hebben. Een accurate beschrijving van deze macromoleculaire basislijn is essentieel voor een goede afschatting van de metabolietsignalen maar ook een interessant onderwerp voor verdere studie. Dit omdat deze signalen op 7T beter van elkaar te onderscheiden zijn dan op lagere veldsterktes en omdat deze grote moleculen in de literatuur zijn verbonden met verschillende ziektebeelden.

Homogeniteit: B_0 veld

Met een verhoging van het statische magnetische veld (B_0) wordt de geinduceerde magnetisatie van het menselijk lichaam groter. Dit leidt tot een groter detecteerbaar signaal aan de ene kant, maar heeft ook tot gevolg dat de absolute verschillen in magnetisatie tussen verschillende weefsels groter wordt. Dit betekent dat het B_0 veld minder homogeen is, bijvoorbeeld op de overgang tussen lucht en weefsel. Daarom moet op 7T meer moeite worden geïnvesteerd om het B_0 veld te homogeniseren. Om dit te bewerkstelligen zijn er extra elektromagnetische spoelen in het systeem geplaatst waarmee spatieel variërende magneetvelden kunnen worden aangelegd. De vorm van deze additionele zogenaamde shimvelden zijn sferisch harmonische functies van tot in de derde orde. Deze shimspoelen worden zo ingesteld dat de variatie van het magneetveld in een klein gebied van interesse wordt geminimaliseerd. Dit leidt tot een goede homogeniteit van het magneetveld in het gebied van interesse, en daardoor een goede spectrale resolutie (hoofdstuk 2, 6 en 7).

Echter, het gebruik van deze steile derde orde velden op een klein gebiedje leidt tot grote variatie buiten dat gebied. Dat heeft tot gevolg dat de onderdrukking van water- en vetsignalen buiten dit gebied niet meer afdoende is. Als verbetering hiervoor is een aanpak ontwikkeld waarbij niet alleen het gebied van interesse wordt meegenomen in de berekeningen van deze shimvelden, maar waarbij tevens wordt gekeken naar de homogeniteit buiten dat gebied. Hierdoor kan toch een effectieve water- en vetonderdrukking worden gerealiseerd in andere gebieden van het brein en in de schedel, zonder dat dit ten koste gaat van de homogeniteit in het gebied van interesse. Deze manier van onderdrukking van water en vet signalen leidt tot een efficiënte sequentie, waardoor hoge spatiële resoluties kunnen worden gerealiseerd (hoofdstuk 3). Deze aanpak kan nog verder worden doorgevoerd, door de optimale aansturing van de shimspoelen te berekenen voor elk onderdeel van de MR sequentie. Tijdens water- en vetonderdrukkingspulsen kan het veld worden gehomogeniseerd over het gehele brein, terwijl tijdens plakselectie en de uitlezing van de data het veld kan worden gehomogeniseerd voor specifiek dat gebied van het brein (hoofdstuk 4). Echter, voor het snel schakelen van deze shimspoelen moeten de geïnduceerde wervelstromen in het systeem goed onder controle gebracht worden.

Niet alleen de spatiële B_0 homogeniteit is belangrijk voor MRS, maar ook de temporele veldstabiliteit is van groot belang. Op ultrahoogveld zijn de effecten van de ademhaling op de homogeniteit van het magneetveld vergroot. De daaraan gerelateerde B_0 veldvariaties (en daardoor variatie op de resonantie frequenties) in het brein bedragen enkele hertz. Dichter bij de longen (bijvoorbeeld in de borst) zijn fluctuaties waarneembaar tot wel 70 Hz. Voor

stabiele en betrouwbare MRS metingen in het menselijk lichaam moeten deze fluctuaties worden gekwantificeerd, en het liefst direct worden gecorrigeerd. Voor dit doel kan een B_0 veldcamera worden gebruikt. Indien uitgerust met snelle analyse software kan dit direct de shimspoelen aansturen om de variërende magneetvelden als gevolg van de ademhaling direct te corrigeren. Het principe van deze correctiestrategie is gedemonstreerd door de globale veldafwijking tijdens ademhaling te corrigeren in de borst (hoofdstuk 5). Bovenop de globale frequentie was ook een sterke lineaire en kleinere hogere orde termen te zien in de borst. Aangezien het veldcorrectiesysteem uitgebreid kan worden met meerdere veldcamera's, kunnen zo de spatiële verdeling van de instabiliteiten gemeten en direct gecorrigeerd worden.

Zoals gedemonstreerd in dit proefschrift zijn deze technieken onmisbaar voor de meting van MR spectra van hoge kwaliteit in de mens op ultrahoogveld. Veel beeldvormingtechnieken vereisen vergelijkbare homogeniteit en stabiliteit van het magneetveld. Daarom zullen deze technieken ook voor andere ultrahoogveldtoepassingen gebruikt kunnen worden.

Homogeniteit: B_1 veld

De energie van het RF veld (B_1 veld) dat wordt gebruikt voor het manipuleren van de nucleaire spins neemt toe op hoger magnetisch veld. Dit leidt tot verhoogde interactie van het RF veld met het menselijk lichaam. Op een resonantiefrequentie van 300 MHz is de golflengte van de RF golven in het lichaam gereduceerd tot ongeveer 12 cm. Dit heeft veel interferentie en absorptie van de RF velden in het lichaam tot gevolg en leidt tot donkere plekken in de MR beelden wanneer traditionele spoelconcepten worden toegepast.

Met het gebruik van multi-element spoelen kunnen deze effecten worden tegengegaan. Hiervoor worden meerdere RF zenders gebruikt. De sterkte en fase van het veld van de verschillende spoelen kan zo worden ingesteld dat de gegenereerde B_1 velden op een klein gebied leiden tot constructieve interferentie om zo het B_1 veld te maximaliseren en daardoor het gebruik van RF pulsen met een hoge bandbreedte voor nauwkeurige lokalisatie mogelijk te maken (hoofdstuk 2 en 6). Een B_1 veld kan ook zo worden aangelegd dat alleen de schedel geëxciteerd wordt voor vetonderdrukking of dat een egale excitatie in het hoofd wordt gegenereerd. Het is mogelijk om snel te schakelen tussen de verschillende RF instellingen. Daarmee kunnen geavanceerde sequenties worden ontwikkeld voor snelle MRS van het brein (hoofdstuk 4).

Onderdrukkingsefficiëntie

Omdat de water- en vetsignalen zijn verhoogd op ultrahoogveld worden hogere prestaties verwacht van de technieken die gebruikt worden voor de onderdrukking van water en vet. Nieuwe onderdrukkingstechnieken zijn ontwikkeld voor efficiënte onderdrukking op ultrahoogveld, binnen de gestelde limieten van RF opwarming van het lichaam (hoofdstuk 3 en 4).

Temporele instabiliteiten kunnen ook een bron van ongewenste signalen zijn. In MRS metingen in de borst is de detectie en correctie van de ademhaling essentieel voor MRS (hoofdstuk 5). Daarnaast kunnen ook in het brein significante instabiliteiten optreden. Bijvoorbeeld, als tijdens een ongunstig punt in de hartcyclus wordt gemeten, dan kan dit de meting van γ-aminoboterzuur (GABA) een behoorlijk beïnvloeden. Dit kan worden opgelost door de meting te synchroniseren met de juiste periode in de hartslag. Daarmee wordt de onderdrukkingsfactor van creatine (een resonantie die overlapt met GABA) verhoogd van (een onvoldoende) 25 keer naar meer dan 200 keer (hoofdstuk 6).

Verder moeten ook de gradiënten worden geoptimaliseerd die worden ingezet voor het verminderen van ongewenste excitaties in een lokalisatiesequentie. De refocusingspulsen kunnen namelijk ongewenste signalen veroorzaken. Door de grote sprongen in het magneetveld op bijvoorbeeld een overgang tussen weefsel en lucht kunnen de aangebrachte defaseringsgradiënten teniet worden gedaan. Daarom moeten deze gradiënten worden verhoogd voor gebruik op ultrahoogveld. Een precieze afstelling is essentieel voor een robuuste detectie van de metabolieten.

In dit proefschrift wordt een aantal methoden gepresenteerd om efficiënte MRS metingen uit te voeren op ultrahoogveld in het menselijk lichaam. Zowel metingen van een enkel volume, als metingen in een twee dimensionaal raster, en van meerdere plakken zijn gedemonstreerd. Daarnaast zijn effectieve technieken gepresenteerd voor de detectie van laaggeconcentreerde metabolieten. GABA is gedetecteerd in het brein door exclusie van de overlappende resonanties van creatine en macromoleculen, en lactaat is gedetecteerd in de kuit door de overlappende vet signalen te minimaliseren tot onder het ruisniveau.

Toekomstperspectief

In dit proefschrift is beschreven hoe MRS kan worden uitgevoerd in het menselijk lichaam, en hoe hoge kwaliteit spectra kunnen worden verkregen. De verschillende technieken maken het mogelijk om snelle en robuuste metingen van het menselijk metabolisme uit te voeren op hoge spatiële en spectrale resoluties.

De directe toepassing van deze technieken in de klinische praktijk vereist echter verdere stroomlijning van de scanprotocollen en optimalisatie van de reconstructie- en analysepijplijn voor de MR data. Met name het gebruik van een multikanaals RF spoel zal essentieel zijn voor de verdere ontwikkeling van ultrahoogveld-MRI. Deze multikanaals RF spoelen voegen een vrijheidsgraad maar ook een moeilijkheidsgraad toe aan het systeem. Daarmee zal het succes van deze techniek afhangen van het vermogen om dit keer op keer goed af te regelen, zonder dat dit veel tijd of interactie van de gebruiker vergt. Ook nieuwe ontwikkelingen, zoals het integreren van versterkers en spoelen en nieuwe spoelontwerpen zullen de prestaties van dit soort systemen nog kunnen verbeteren. Daarbij zal vooral het dynamisch gebruik van multikanaals RF pulsen en B_0 shimvelden het potentieel nut van ultrahoogveld-MRI systemen verhogen. Hiermee kan namelijk zowel de B_0 als B_1 veldhomogeniteit worden geoptimaliseerd voor elk individueel onderdeel van de MR

sequenties.

Het tegengaan van temporele instabiliteiten van het B_0 veld met een veldcamera en directe veldcorrectie met de shimspoelen is essentieel voor MRS van de borst op 7T. Daarnaast zal een dergelijk systeem van nut zijn om de stabiliteit te verhogen in MRS, maar ook in MRI van andere lichaamsdelen, zowel op hogere als op lagere veldsterktes. Zo'n systeem kan in potentie het magneetveld homogeen houden ondanks ademhaling en beweging van de persoon in de magneet en kan daardoor veel artefacten verhelpen, veroorzaakt door instabiliteit van de magneet en ten gevolge van beweging en fysiologie in de mens.

Concluderend kan gezegd worden dat met het gebruik van een ultrahoogveld magneet een nieuwe stap wordt gezet in de haalbare spectrale en spatiële resoluties voor MRS. Spectra kunnen worden verkregen van kleine volumina, en metabolieten die niet betrouwbaar gedetecteerd konden worden op lagere veldsterktes kunnen nu robuust worden gemeten.

In dit proefschrift worden de technische haalbaarheid en de reële potentie van ultrahoogveld-MRS gedemonstreerd voor het bestuderen van het normale en het pathologische metabolisme in de mens.

List of publications

van den Bergen, B, Klomp DWJ, Raaijmakers AJE, de Castro CA, **Boer VO**, Kroeze H, Luijten PR, Lagendijk JJW, van den Berg CAT. "Uniform prostate imaging and spectroscopy at 7T: comparison between a microstrip array and an endorectal coil", NMR in Biomedicine 2011; 24(4) 358-365

Kan HE, Klomp DWJ, Wong CS, **Boer VO**, Webb AG, Luijten PR, Jeneson JA. "In vivo 31P MRS detection of an alkaline inorganic phosphate pool with short T_1 in human resting skeletal muscle", NMR in Biomedicine 2010; 23(8) 995-1000

Klomp, DWJ, Scheenen TWJ, Arteaga CS, van Asten, J, **Boer VO**, Luijten PR. "Detection of fully refocused polyamine spins in prostate cancer at 7T", NMR in Biomedicine 2011; 24(3) 299-306

Boer VO, van Lier AL, Hoogduin JM, Wijnen JP, Luijten PR, Klomp DWJ. "7T ^{1}H MRS with adiabatic refocusing at short TE using radiofrequency focusing with a dual-channel volume transmit coil", NMR in Biomedicine 2011; 24(9) 1038-46

Klomp DWJ, van de Bank BL, Raaijmakers A, Korteweg MA, Possanzini C, **Boer VO**, van de Berg CA, van de Bosch MA, Luijten PR. "^{31}P MRSI and ^{1}H MRS at 7T: initial results in human breast cancer", NMR in Biomedicine 2011; in press DOI: 10.1002/nbm.1696

Boer VO, Siero JC, Hoogduin H, van Gorp JS, Luijten PR, Klomp DWJ. "High-field MRS of the human brain at short TE and TR", NMR in Biomedicine 2011; 24(9) 1081-8

Mandl RC, van den Heuvel MP, Klomp DWJ, **Boer VO**, Siero JC, Luijten PR, Hulshoff Pol HE. "Tract-based magnetic resonance spectroscopy of the cingulum bundles at 7T", Human Brain Mapping 2011; in press DOI: 10.1002/hbm.21302

Boer VO, Klomp DWJ, Juchem C, Luijten PR, de Graaf RA. "Multi-slice ^{1}H MRSI of the human brain at 7 Tesla using dynamic B_0 and B_1 shimming", Magnetic Resonance in Medicine 2011; in press

Boer VO, Bank BL, van Vliet G, Luijten PR, Klomp DWJ. "Direct B_0 field monitoring and real-time B_0 field updating in the human breast at 7T", Magnetic Resonance in Medicine 2011; in press

Andreychenko A, **Boer VO**, Luijten PR, Klomp DWJ. "Efficient spectral editing at 7T: GABA detection with MEGA-sLASER", Magnetic Resonance in Medicine 2011; in press

Juchem C, Nixon TW, McIntyre S, **Boer VO**, Rothman DL, de Graaf RA. "Dynamic multi-coil shimming of the human brain at 7T", Journal of Magnetic Resonance 2011; 212(2) 280-8

van Kalleveen IML, Koning W, **Boer VO**, Luijten PR, Zwanenburg JJM, Klomp DWJ. "Adiabatic turbo spin echo in human applications at 7 Tesla", Magnetic Resonance in Medicine 2011; in press

Van der Kemp WJM, **Boer VO**, Luijten PR, Wijnen JP, Klomp DWJ. "Increase in SNR for 31P MR spectroscopy by integrating polarization transfer with direct detection", Magnetic Resonance in Medicine 2011; in press

Curriculum Vitae

Vincent Oltman Boer was born on the 22nd of August 1984 in Nieuwegein, The Netherlands. After finishing high school, he started his Bachelors Physics and Astronomy at the Utrecht University, The Netherlands. During his study he did an internship at the Biophysics group in the Physics department on two-photon excitation fluorescence microscopy.

After receiving his BSc degree in 2005, he continued with his Masters studies in Biomedical Imaging Sciences at the Utrecht University where he first encountered the fascinating world of MRI. His masters research project concerned the real-time motion tracking of the kidneys for MR thermometry, which was performed at the University of Bordeaux, France. He received his MSc degree in 2007, after which he continued with a PhD project on ultra-high field MR Spectroscopy at the University Medical Center Utrecht, The Netherlands. During his research project, under supervision of Prof. Dr. Peter Luijten, he investigated the use of the 7 Tesla MRI magnet for *in vivo* MR spectroscopy of the human brain and body. During the project he performed a 5-month research project as a Postgraduate Fellow at Yale University, U.S. under the supervision of Dr. Robin de Graaf.

In september 2011 he started a post-doc project in the UMC Utrecht on real-time B_0 shimming for MRI.

Dankwoord

Na dit promotietraject (die vier jaar zijn voorbij gevlogen!) wil ik graag een woord van dank richten aan iedereen die me heeft bijgestaan in deze periode. Een proefschrift maak je niet alleen, maar gelukkig ben ik de afgelopen jaren geholpen door een fijne groep mensen in een open werksfeer waar bij iedereen de deur altijd openstaat.

Allereerst veel dank aan mijn promotor en co-promotor.

Professor P.R. Luijten, beste Peter, als baas van de 7T heb je een grote, jonge en inspirerende groep mensen bij elkaar weten te krijgen. En met je spectro achtergrond wist je ook meestal gelijk wat wel en wat niet de moeite van het uitzoeken waard was in mijn onderzoek. Dank je voor alle input in het onderzoek.

Dennis Klomp, beste Dennis, mr D, dank voor alle inspiratie en steun. Meestal als ik met weer een mislukte meting bij jou op de stoep stond, ging ik weer weg met ideeën voor minimaal twee nieuwe publicaties. En je grenzenloze en aanstekelijke enthousiasme laat je zelfs in de vroege uurtjes niet in de steek, daardoor was het vaak moeilijk om te stoppen op maandagavond (dinsdagochtend)!

Robin de Graaf, beste Robin, dankjewel voor je creativiteit en je kritische blik bij het doen van een onderzoek in New Haven. Ik heb in die 5 maanden gigantisch veel van je kunnen leren over alles wat met pulssequenties te maken heeft, maar daarnaast was er ook altijd tijd voor gezellige BBQ's in je steeds weer verbouwde huis en tuin!

De leden van de beoordelingscommissie, prof. dr. ir. J.J.W. Lagendijk, prof. dr. M.A.A.J. van den Bosch, prof. dr. ir. M.A. Viergever, prof.dr. K. Nicolay en prof. dr. A. Heerschap wil ik bedanken voor het beoordelen en goedkeuren van dit manuscript.

Beste coauteurs, bedankt voor alle goede ideeën en jullie bijdrage aan de hoofdstukken in dit proefschrift.

Professor C.T.W Moonen, beste Chrit, ook een woord van dank naar jou. Niet alleen voor het leuke jaar van onderzoek dat ik heb mogen doen in Bordeaux voorafgaand aan mijn promotieonderzoek, maar ook voor het aanraden van een promotieplek in Utrecht. Het is erg goed bevallen!

Sylvia, zonder jouw ondersteuning zou de 7T groep een grote chaos zijn. Een hele grote dankjewel voor al je inzet en hulp bij de administratie die bij het maken van een proefschrift komt kijken, en natuurlijk voor het regelen van alle vrijwilligers de afgelopen jaren!

Hans, bedankt voor je hulp bij het B_0 shimmen, B_1 shimmen en al je hulp bij het programeren op de Multix!

Beste Fredy, al vanaf onze eerste dag hier kamergenoten. Zonder deze Fredy factor was onze 7T groep niet zo ver gekomen!

Gerard, bedankt voor al je hulp met de Varian console, zelfs als we 's avonds laat weer de boel hadden opgeblazen was je bereid te komen helpen!

All the guys/girl at Yale, thanks for making my stay in New Haven an enjoyable one! Christoph, Henk, Terry, Scot, Dorit, Elany, Roger, Yang, Barak, Sho and Maggie; thanks! I had a wonderful summer in New Haven! En ook Maartje natuurlijk, gezellig dat ik je daar tegenkwam!

Daarnaast heb ik ook een aantal studenten mogen begeleiden, die gelukkig soms wat werk van je over kunnen nemen. Sjoerd, Henk, Hans en Irene, dankjulliewel!

En natuurlijk een hele grote thank you naar alle collega's voor de gezelligheid, de goede werksfeer, leuke borrels en alle zelfgemaakte baksels bij verjaardagen en publicaties! (Keep it up!) Oppervrijdagmiddagborrel Daniel, altijd in voor een goede discussie over bier en/of T_1! Catalina (gracias!), Anna (спасибо!), Jeroen en natuurlijk alle collega's van de 7T! Irene, Jannie, Bart, Jaco, Wouter & Allesandro, Alex, Mandy, Mies, Anja, Bertine, Laura, Wybe, Natalia and Taro. En iedereen van radiotherapie/radiologie (ook goed geïntegreerd op Q4!); Mariska, Astrid, Hanneke, Ozlem, Alexander, Nico, Nolan en alle anderen. En natuurlijk de ISI/IMAGO-ers Hendrik, Roel, Lisette, Mark en alle anderen, bedankt voor de gezelligheid en leuke discussies!

Ook een bedankje voor de technische ondersteuning is hier zeker op z'n plek. Met name naar het technisch cluster, de digitale beeldverwerking en de medische technologie. Ook alle spoelenbouwers en interfaceconstructeurs bedankt, Ingmar, Michel en alle andere jongens, bedankt!

Naast het ploeteren op het proefschrift is het ook nodig om af en toe te ontspannen. Gelukkig kan ik mee een paar keer per weer uitleven bij korfbal vereniging VIKO. Wessel en Mandy met name bedankt voor de logistiek afgelopen tijd! En Wessel daarbovenop dank dat je paranimf wilt zijn!

Daarnaast ook nog vaak hardlopen, en dan zit het met je conditie wel goed. Geerte, dankjewel voor de hardloopmotivatie, en ook dat je me wilt bijstaan als paranimf bij mijn promotie!

Lieve pap en mam, dit was me niet gelukt zonder jullie steun, goede raad en alles wat jullie me geleerd hebben. Simon en Caryn, a big thank you! voor de gezelligheid, en Simon heel erg bedankt voor de supergave lay-out!

Lieve Anouk, gewoon een hele dikke kus! Hvj!